Supporting Information

One-Pot Fluorescent Labeling Protocol for Complex Hydroxylated Bioactive Natural Products

Saikat Haldar, [†] *Santosh Kumar,* [‡, #] *Swati P. Kolet,* [†, #] *Harshal S. Patil,* [†] *Dhiraj Kumar,* [‡] *Gopal C. Kundu,* [‡] *Hirekodathakallu V. Thulasiram* [*, †, §]

[†] Chemical Biology Unit, Division of Organic Chemistry, CSIR-National Chemical Laboratory, Pune-411008, India.

[§] CSIR-Institute of Genomics and Integrative Biology, Mall Road, New Delhi-110007, India.

[‡] National Center for Cell Science, Pune-411007, India.

Corresponding Author. Fax: +91 2025902636; Tel: +91 2025902478; E-mail: hv.thulasiram@ncl.res.in

[#] Authors contributed equally.

Table of Contents

General Information.

Technical grade solvents were distilled prior to use for preparative chromatography purpose. Compounds were purified over silica gel (230-400 mesh) flash chromatography columns using dichloromethane/methanol gradient mixture as the eluent. HPLC runs were performed on HPLC system coupled with UV-Vis detector and analytical XBridge C_{18} column (4.6 x 100 mm) at a flow rate of 1 mL/min with a gradient solvent programme of: 0 min, 40% methanol/water; 10 min, 60% methanol/water; 25 min, 90% methanol/water; 28 min, 60% methanol/water; 30 min, 40% methanol/water; and monitored at 230 nm. Reactions and purification processes were monitored by thin layer chromatography, which was carried out on precoated silica gel plates using UV light (254 nm) as the visualization medium and anisaldehyde charring solution as the staining agent. Thin film IR spectra were recorded in $CHCl_3$ and optical rotations were determined in the same solvent at 589 nm using 10 mm cell (*c* in gm/100 mL unit). Chemical shift values in NMR (^{1}H, ^{13}C, DEPT-135) spectra were reported in ppm with respect to the residual solvent or TMS signals as the reference. HRMS data were collected on Q Exactive Quadrupole-Orbitrap Mass Spectrometer. The human cervical carcinoma (HeLa), breast adenocarcinoma (MDA-MB-231), and skin carcinoma (A375) cells were procured from American Type Culture Collection (ATCC, Manassas, VA, USA) and maintained in L-15 (MDA-MB-231), MEM (HeLa) and DMEM (A375, NIH-3T3) media (Gibco BRL) supplemented with 10% FBS, 100 units penicillin and 100 gm/mL streptomycin. The cells were maintained under humidified atmosphere of 5% CO_2 and 95% air at 37 ºC. Cell imaging was performed on confocal microscope. LC-ESI-HRMS runs were performed on Q Exactive Orbitrap attached with LC system. Samples were resolved through Hypersil Gold C_{18} column of particle size 5 μm with a flow rate of 0.5 mL/min and gradient solvent program of 35 min (0.0 min, 10% methanol/water; 0.5 min, 10.0% methanol/water; 3.0 min, 45% methanol/water; 6.0 min, 60% methanol/water; 30.0 min, 90% methanol/water; 32.0 min, 90% methanol/water; 32.5 min, 10% methanol/water; 35.0 min, 10% methanol/water). 0.1% LC-MS grade formic acid was also added to the solvents (methanol and water). HRMS data were recorded in ESI-positive ion mode within the mass range *m/z* 100 to 1000 using the tune method as followed: sheath gas flow rate 45, auxiliary gas flow rate 10, sweep gas flow rate 2, spray voltage (|KV|) 3.60, spray current (μA) 3.70, capillary temperature (ºC) 320, s-lens RF level 50, heater temperature (ºC) 350.

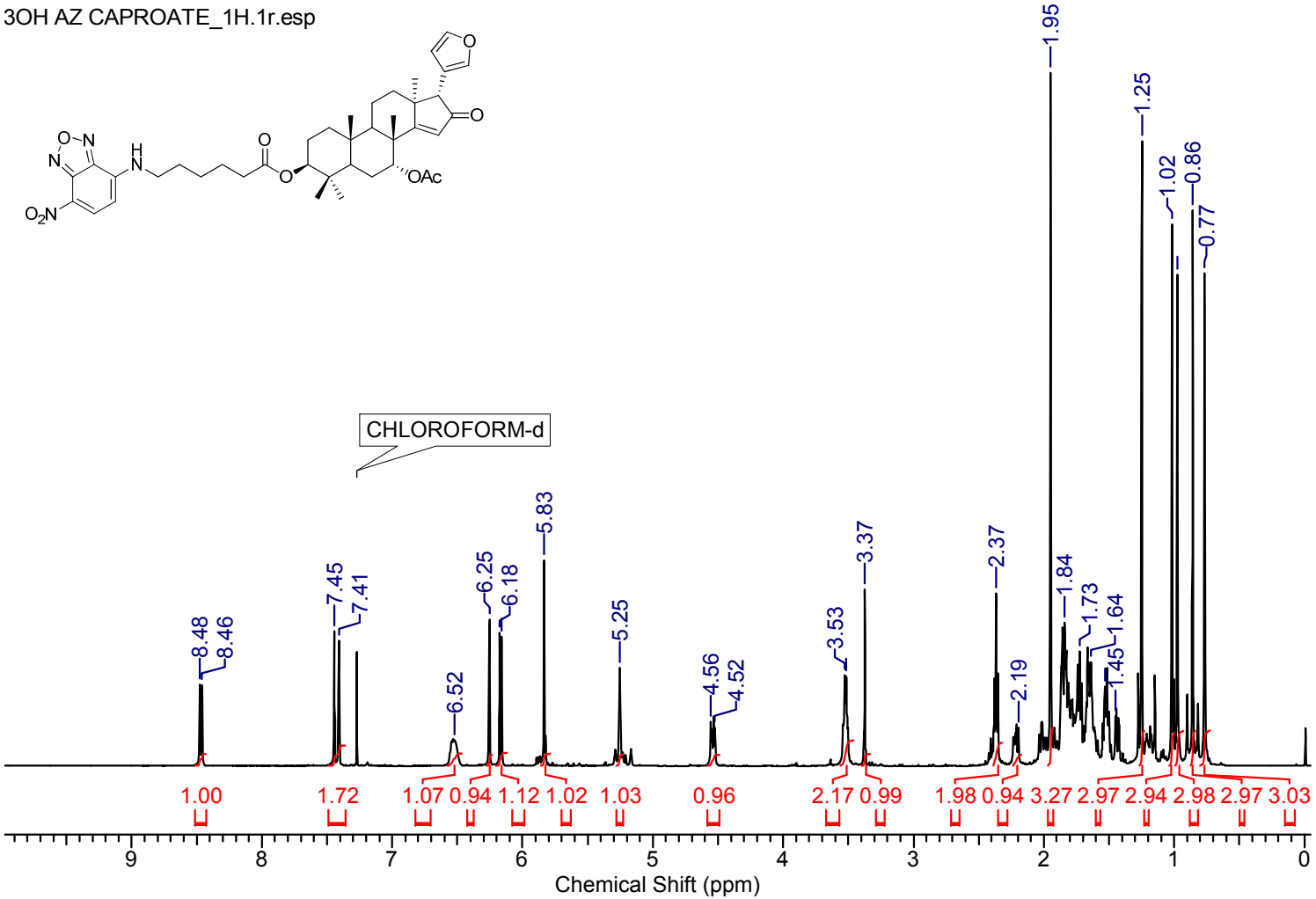

Fig. 1. ^{1}H NMR of **1a** in $CDCl_3$ at 400 MHz.

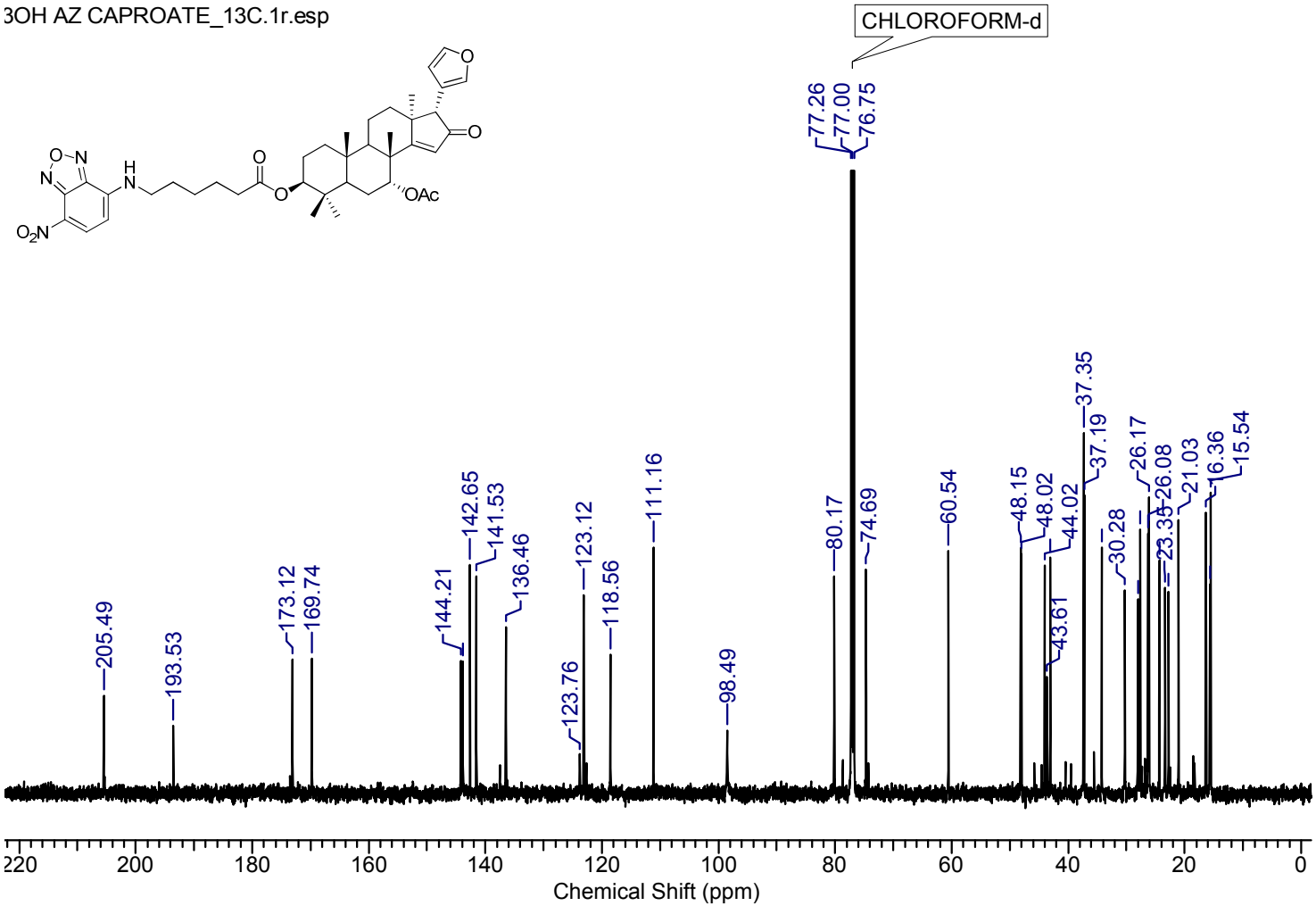

Fig. 2. ^{13}C NMR of **1a** in $CDCl_3$ at 100 MHz.

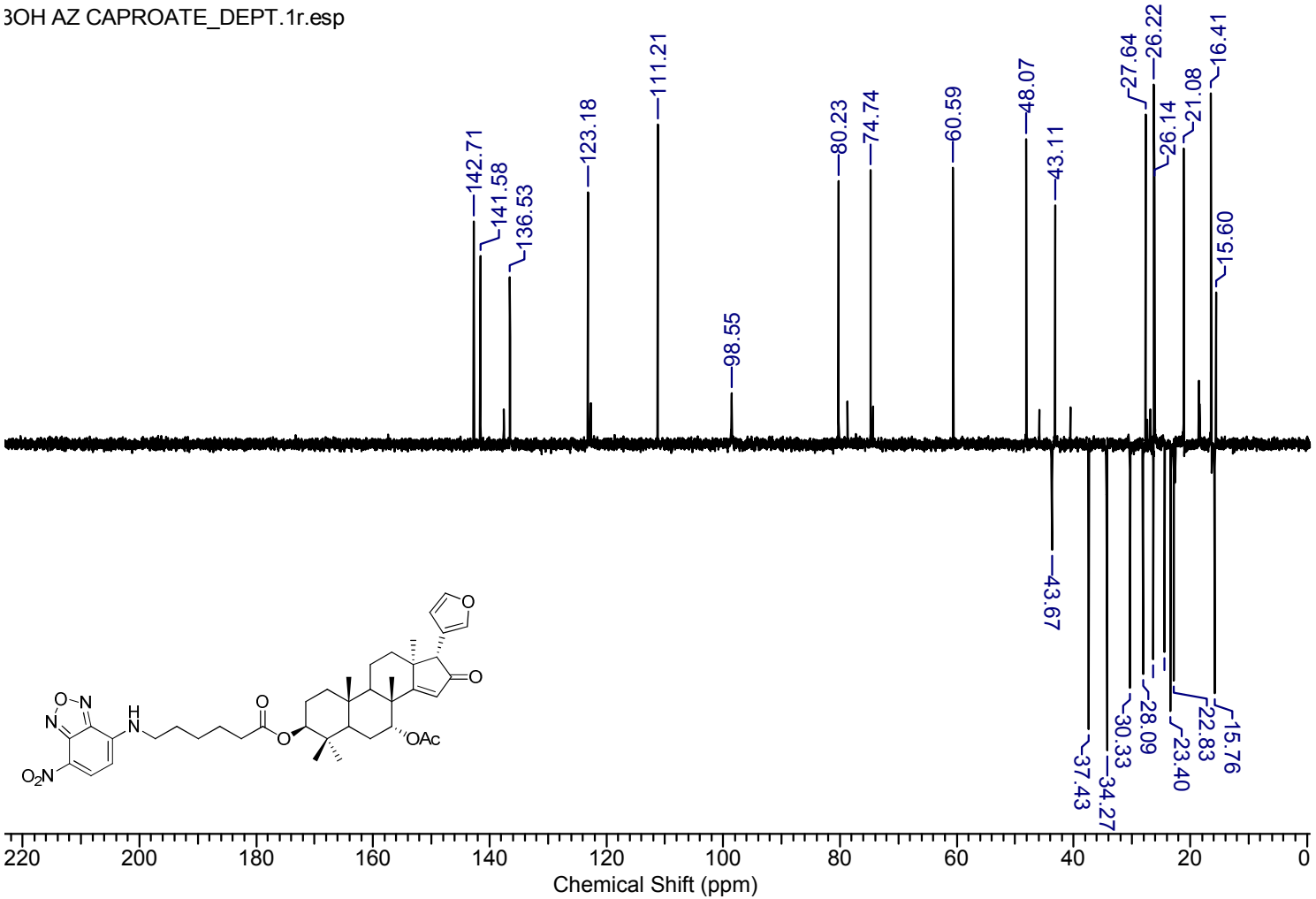

Fig. 3. DEPT-135 NMR of **1a** in $CDCl_3$ at 100 MHz.

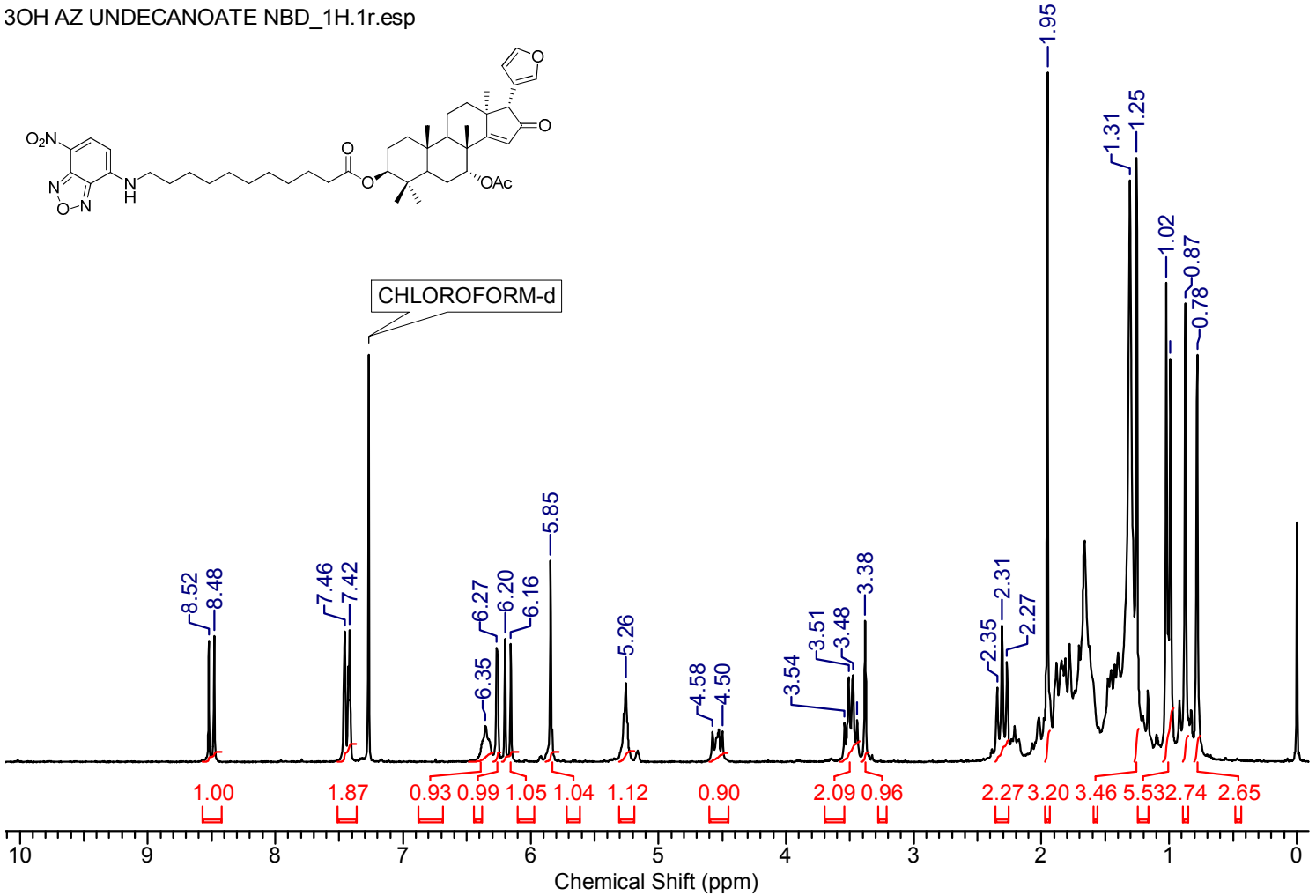

Fig. 4. ^{1}H NMR of **1b** in $CDCl_3$ at 400 MHz.

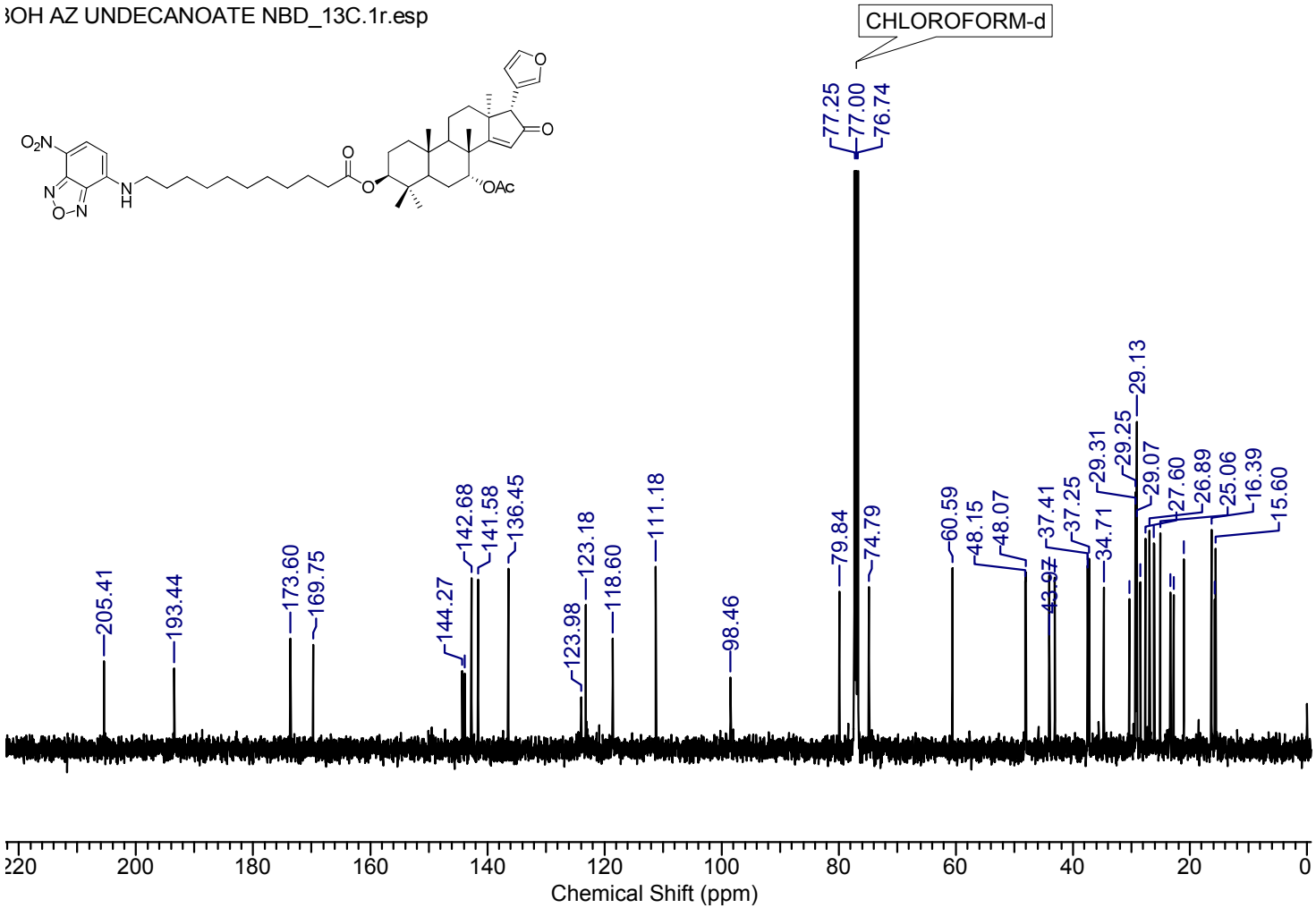

Fig. 5. ^{13}C NMR of **1b** in $CDCl_3$ at 100 MHz.

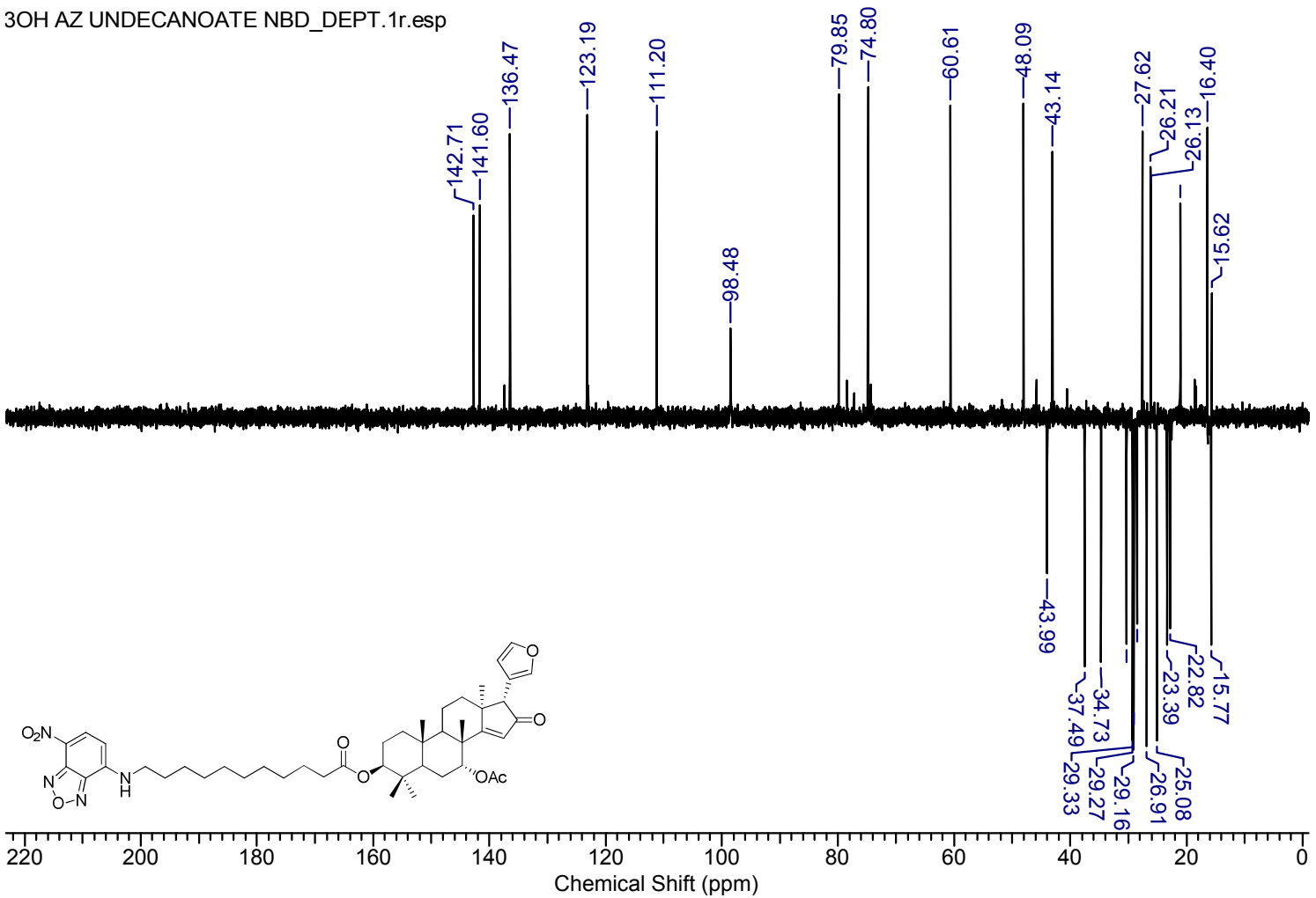

Fig. 6. ^{1}H NMR of **1b** in $CDCl_3$ at 100 MHz.

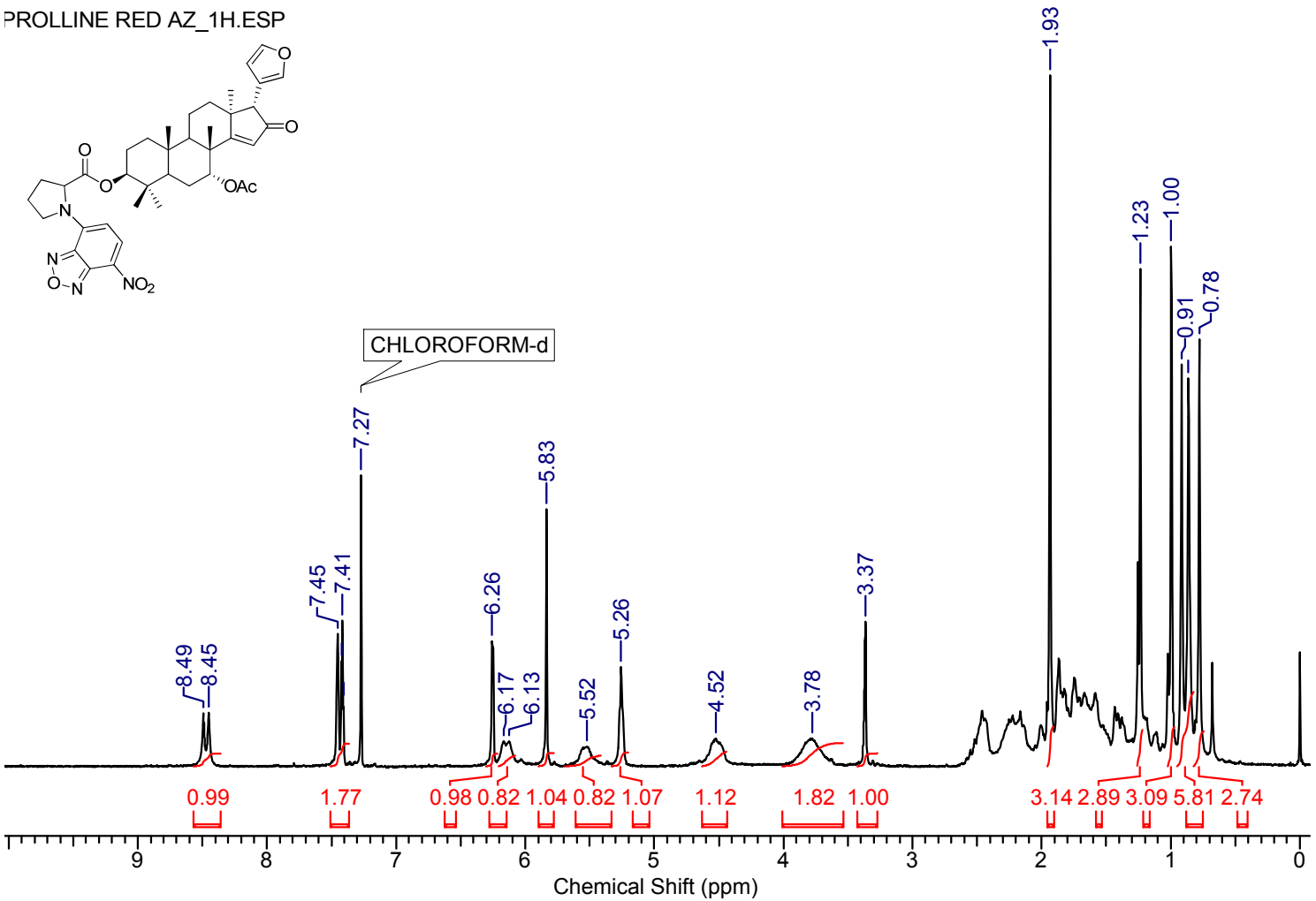

Fig. 7. ^{1}H NMR of **1c** in $CDCl_3$ at 400 MHz.

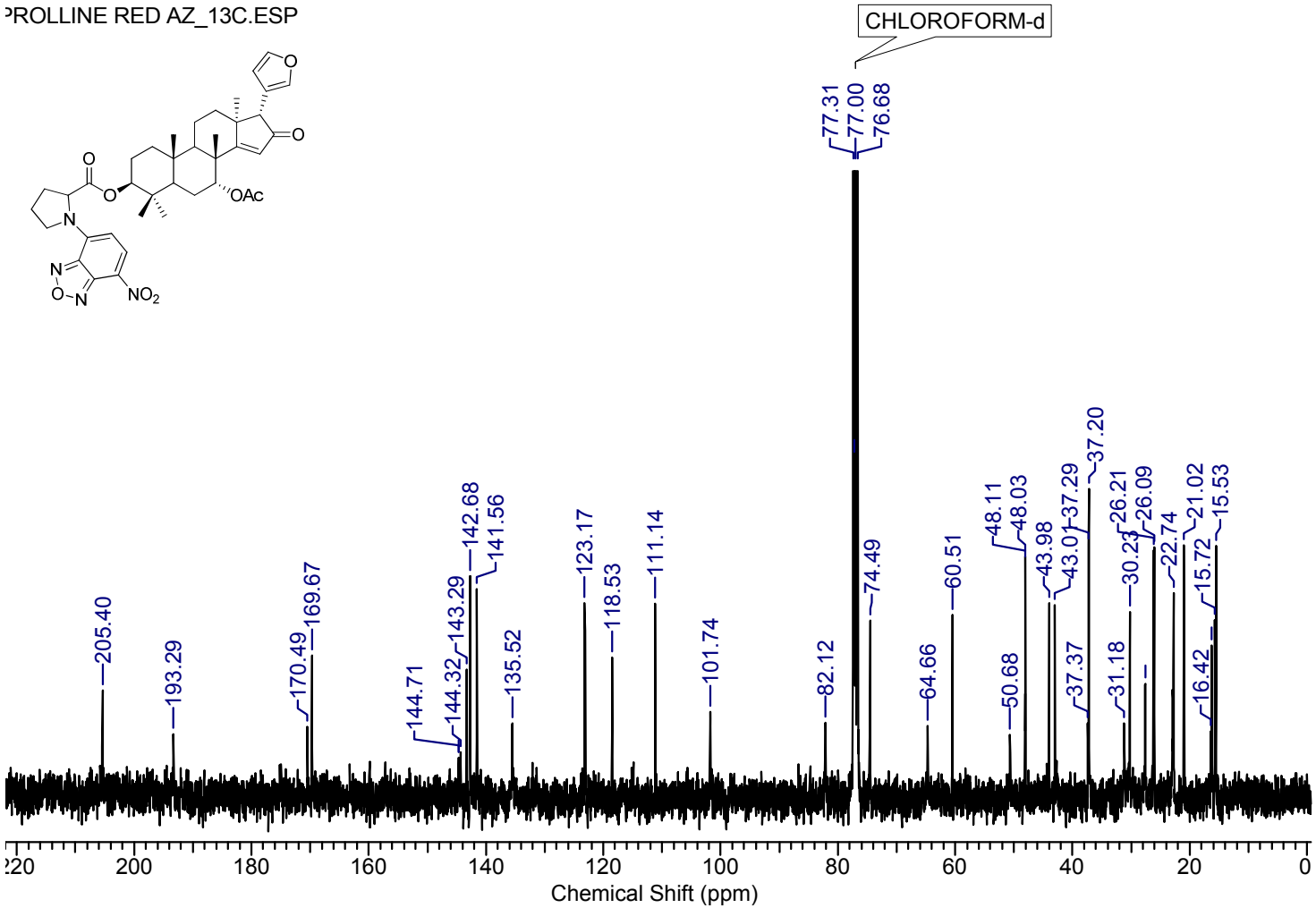

Fig. 8. ^{13}C NMR of **1c** in $CDCl_3$ at 100 MHz.

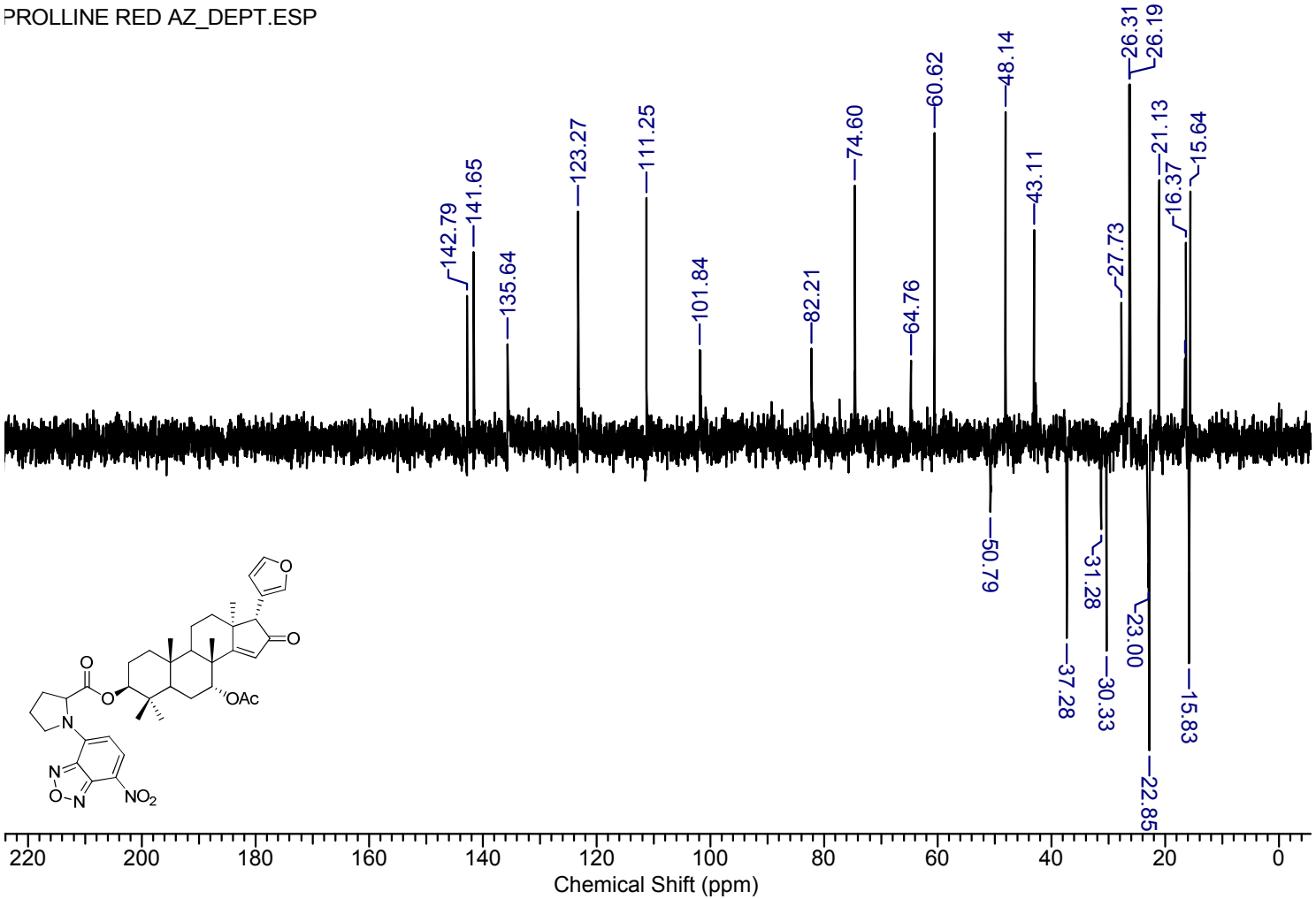

Fig. 9. DEPT-135 NMR of **1c** in $CDCl_3$ at 100 MHz.

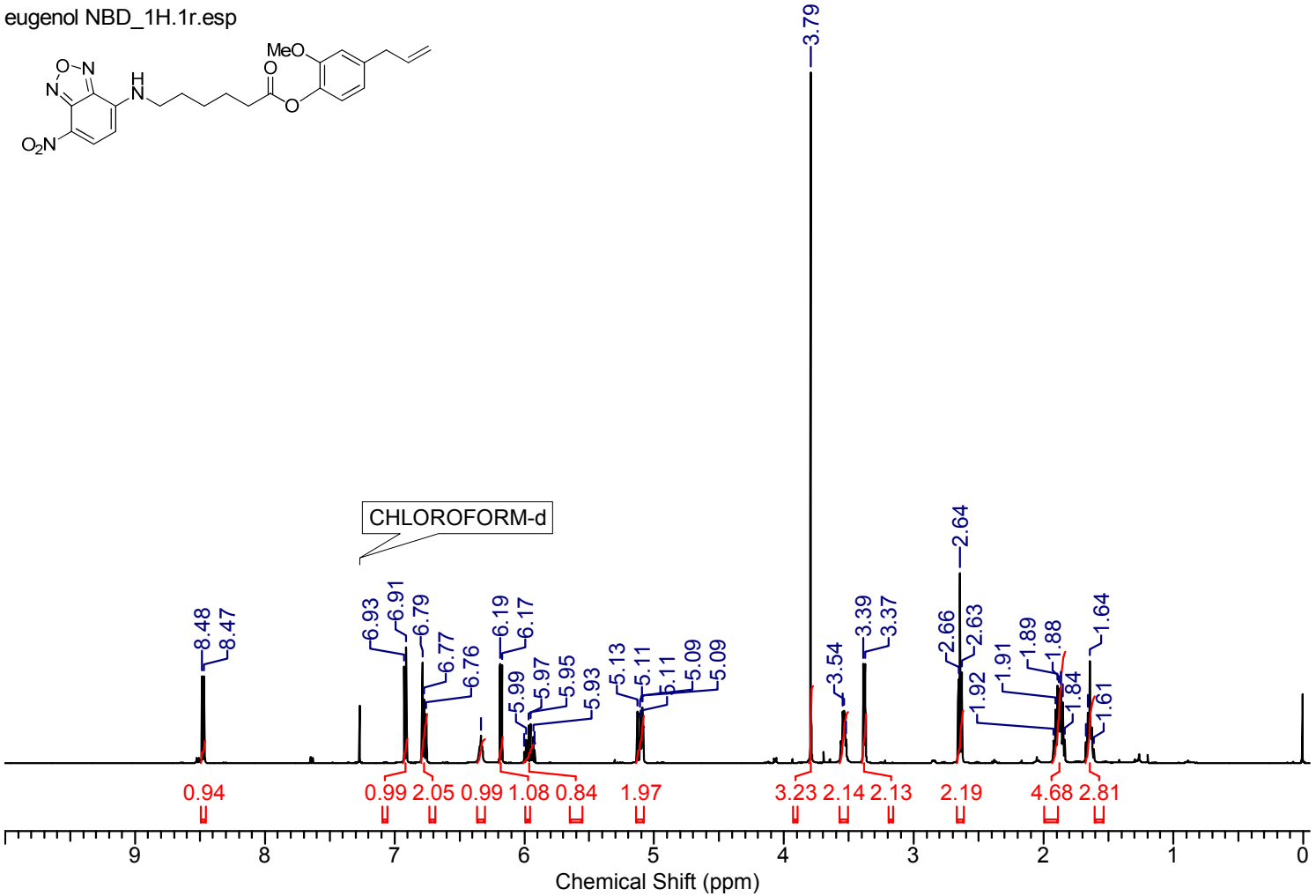

Fig. 10. ^{1}H NMR of **2a** in $CDCl_3$ at 400 MHz.

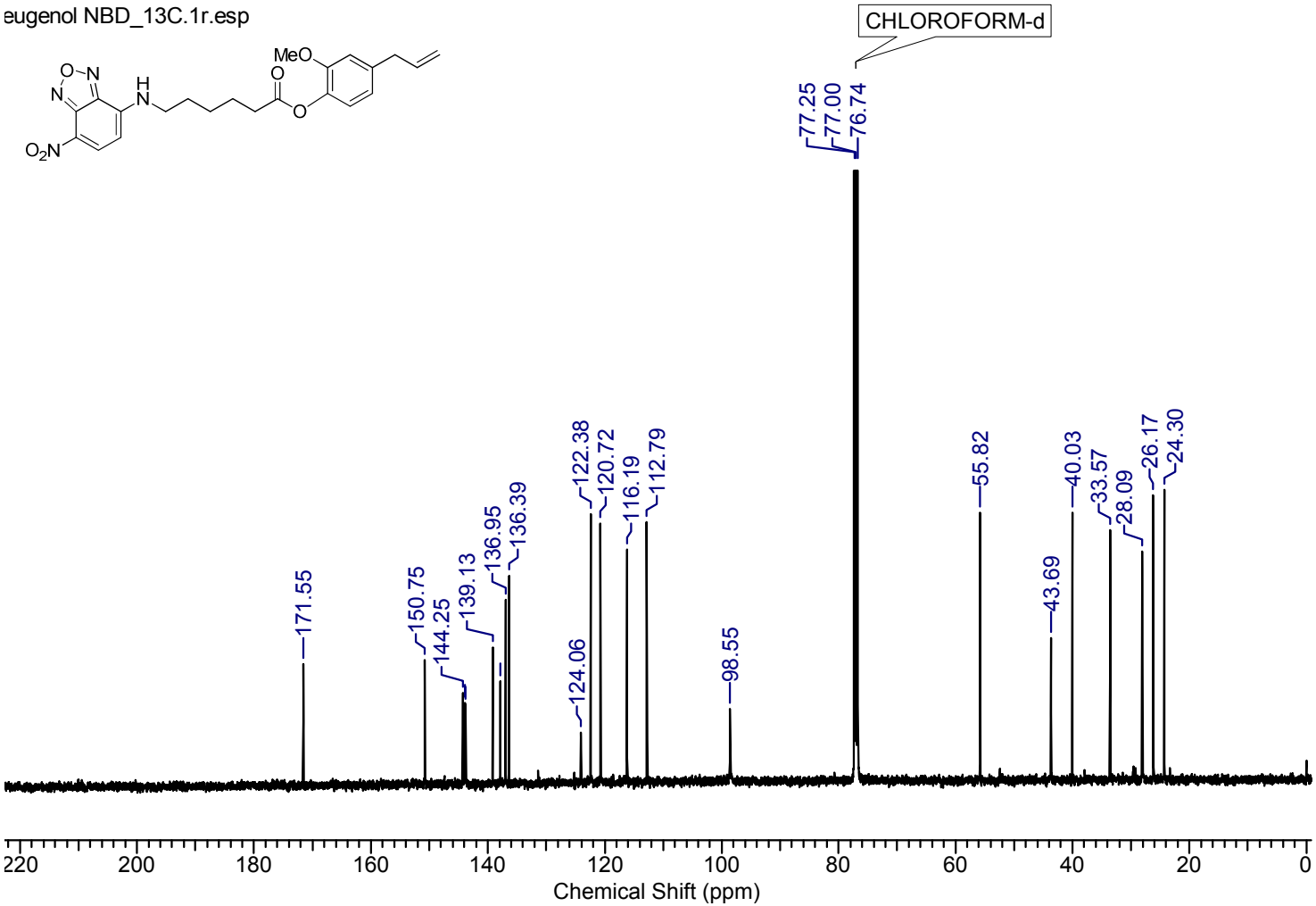

Fig. 11. ^{13}C NMR of **2a** in $CDCl_3$ at 100 MHz.

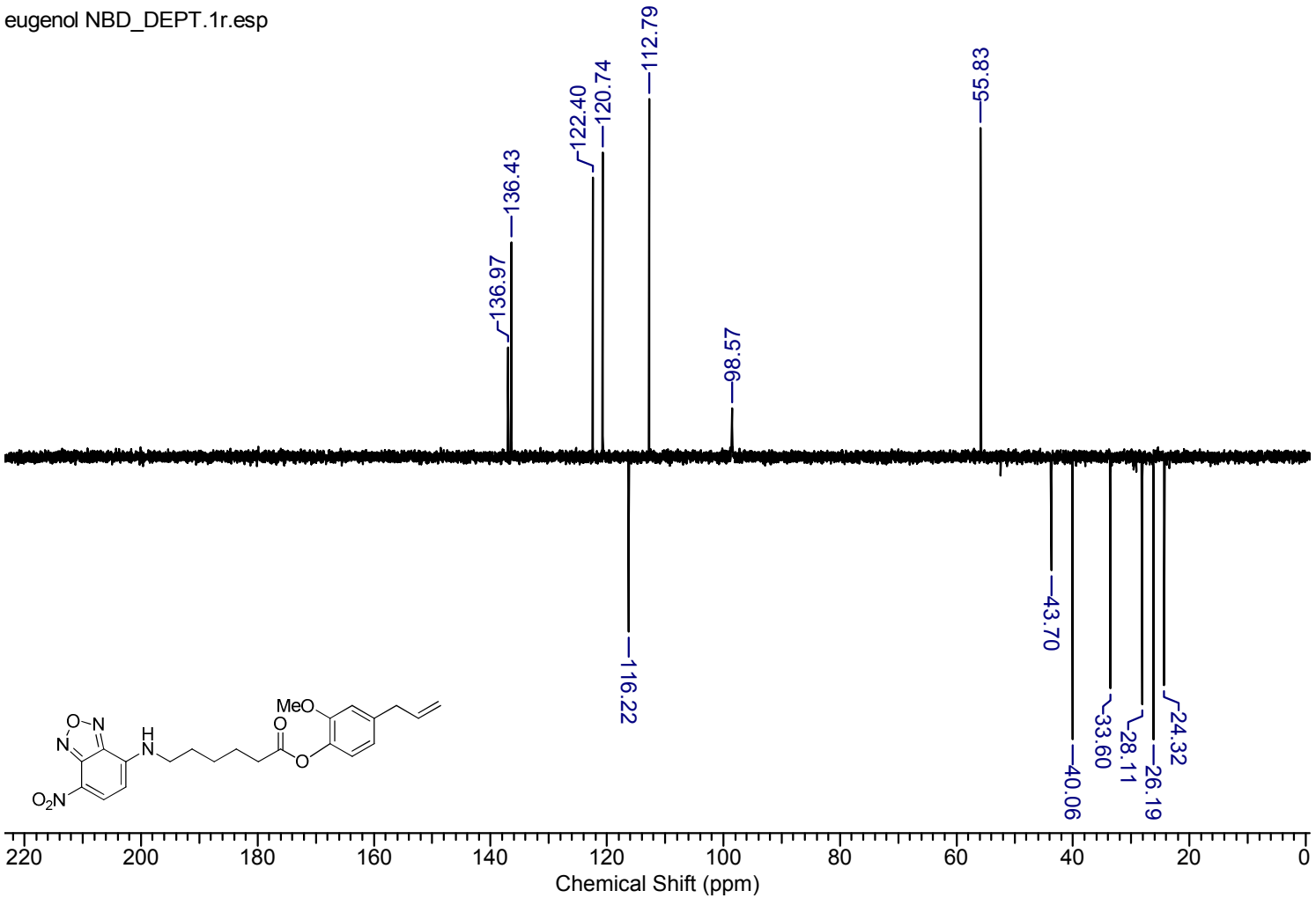

Fig. 12. DEPT-135 NMR of **2a** in $CDCl_3$ at 100 MHz.

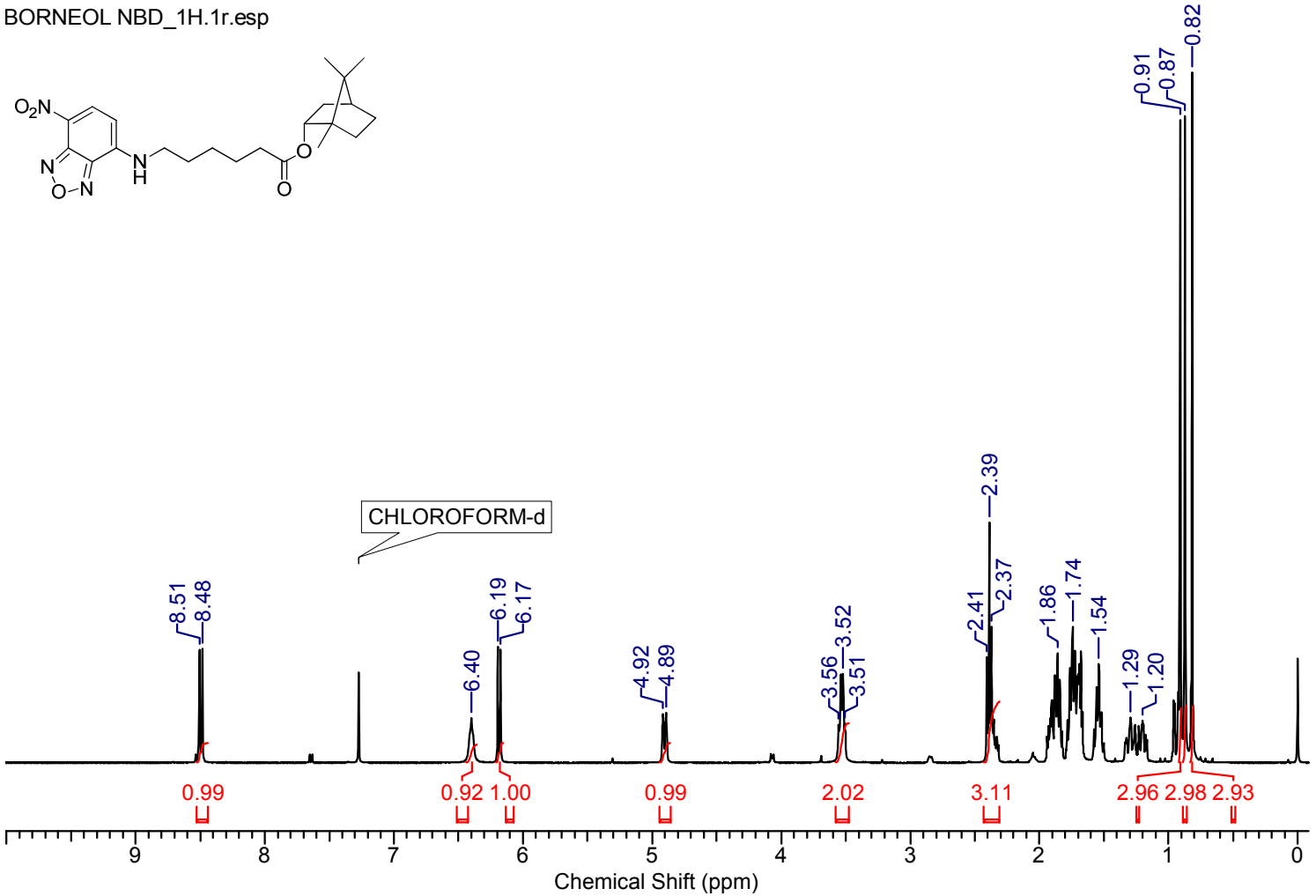

Fig. 13. ^{1}H NMR of **3a** in $CDCl_3$ at 400 MHz.

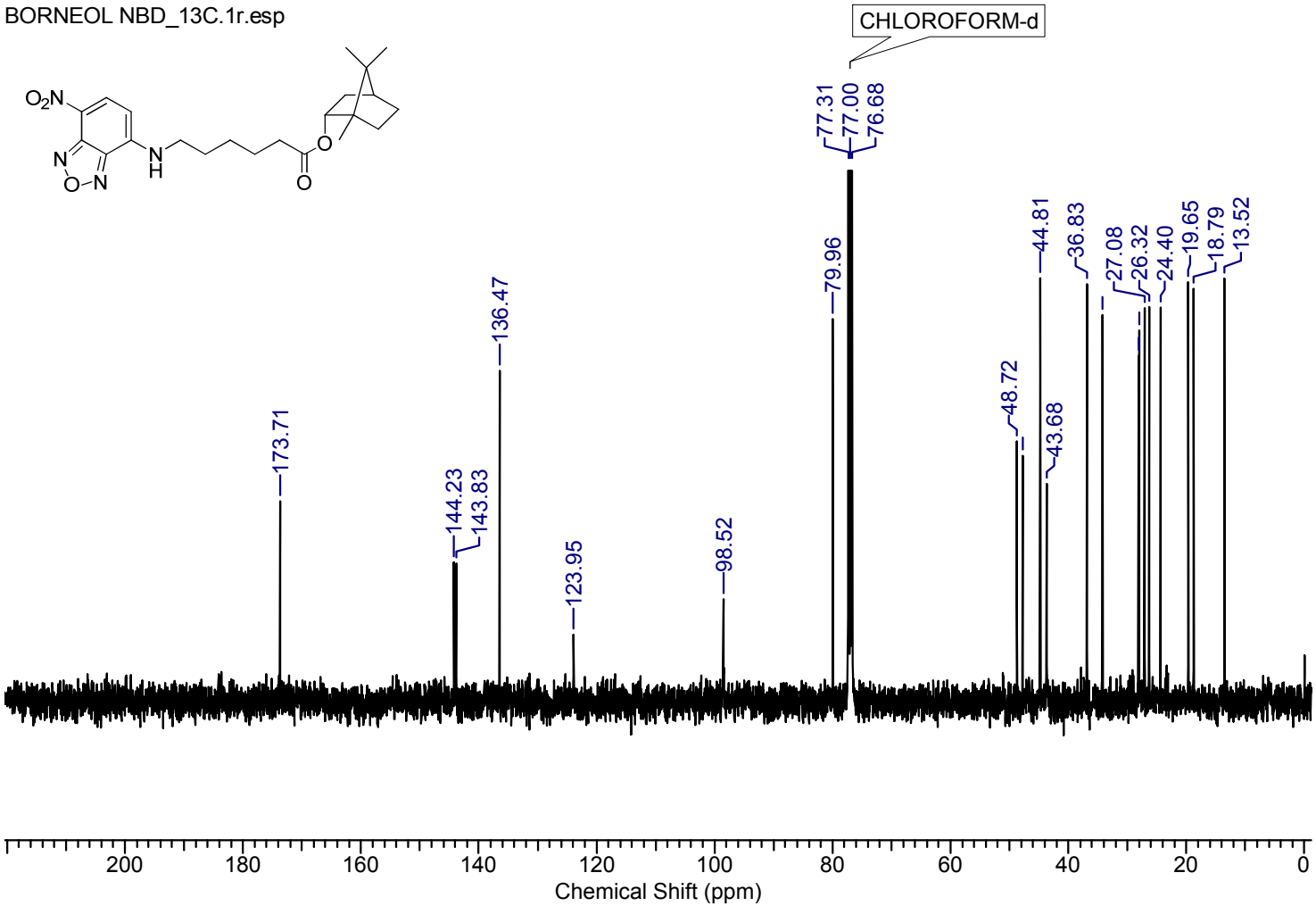

Fig. 14. ^{13}C NMR of **3a** in $CDCl_3$ at 100 MHz.

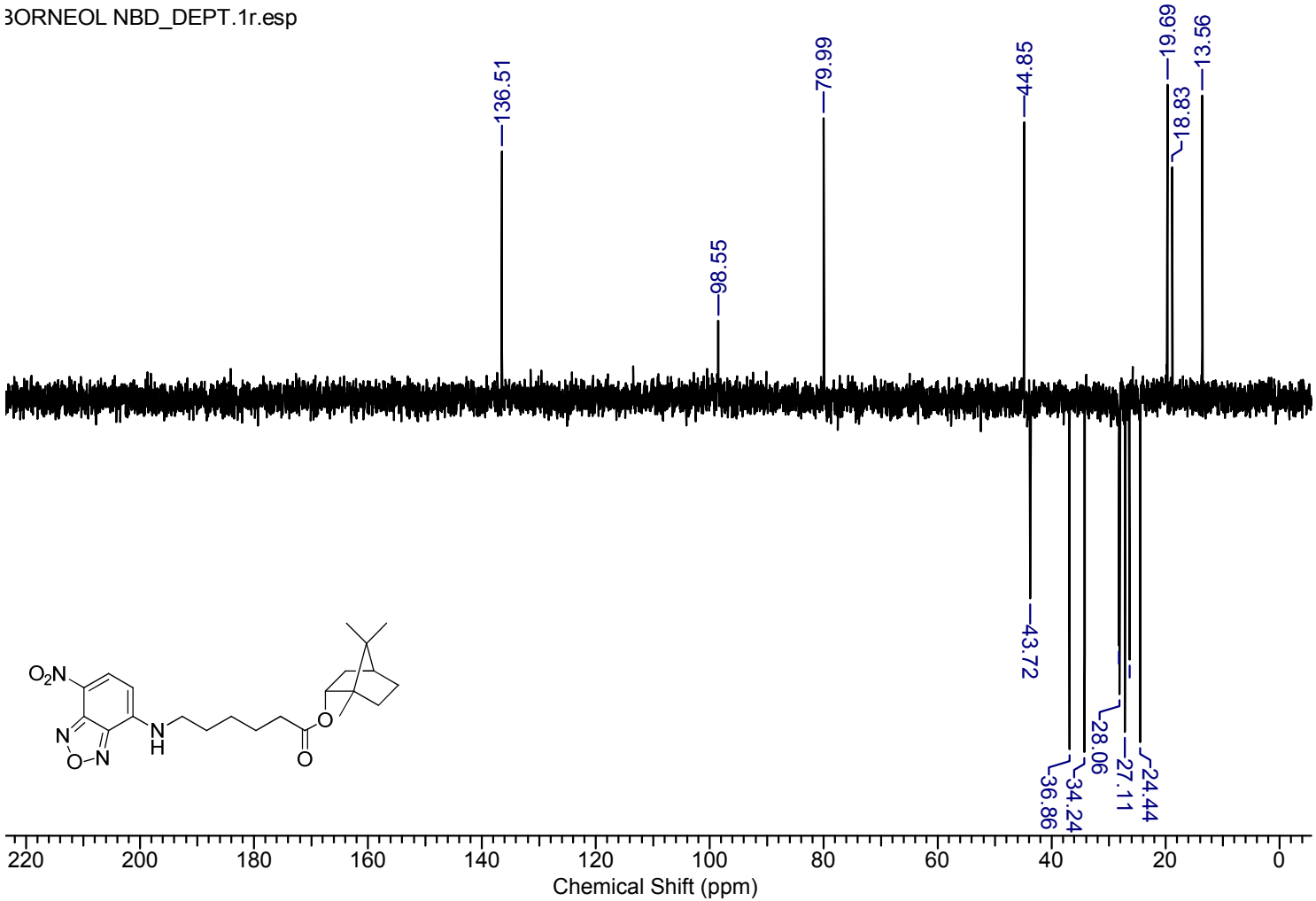

Fig. 15. DEPT-135 NMR of **3a** in $CDCl_3$ at 100 MHz.

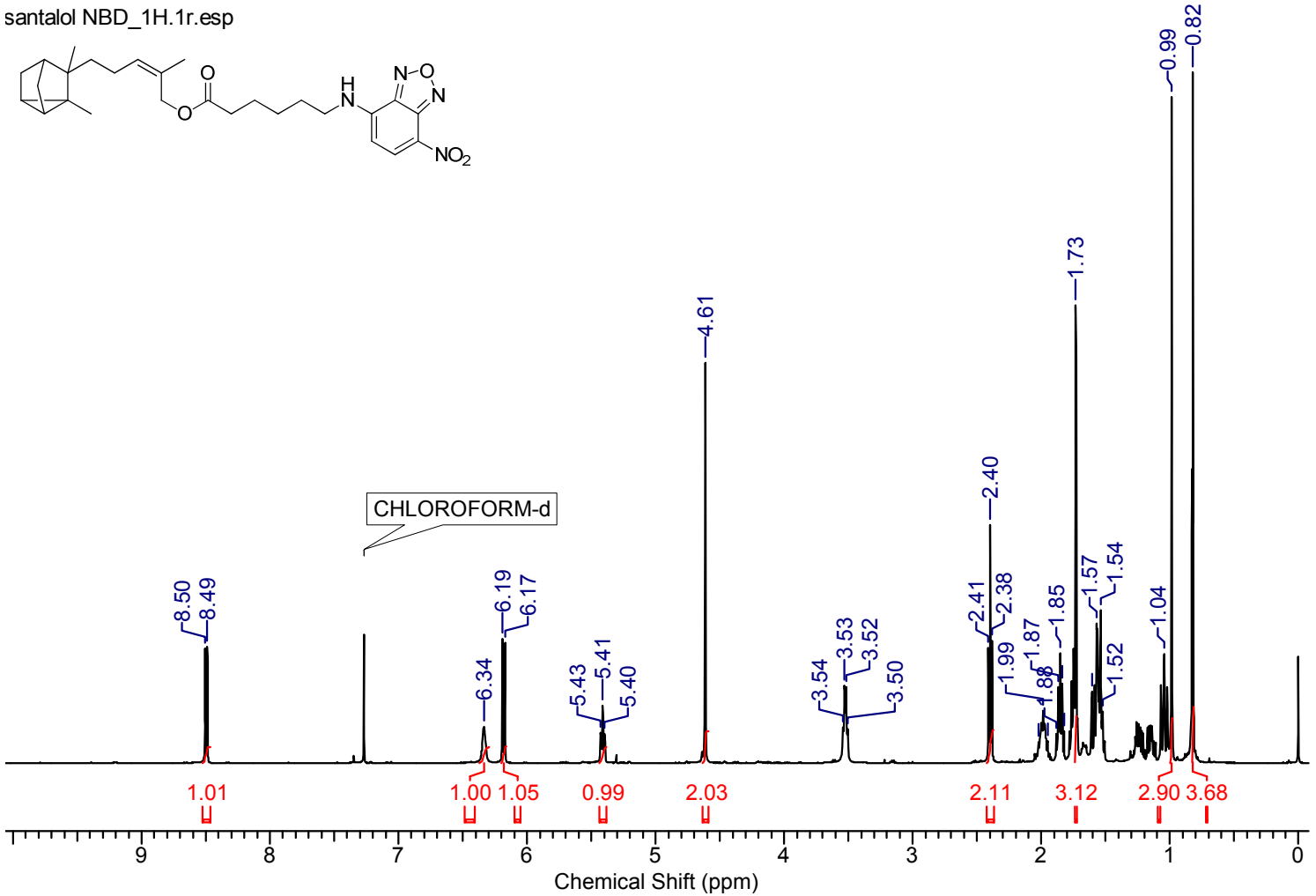

Fig. 16. ^{1}H NMR of **4a** in $CDCl_3$ at 400 MHz.

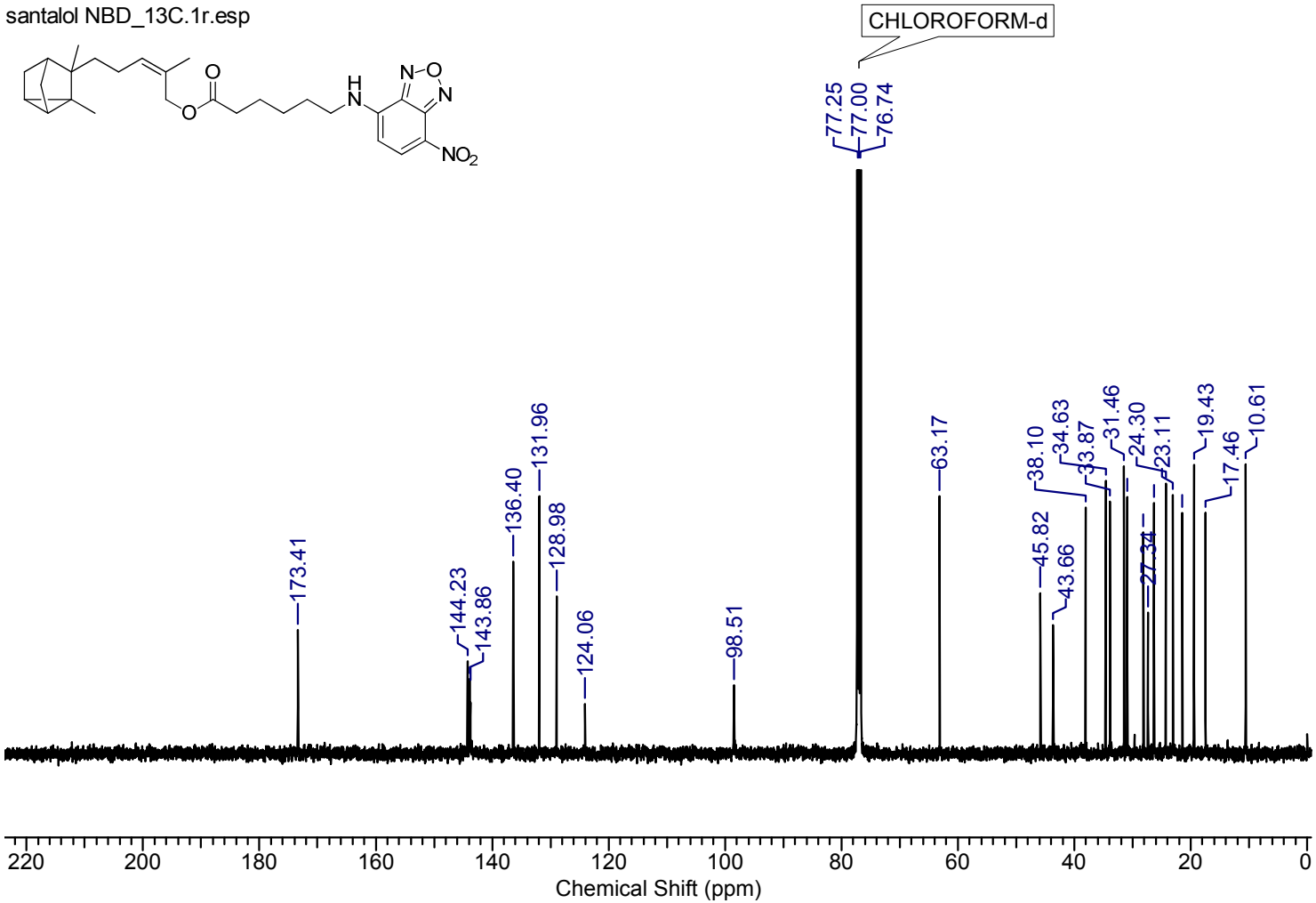

Fig. 17. ^{13}C NMR of **4a** in $CDCl_3$ at 100 MHz.

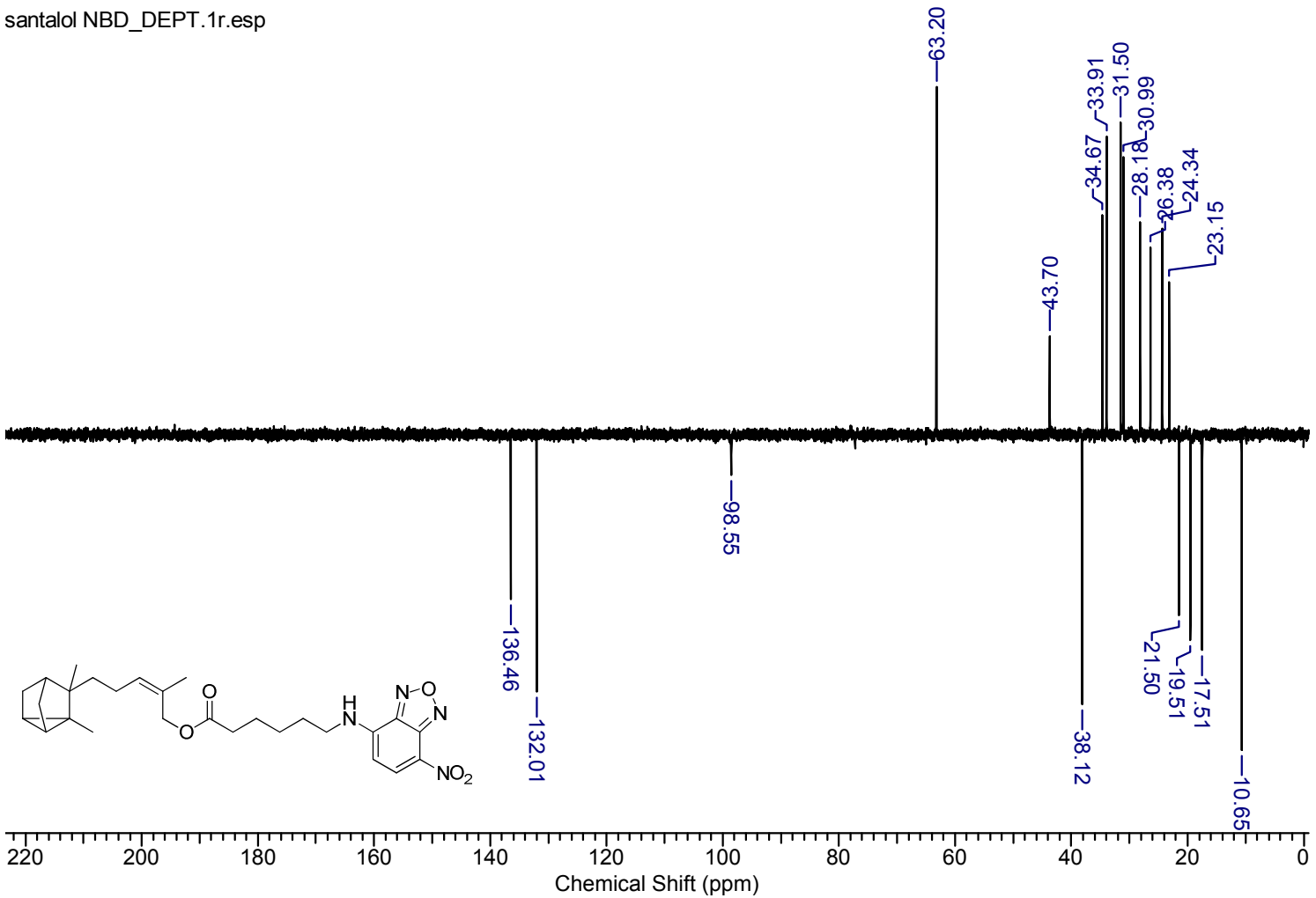

Fig. 18. DEPT-135 NMR of **4a** in $CDCl_3$ at 100 MHz.

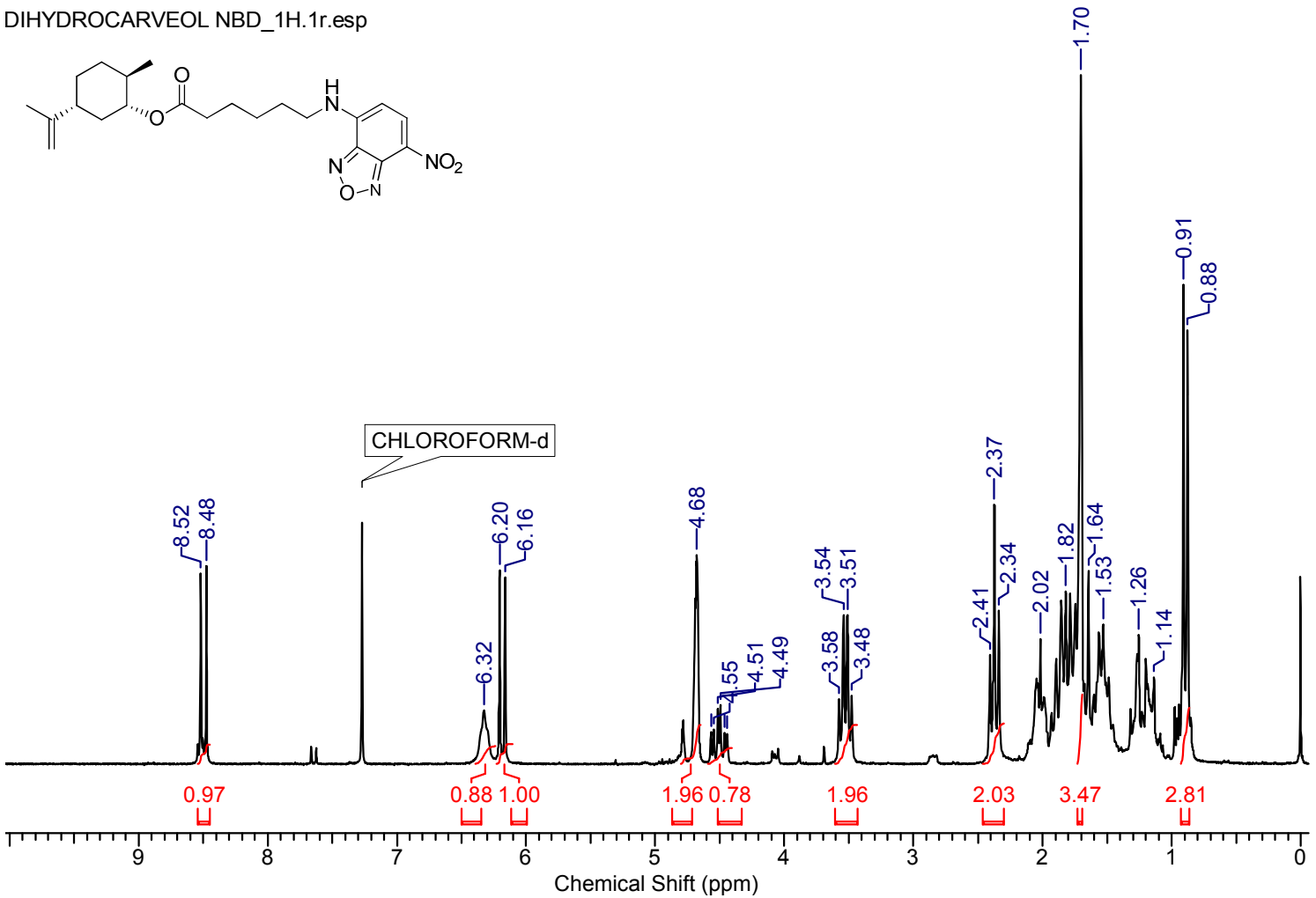

Fig. 19. ^{1}H NMR of **5a** in $CDCl_3$ at 400 MHz.

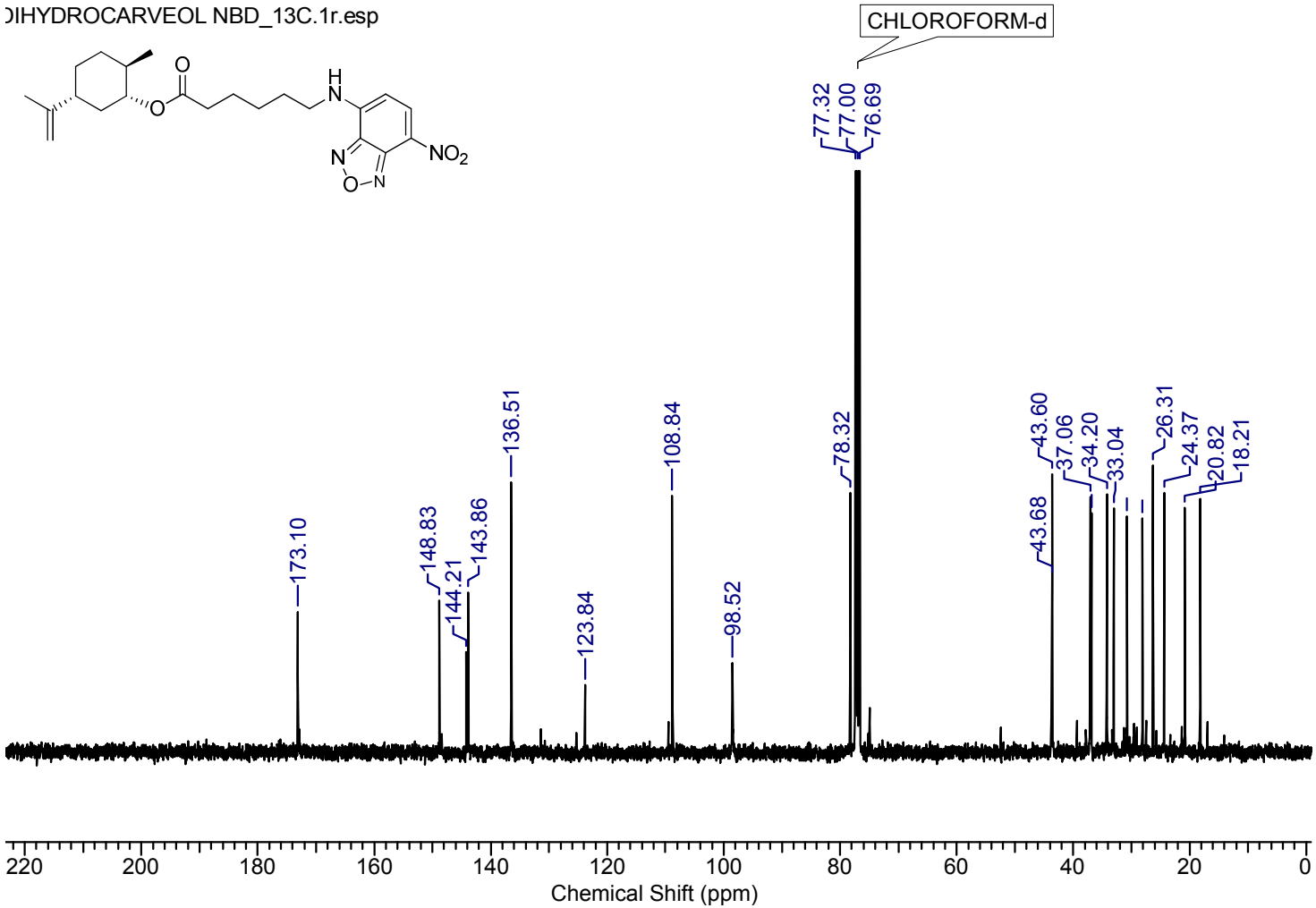

Fig. 20. ^{13}C NMR of **5a** in $CDCl_3$ at 100 MHz.

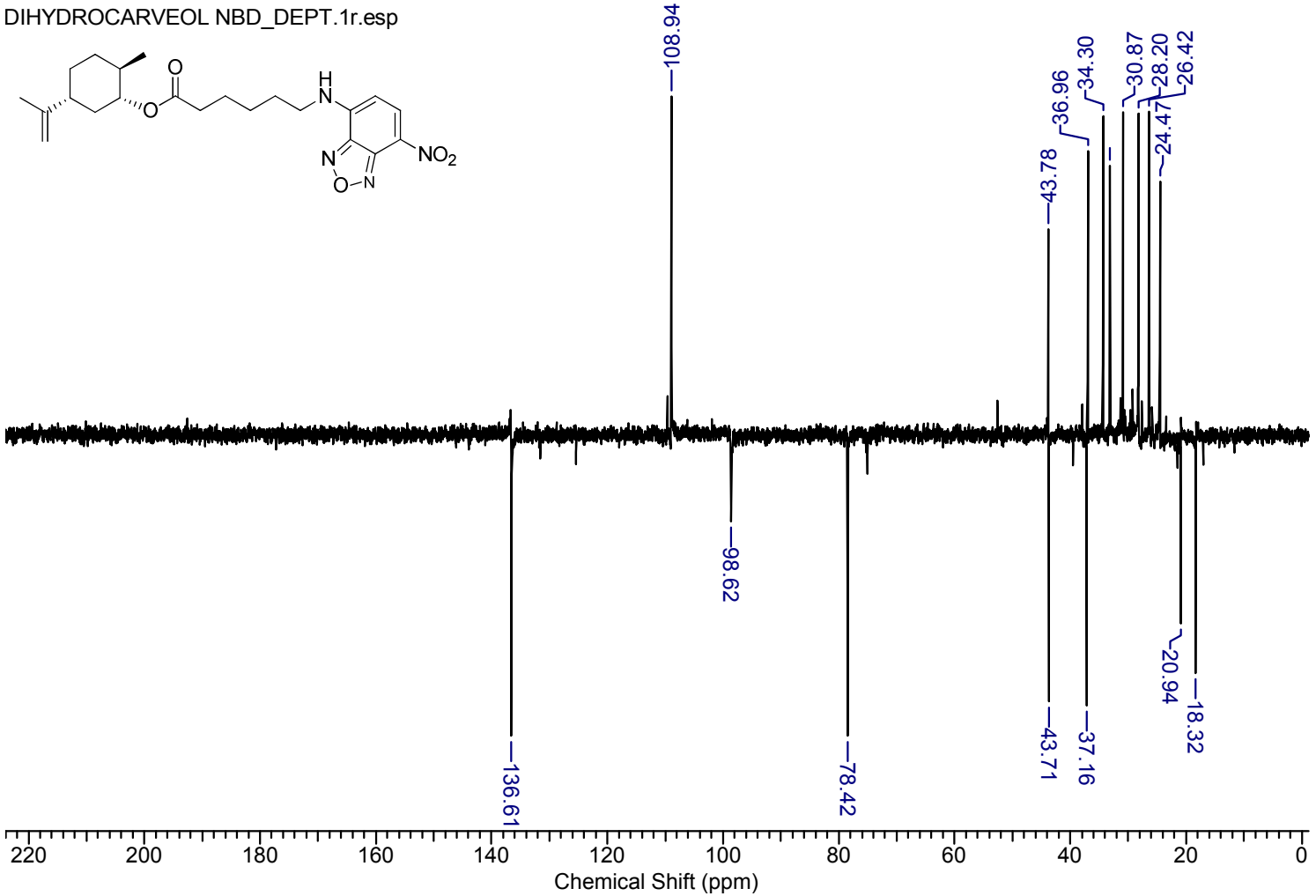

Fig. 21. DEPT-135 NMR of **5a** in $CDCl_3$ at 100 MHz.

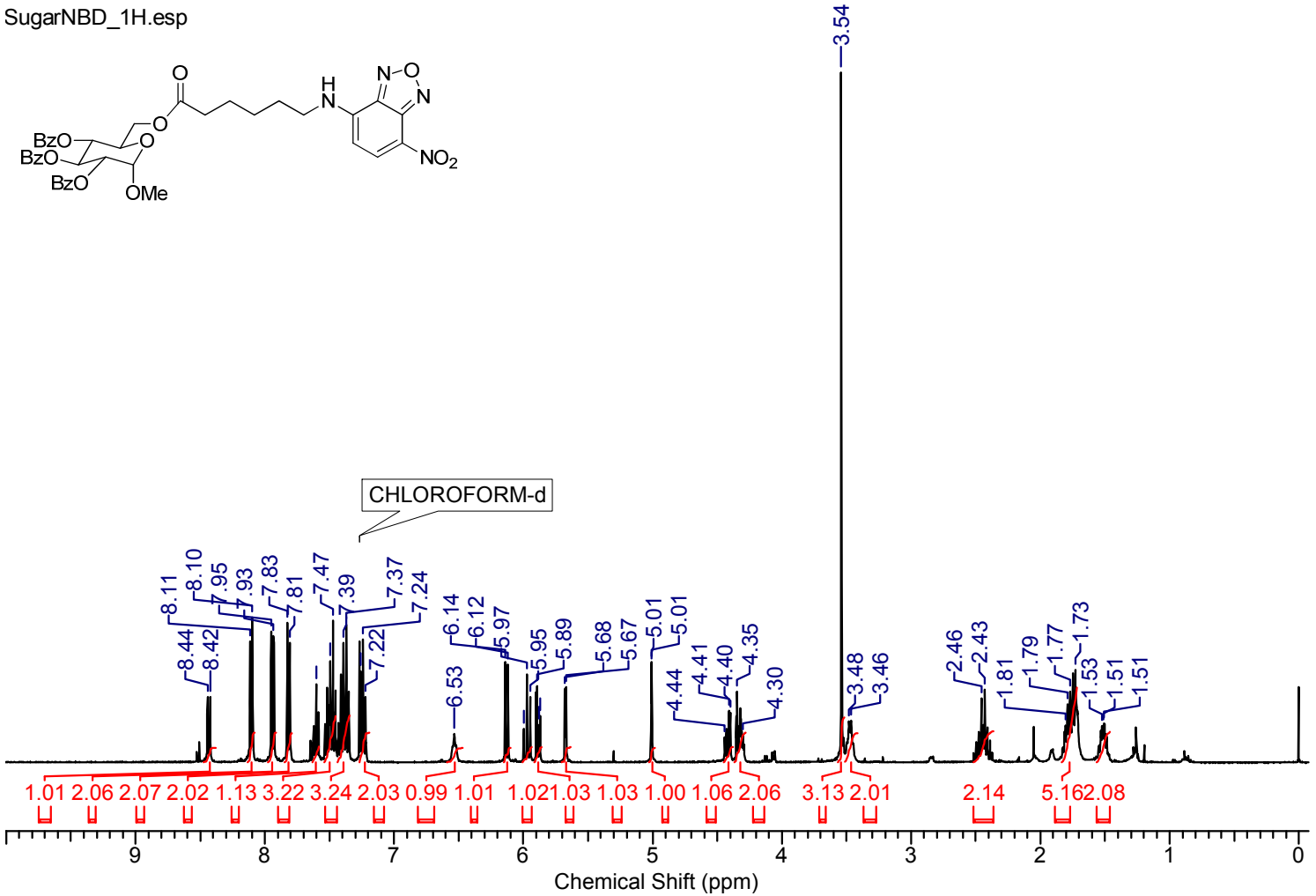

Fig. 22. ^{1}H NMR of **6a** in $CDCl_3$ at 400 MHz.

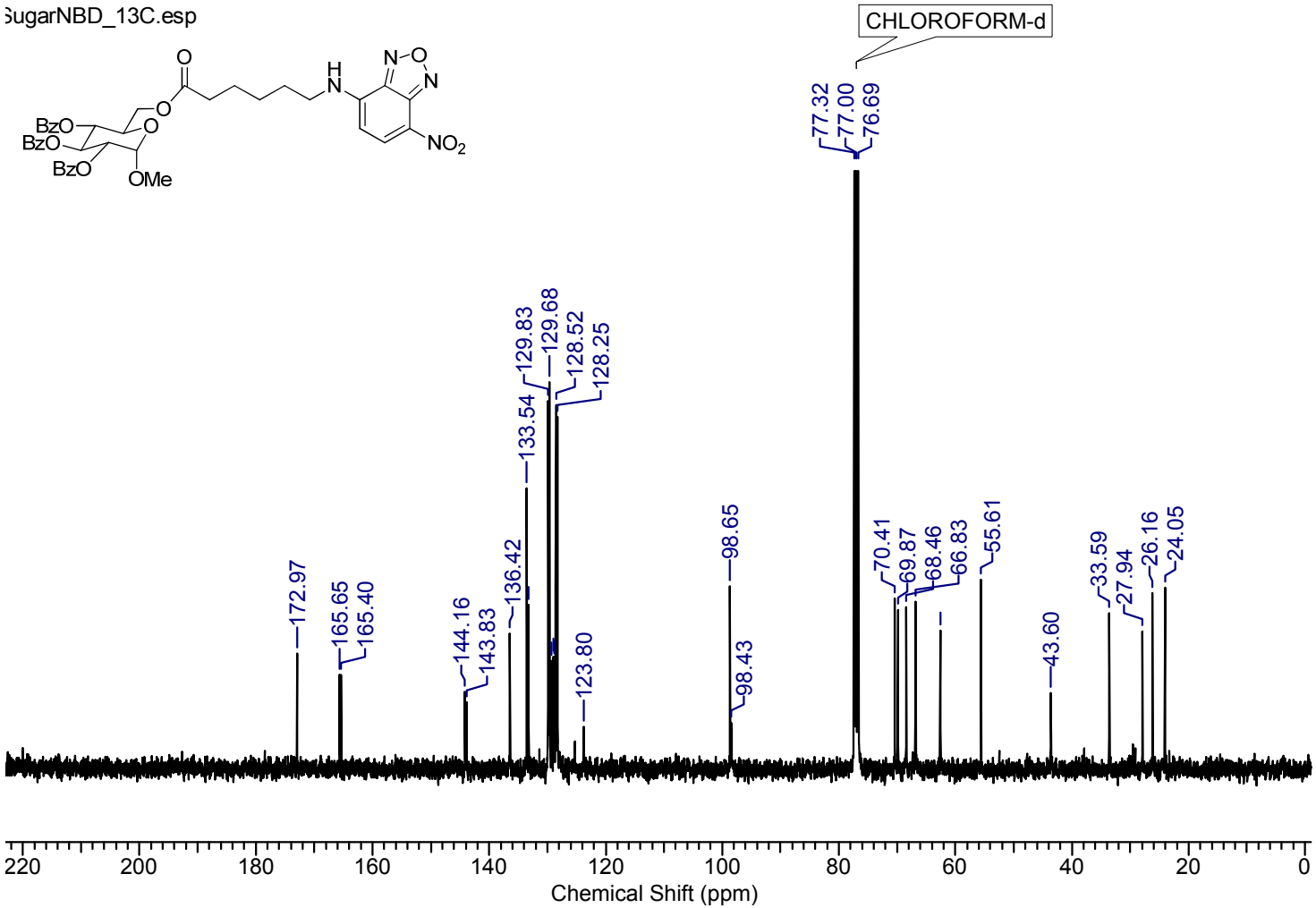

Fig. 23. ^{13}C NMR of **6a** in $CDCl_3$ at 100 MHz.

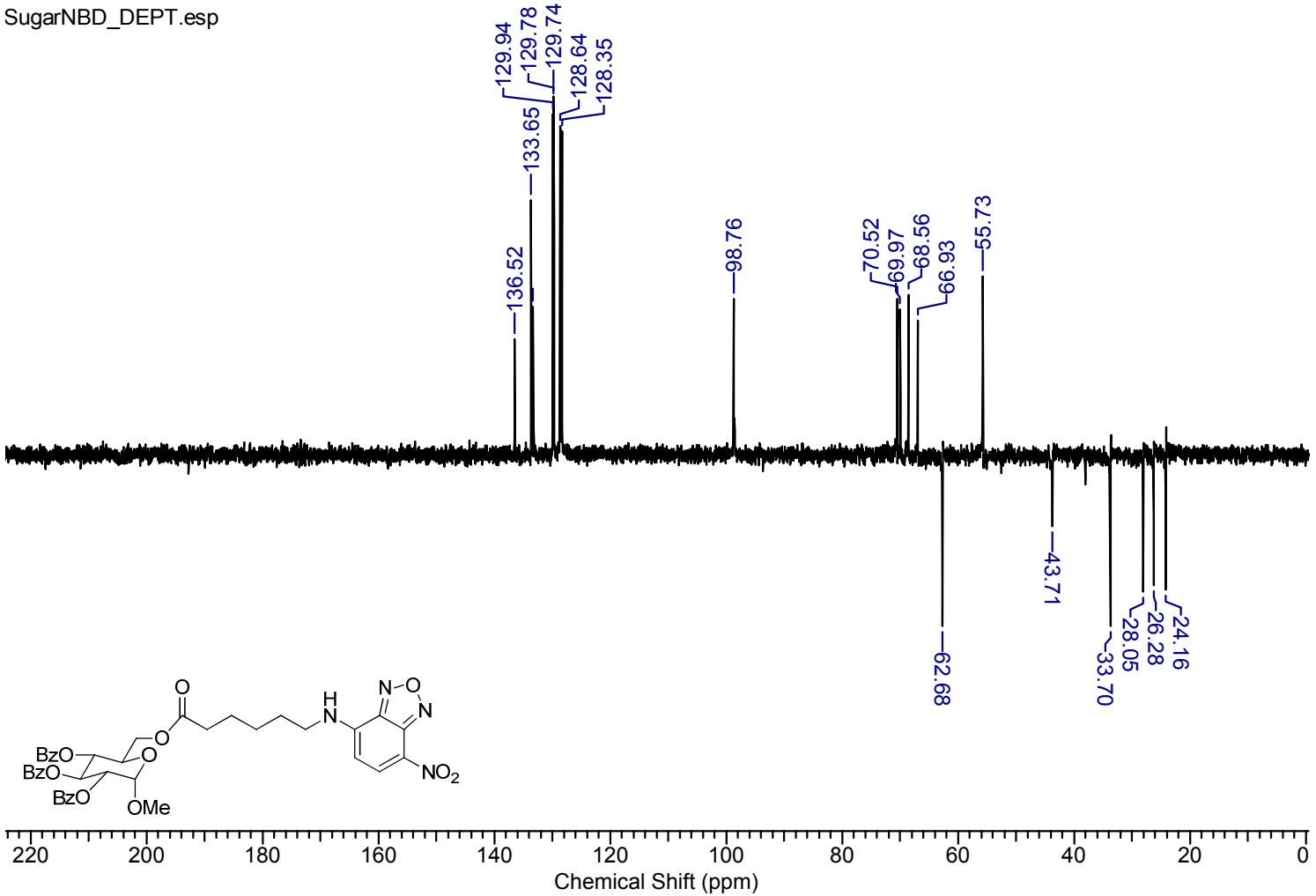

Fig. 24. DEPT-135 NMR of **6a** in $CDCl_3$ at 100 MHz.

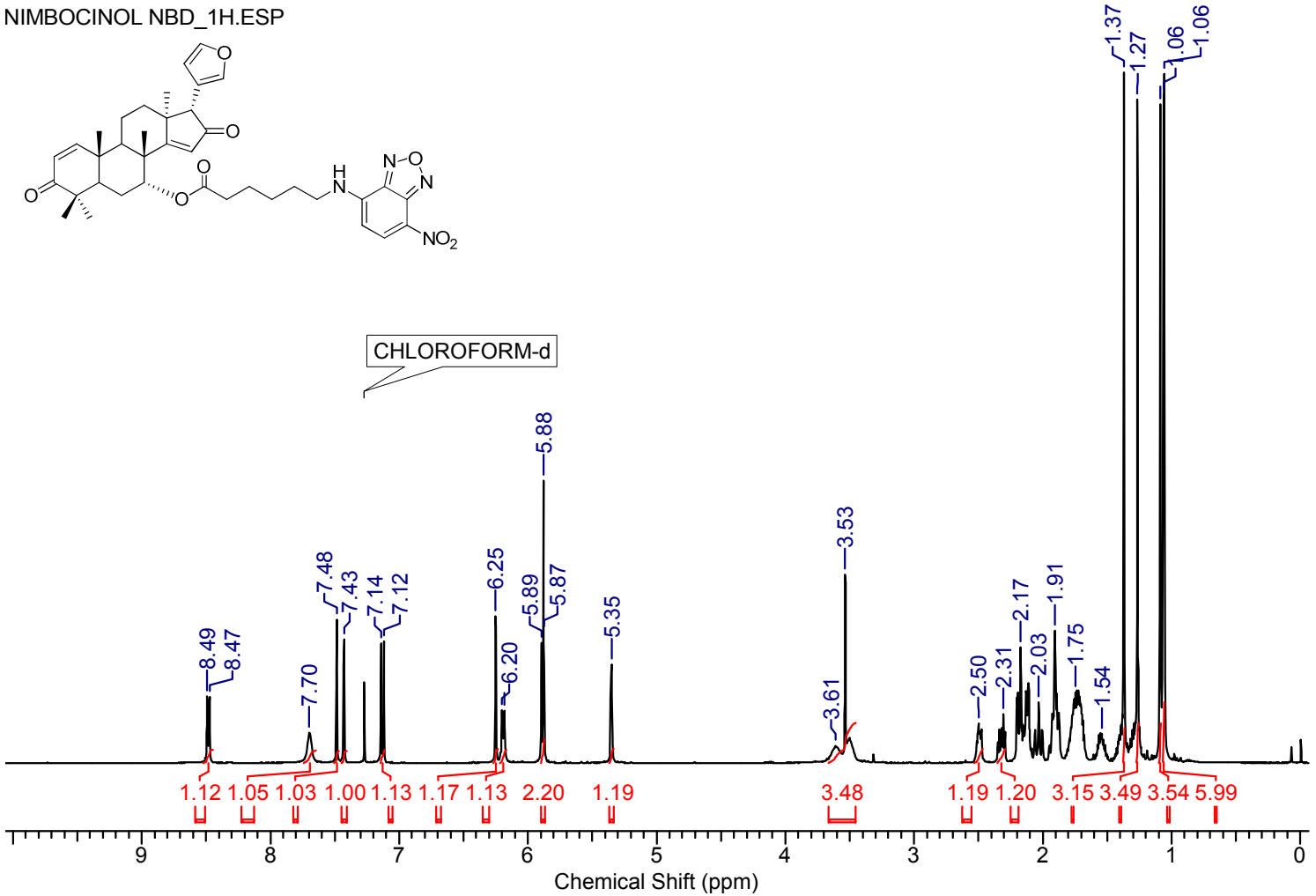

Fig. 25. ^{1}H NMR of **8a** in $CDCl_3$ at 400 MHz.

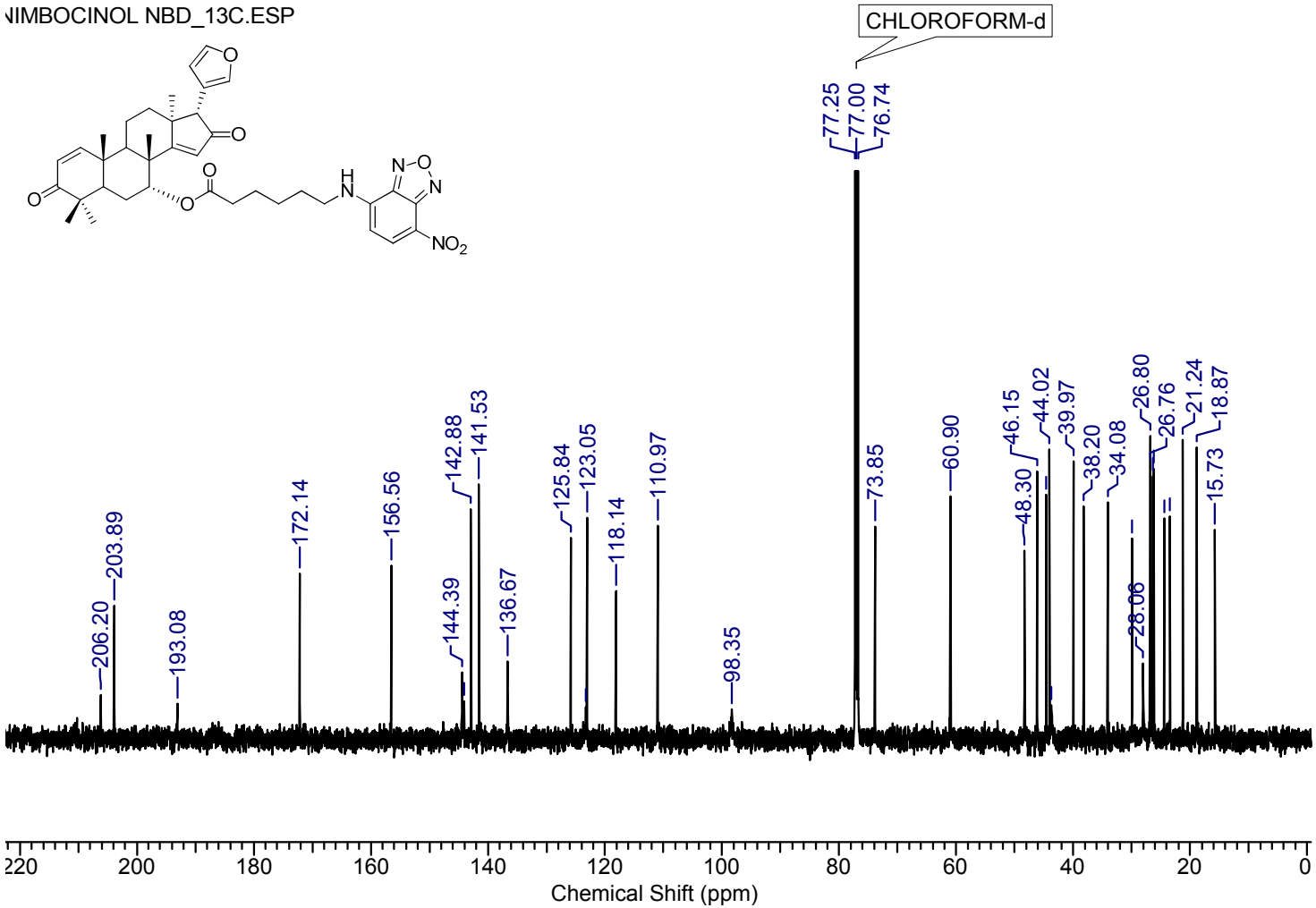

Fig. 26. ^{13}C NMR of **8a** in $CDCl_3$ at 100 MHz.

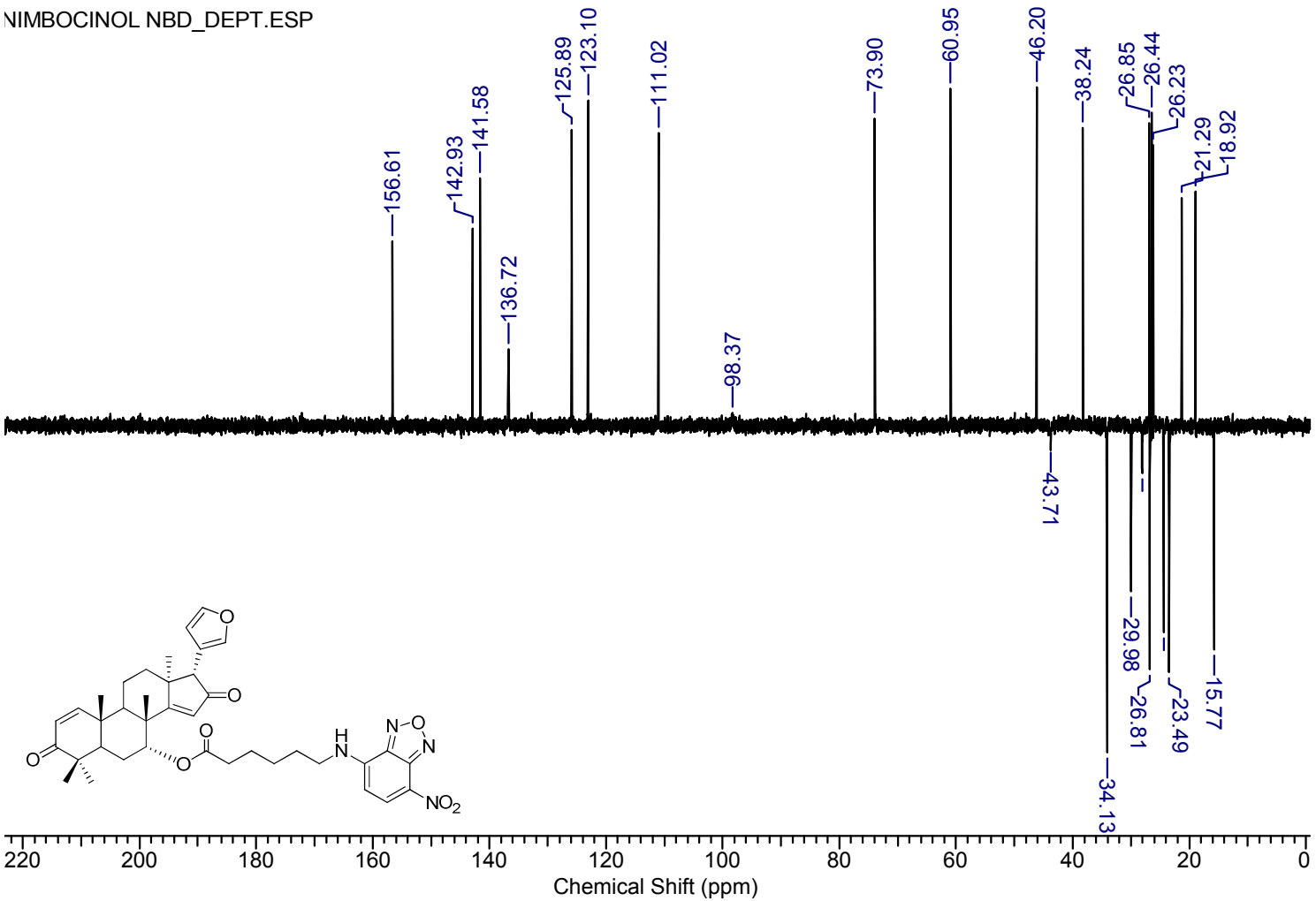

Fig. 27. DEPT-135 NMR of **8a** in $CDCl_3$ at 100 MHz.

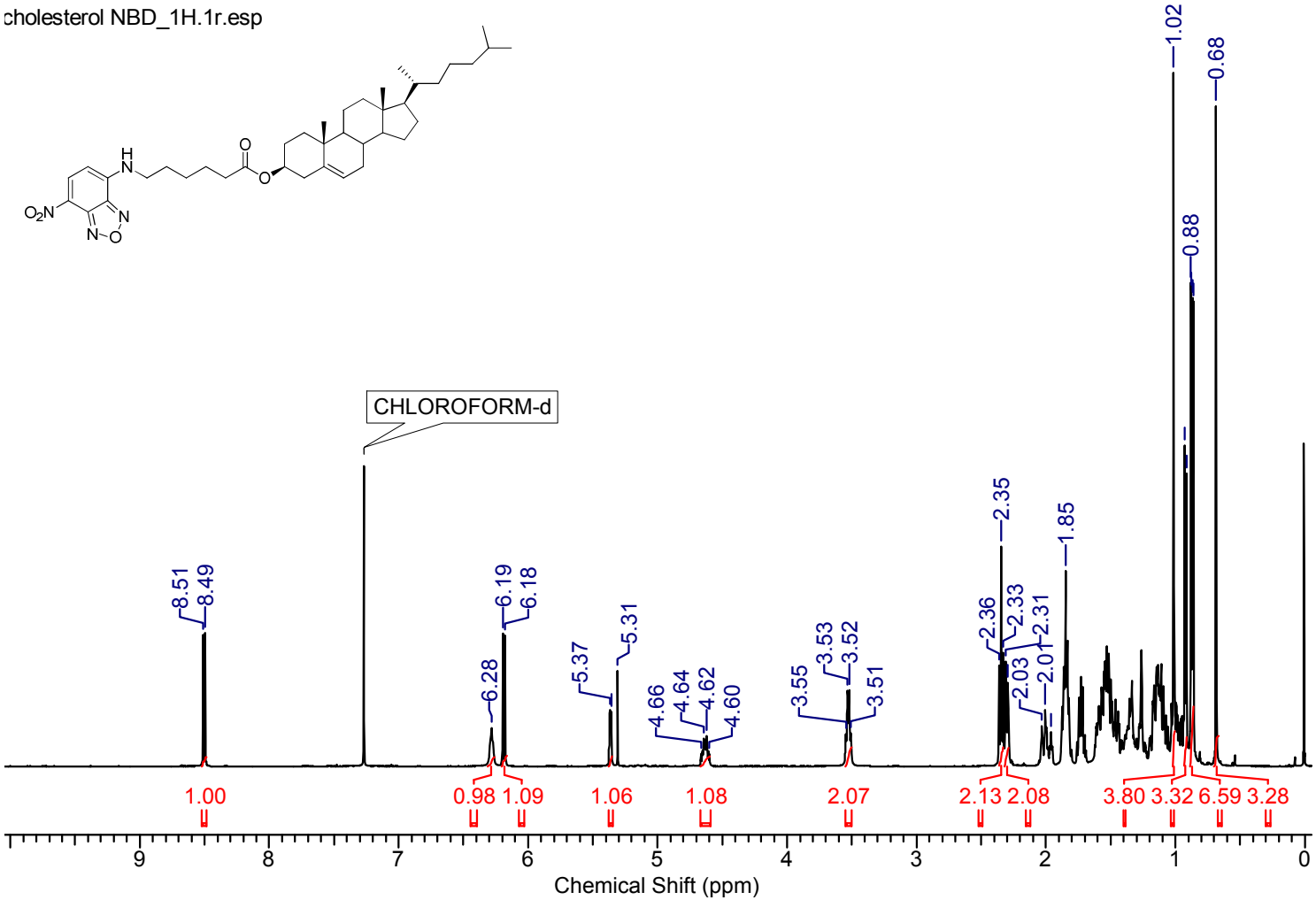

Fig. 28. ^{1}H NMR of **9a** in $CDCl_3$ at 400 MHz.

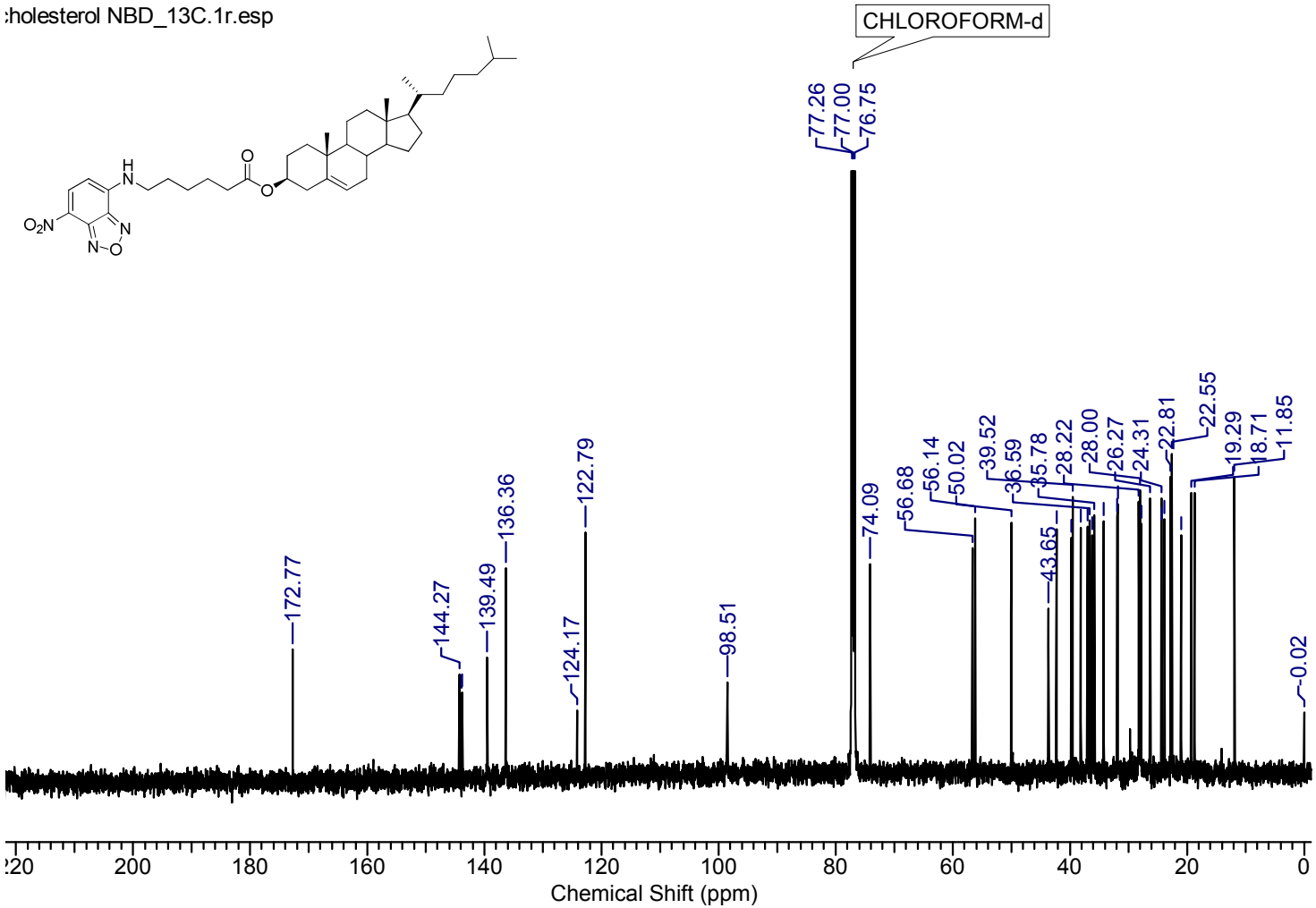

Fig. 29. ^{13}C NMR of **9a** in $CDCl_3$ at 100 MHz.

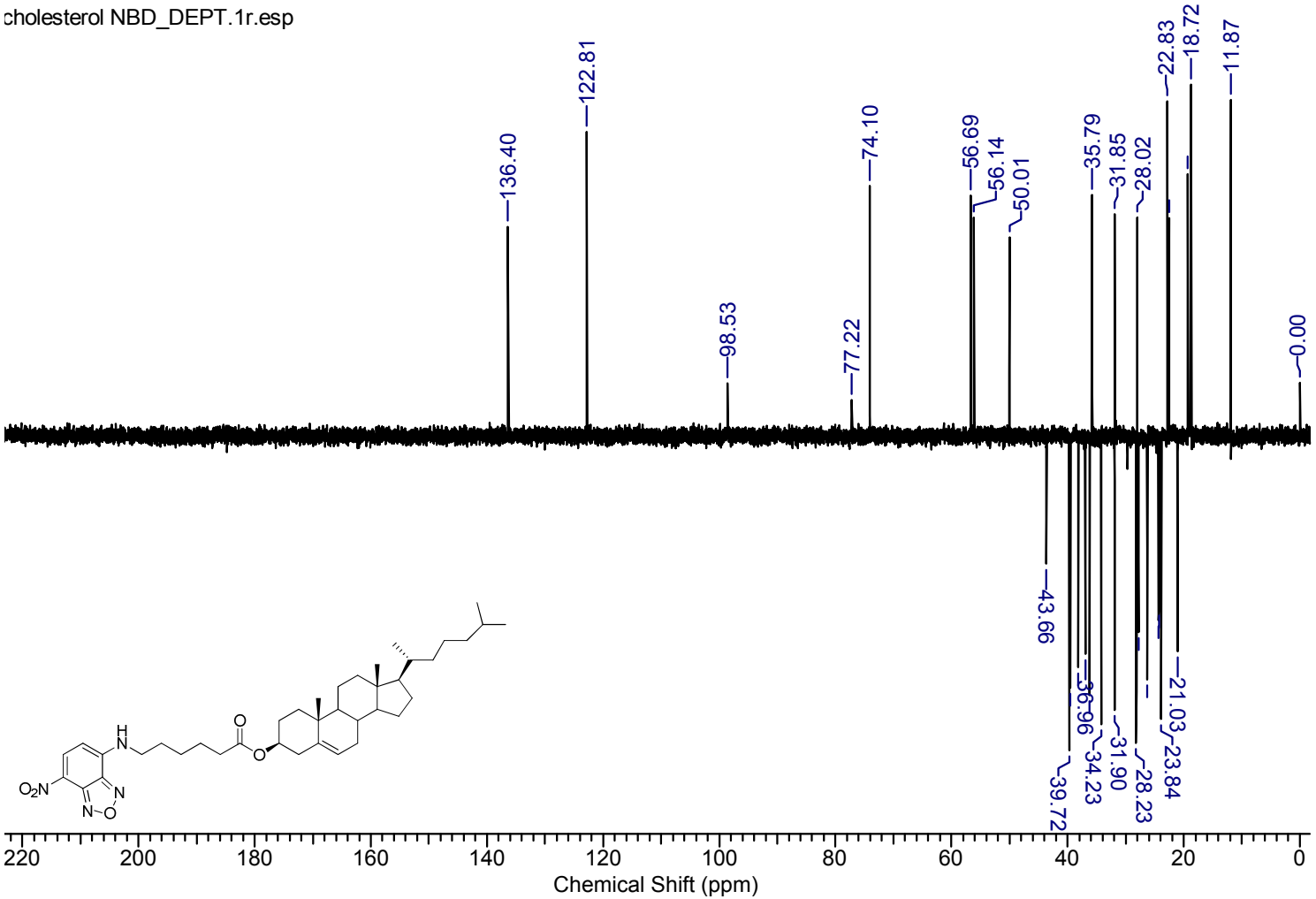

Fig. 30. DEPT-135 NMR of **9a** in $CDCl_3$ at 100 MHz.

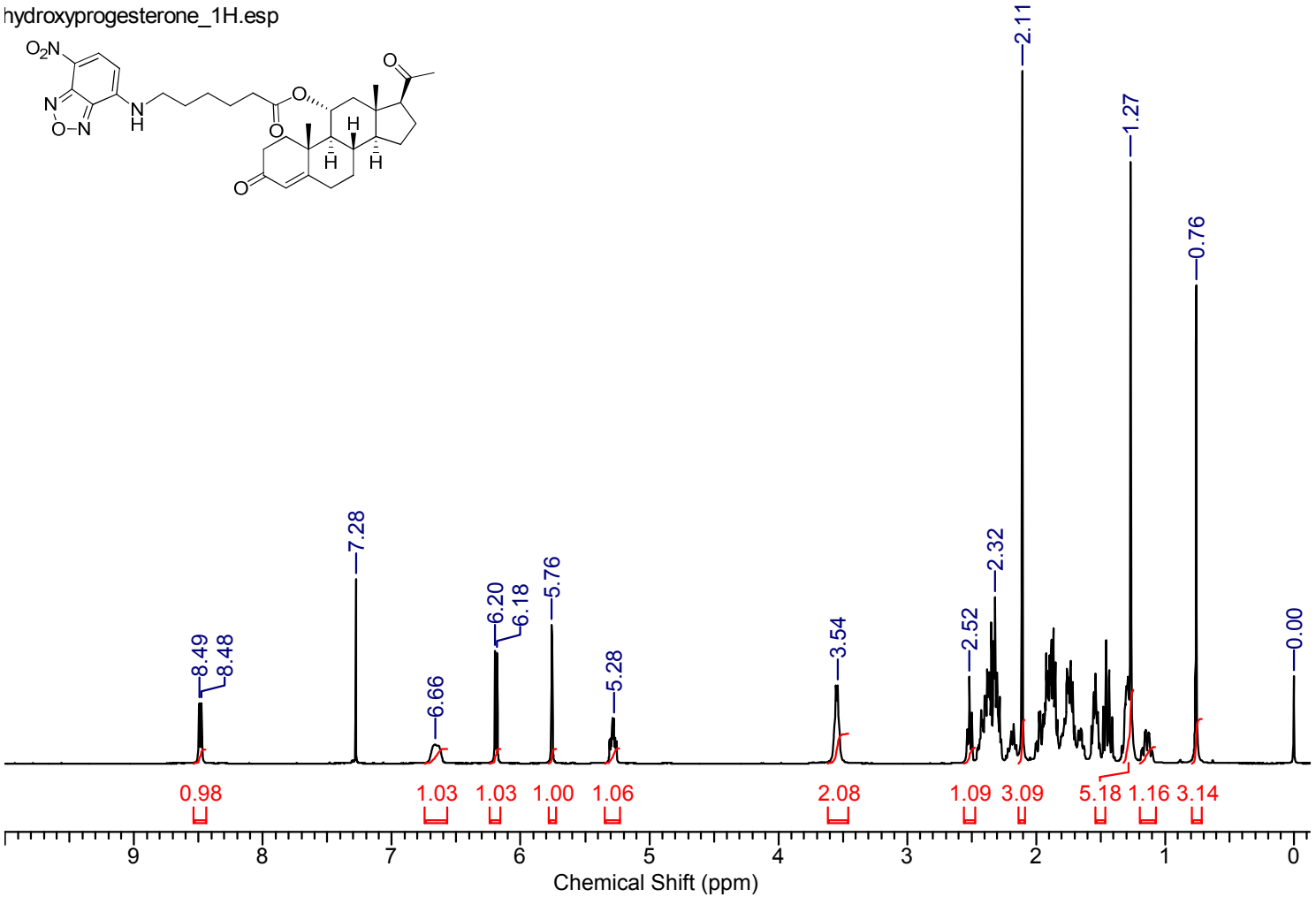

Fig. 31. ^{1}H NMR of **10a** in $CDCl_3$ at 400 MHz.

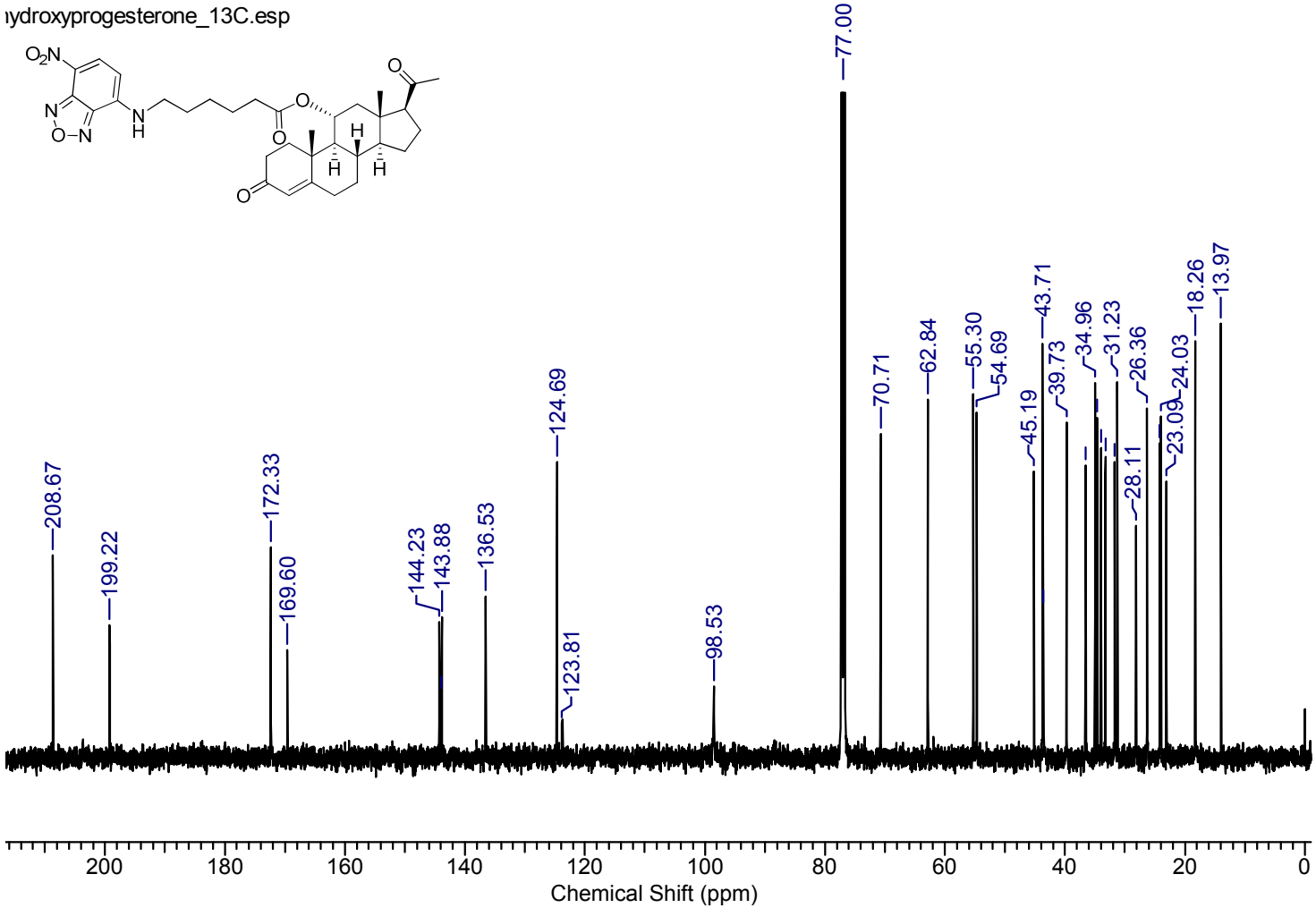

Fig. 32. ^{13}C NMR of **10a** in $CDCl_3$ at 100 MHz.

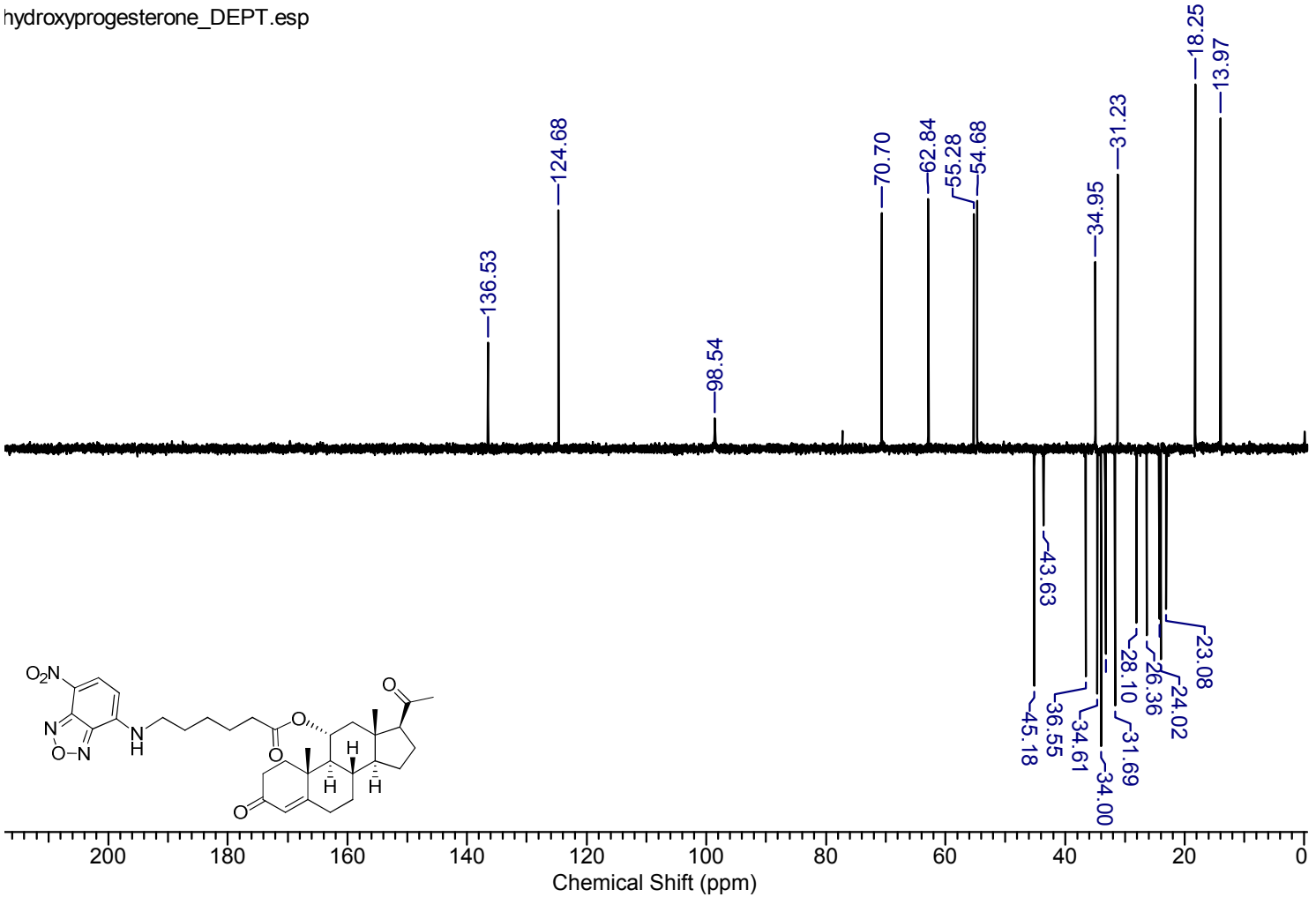

Fig. 33. DEPT-135 NMR of **10a** in $CDCl_3$ at 100 MHz.

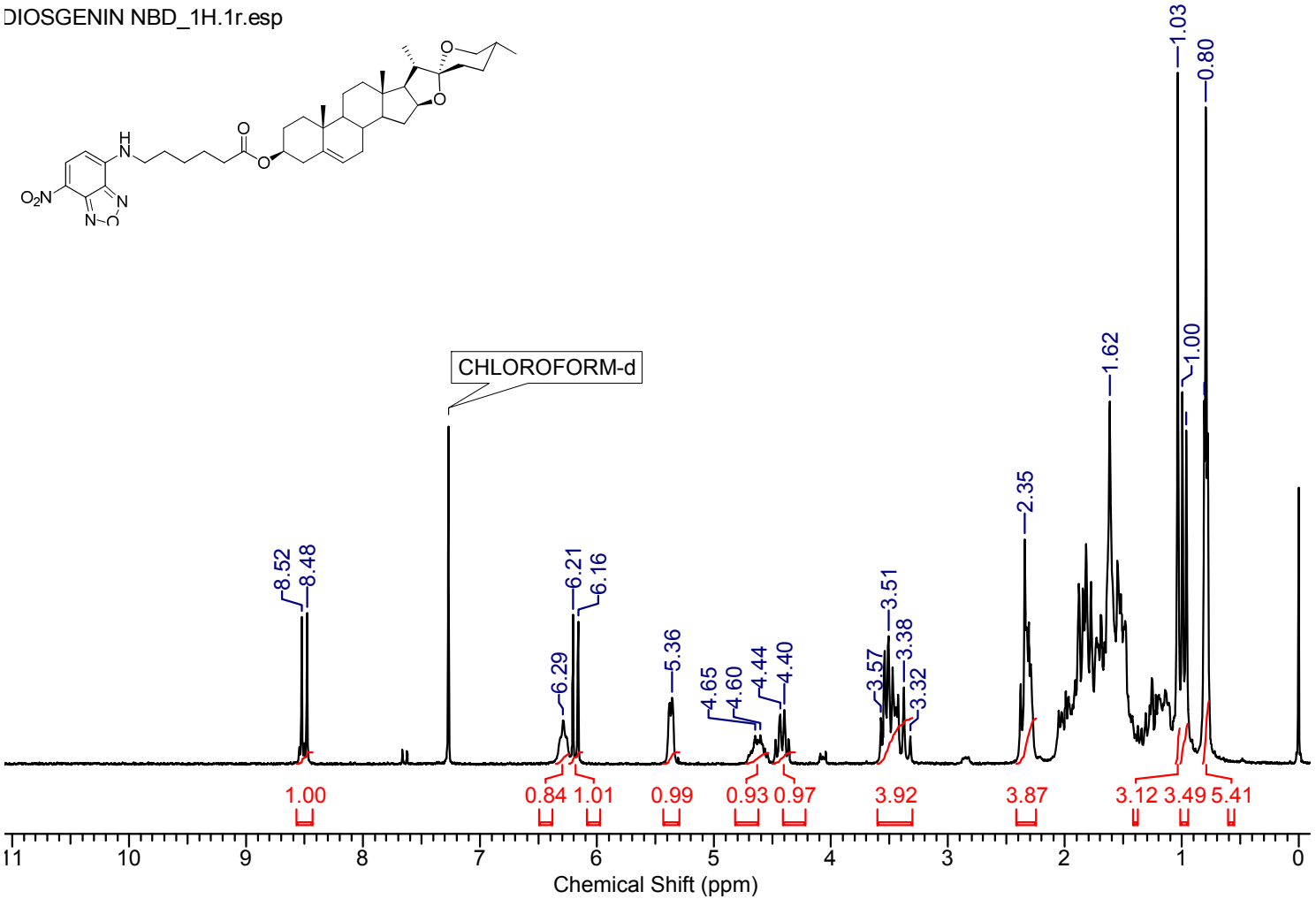

Fig. 34. ^{1}H NMR of **11a** in $CDCl_3$ at 400 MHz.

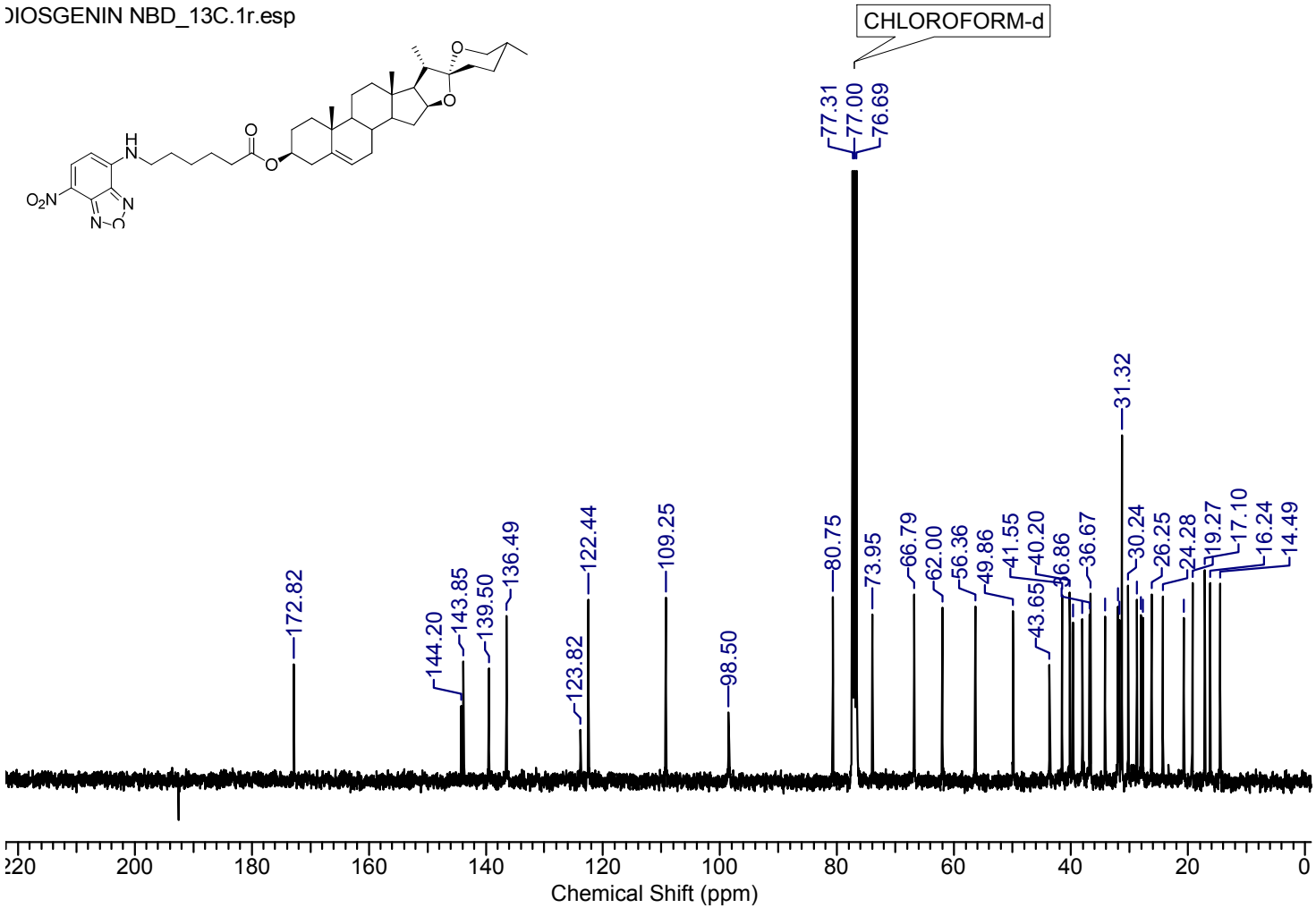

Fig. 35. ^{13}C NMR of **11a** in $CDCl_3$ at 100 MHz.

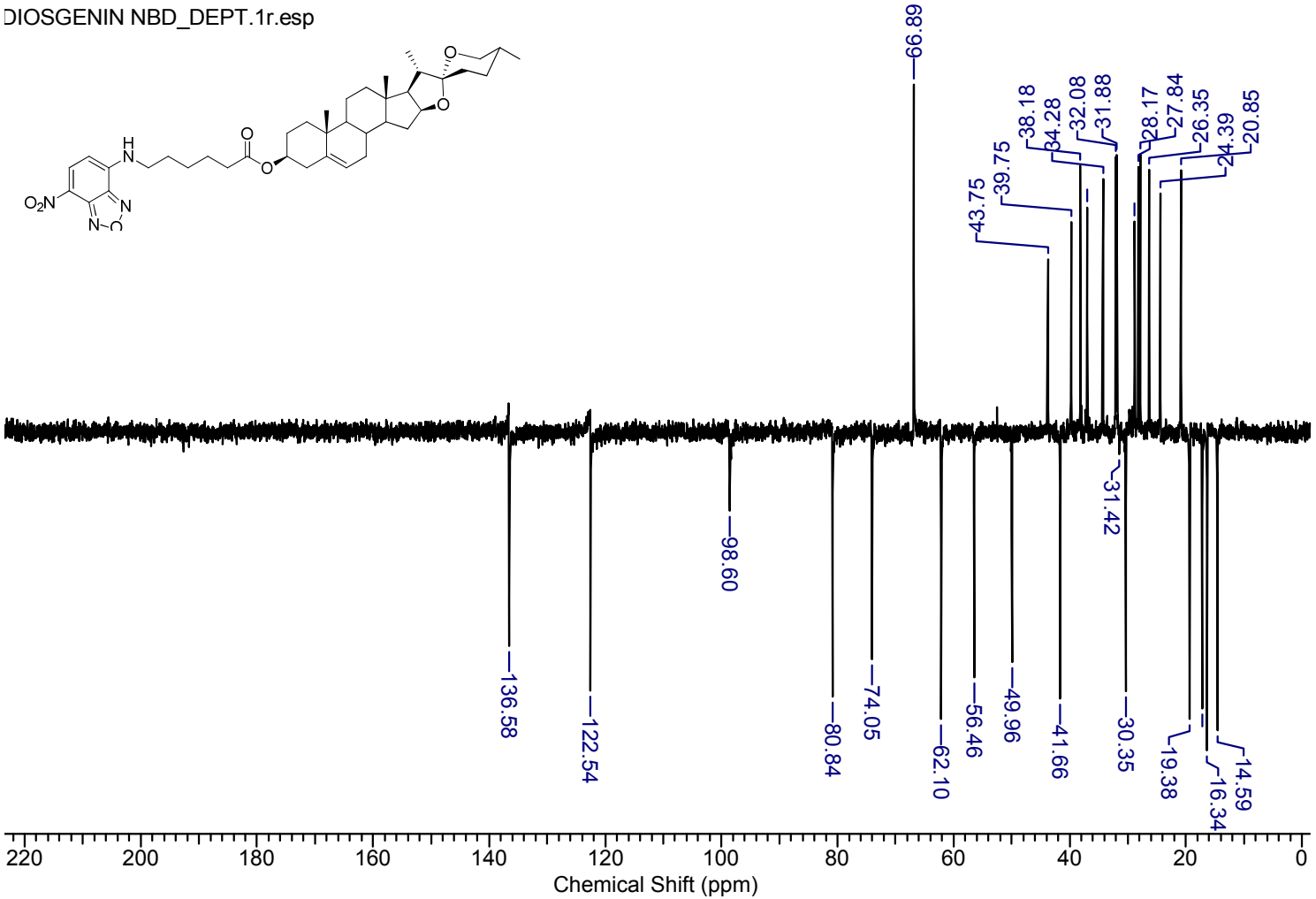

Fig. 36. DEPT-135 NMR of **11a** in $CDCl_3$ at 100 MHz.

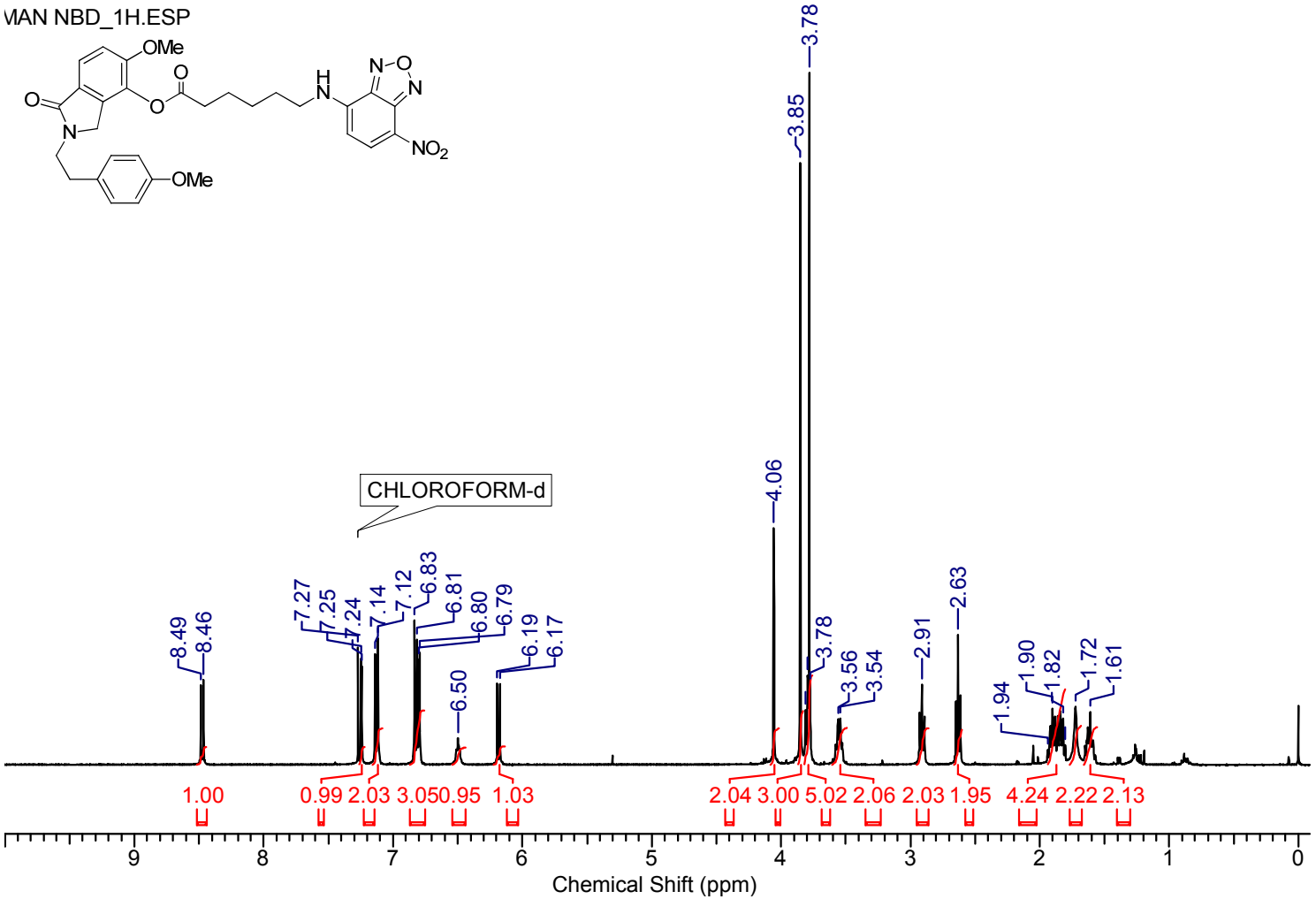

Fig. 37. ^{1}H NMR of **12a** in $CDCl_3$ at 400 MHz.

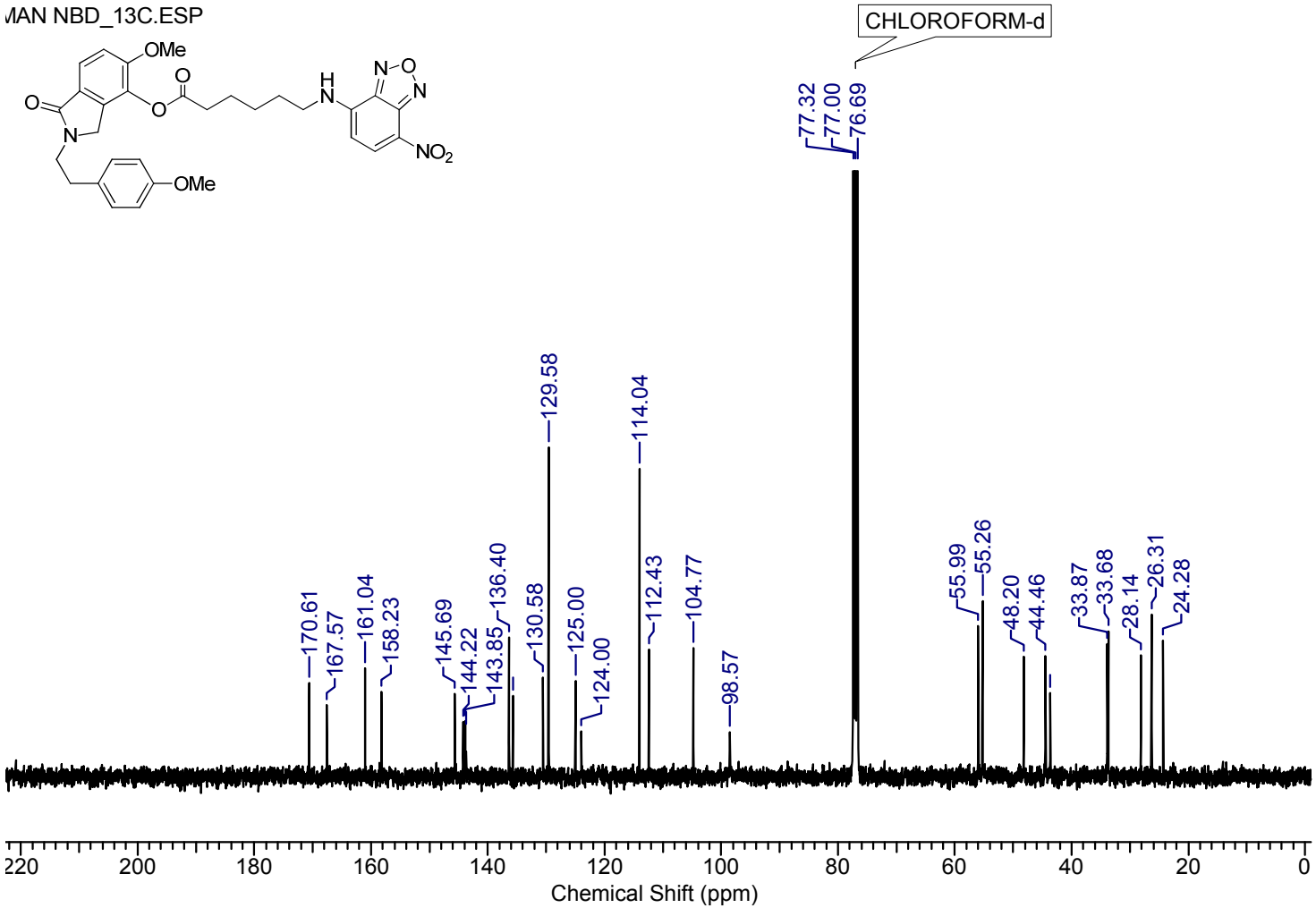

Fig. 38. ^{13}C NMR of **12a** in $CDCl_3$ at 100 MHz.

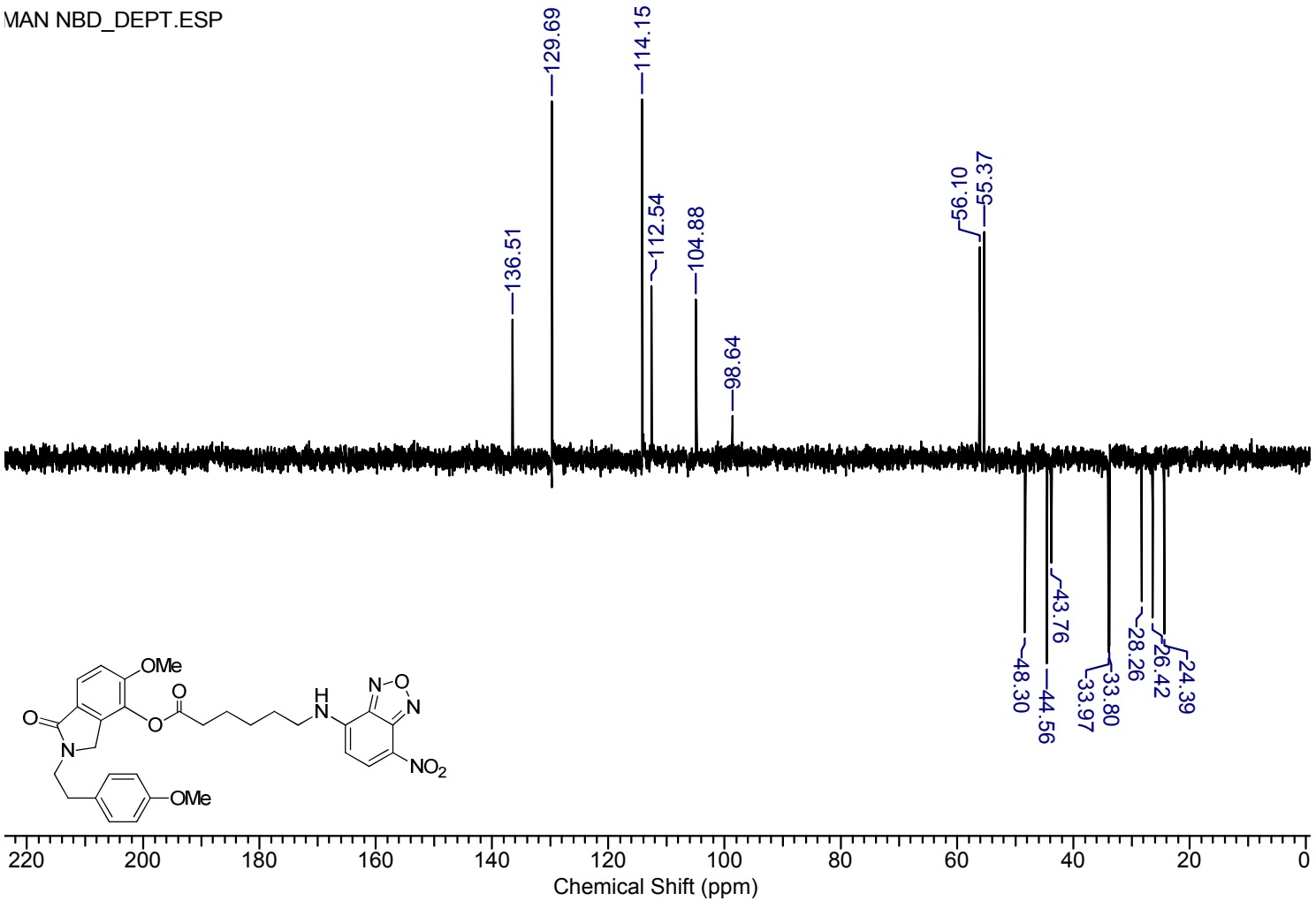

Fig. 39. DEPT-135 NMR of **12a** in $CDCl_3$ at 100 MHz.

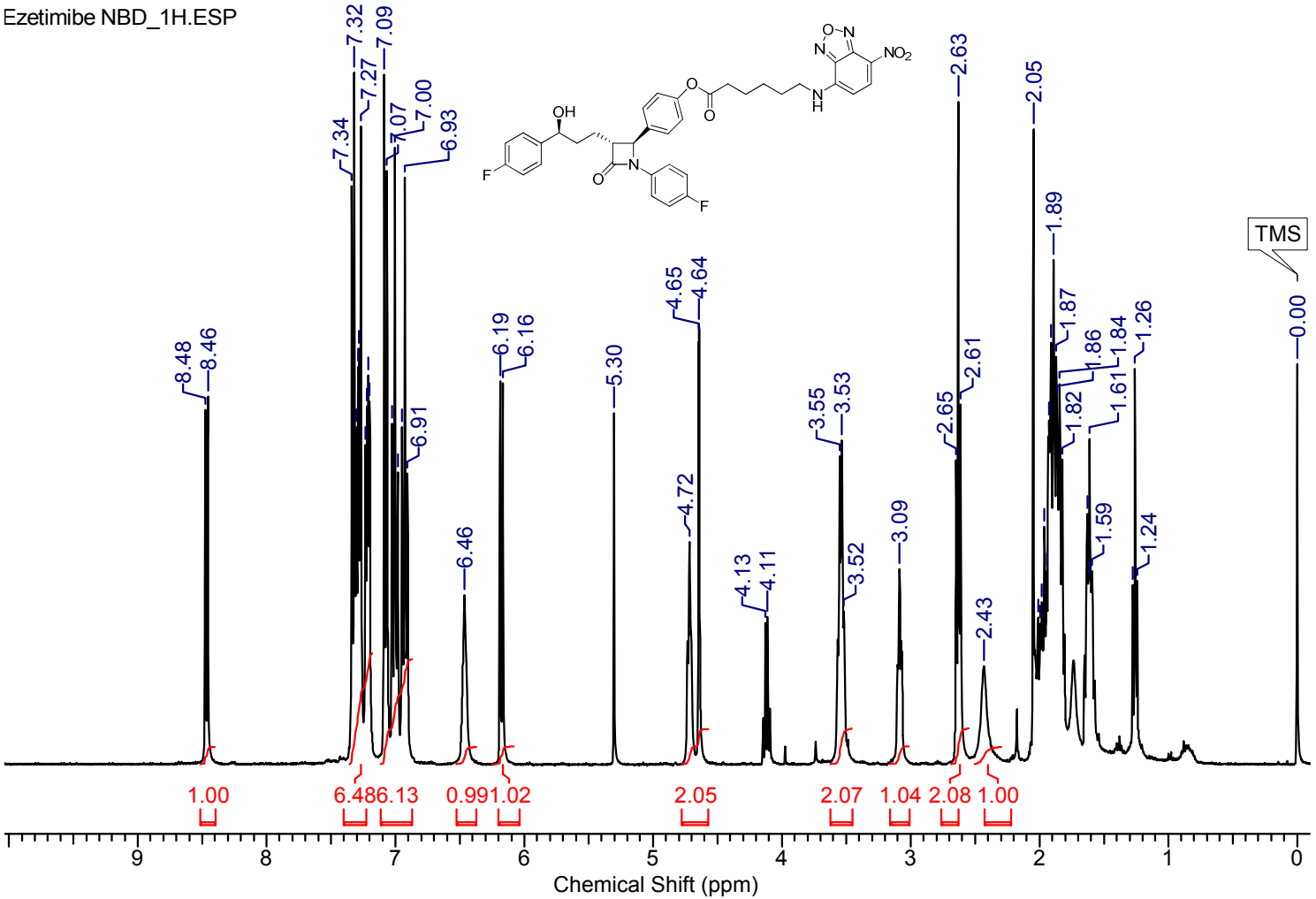

Fig. 40. ^{1}H NMR of **13a** in $CDCl_3$ at 400 MHz.

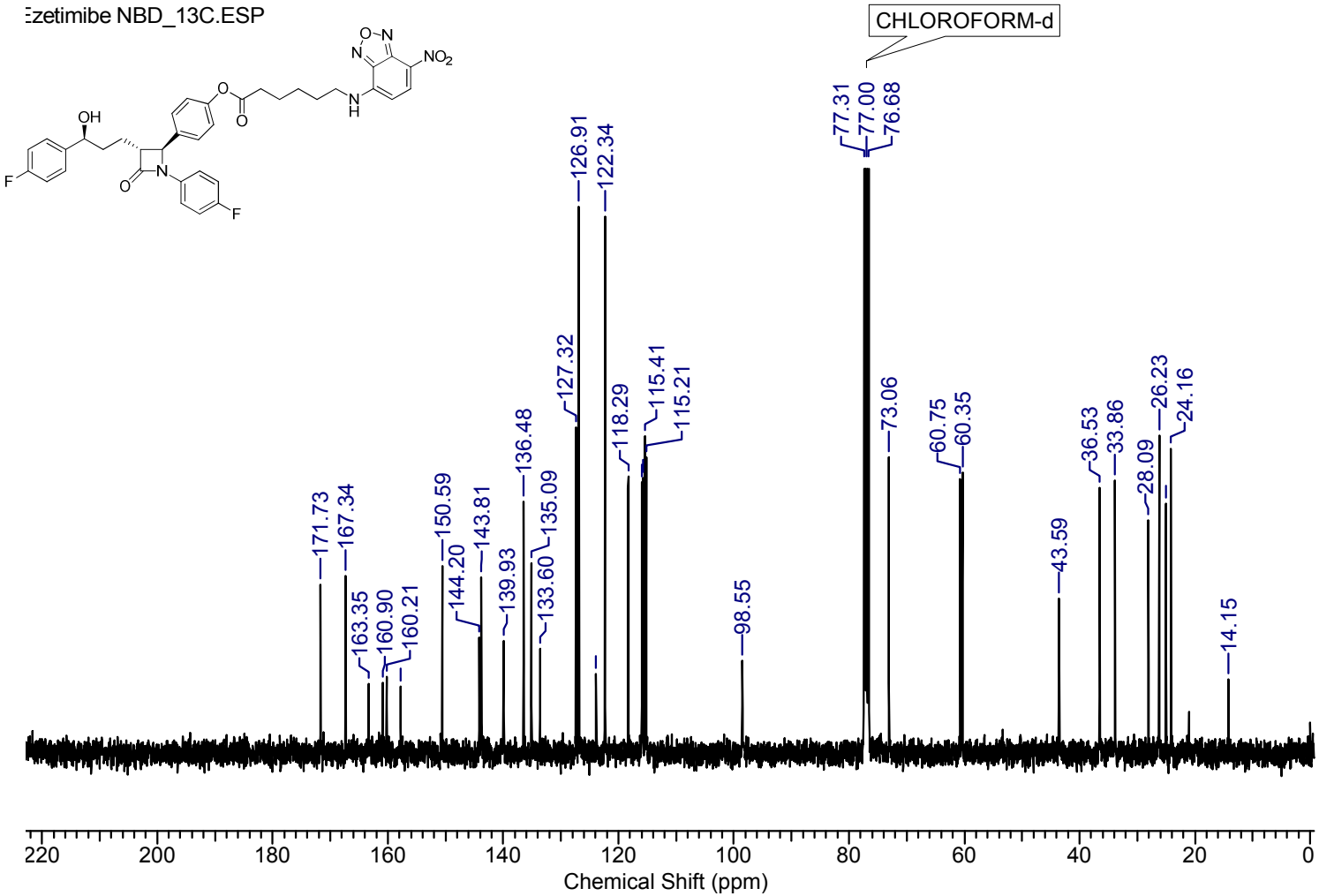

Fig. 41. ^{13}C NMR of **13a** in $CDCl_3$ at 100 MHz.

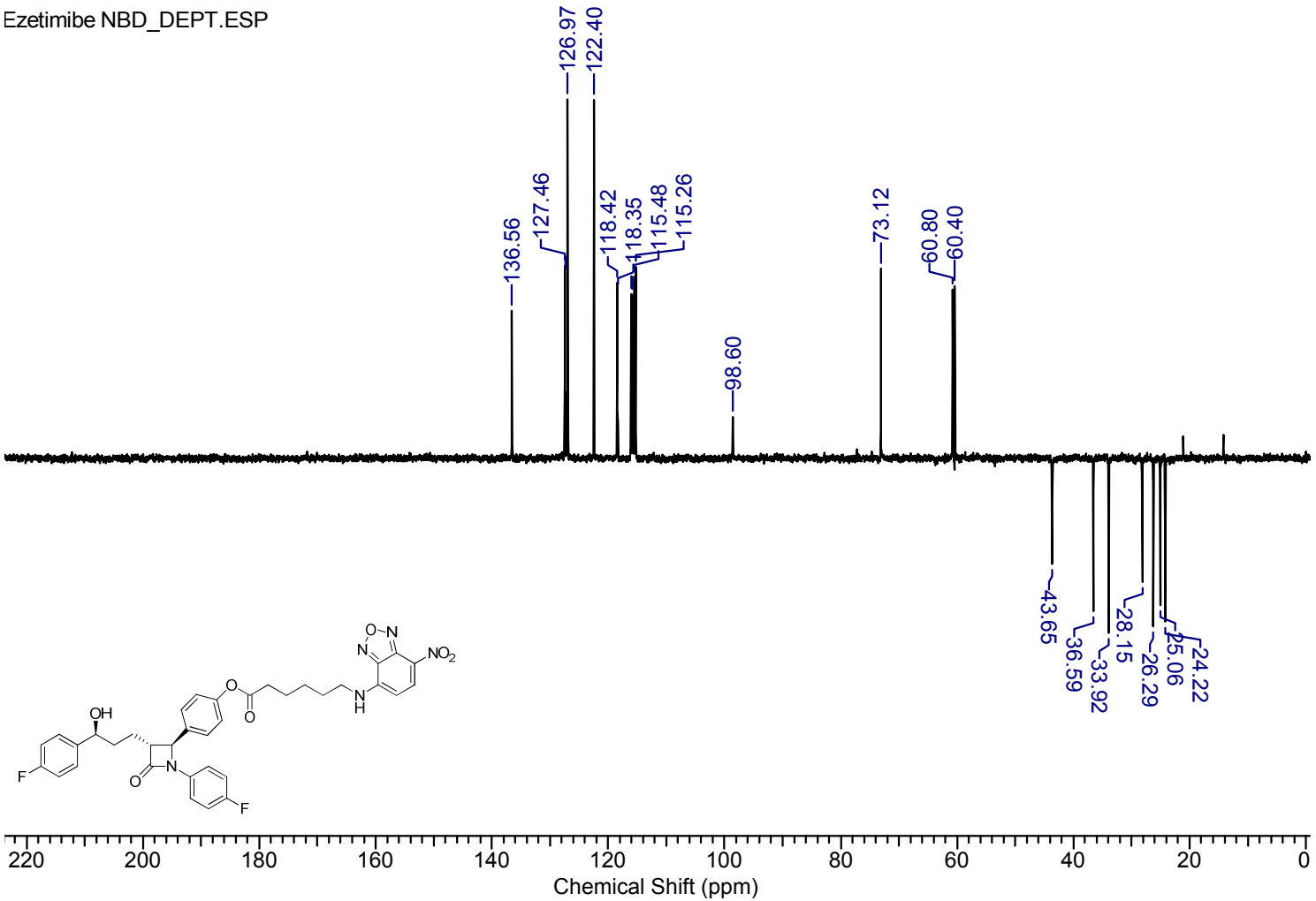

Fig. 42. DEPT-135 NMR of **13a** in $CDCl_3$ at 100 MHz.

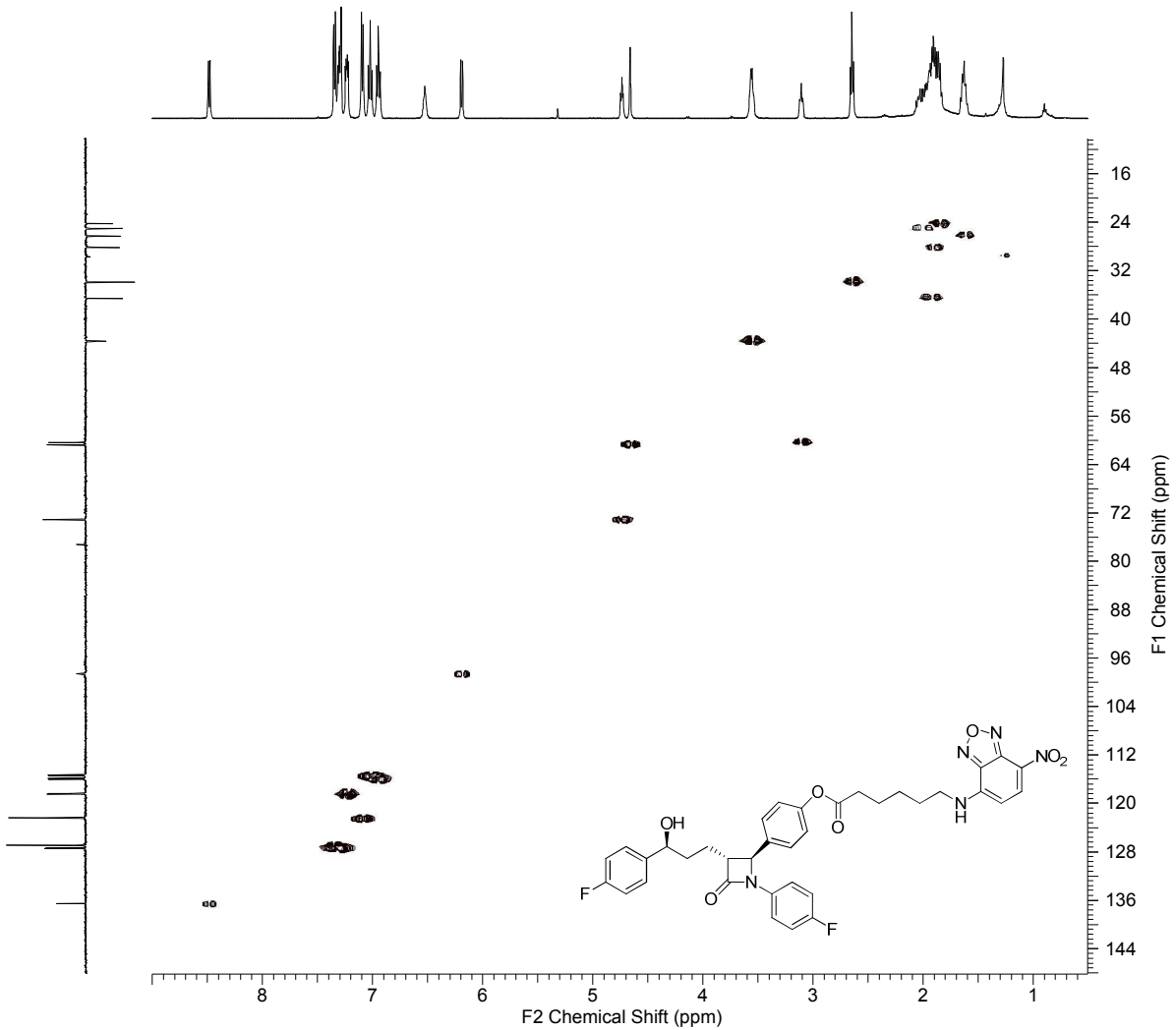

Fig. 43. HSQC NMR spectrum of **13a** in $CDCl_3$.

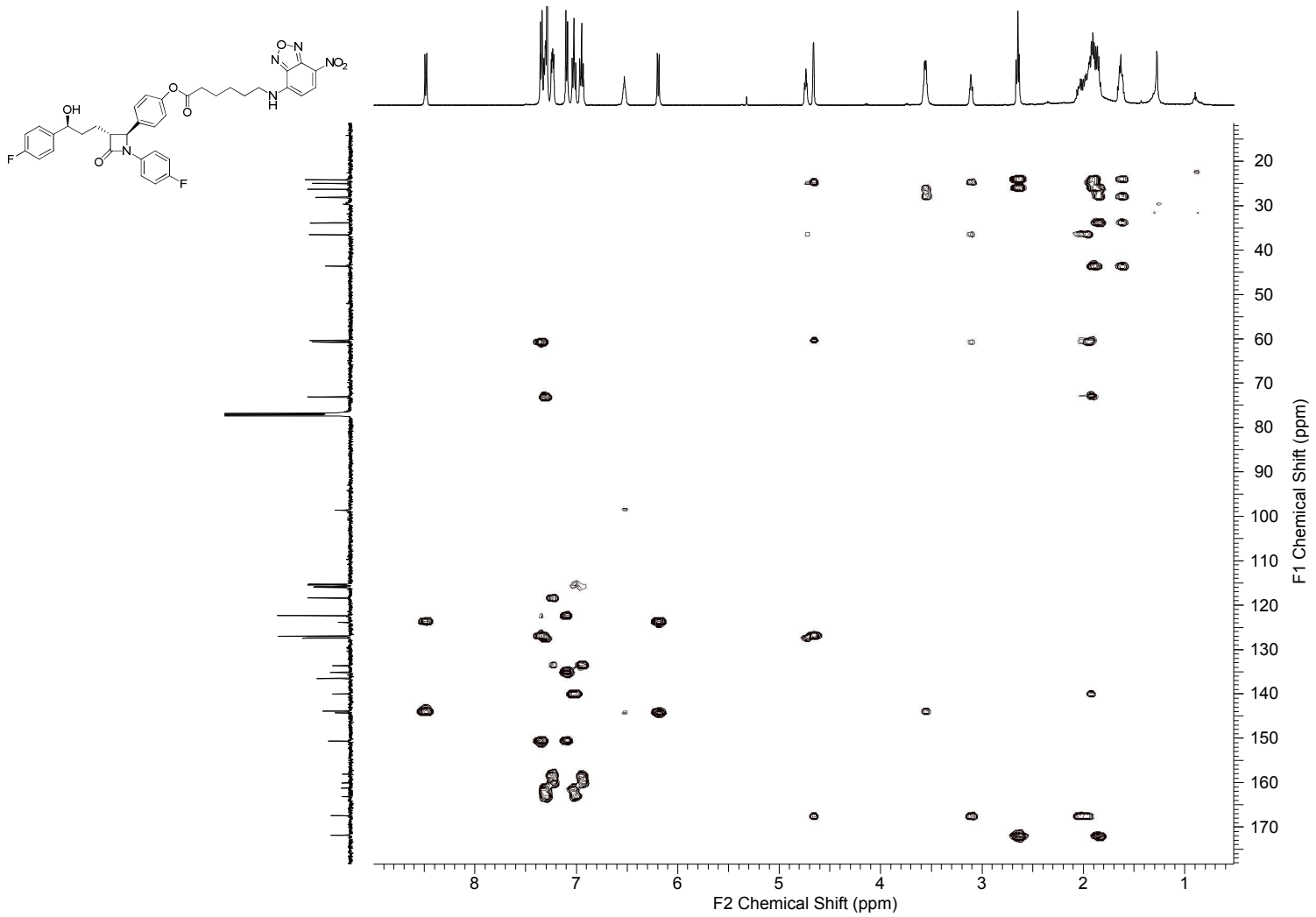

Fig. 44. HMBC NMR spectrum of **13a** in $CDCl_3$.

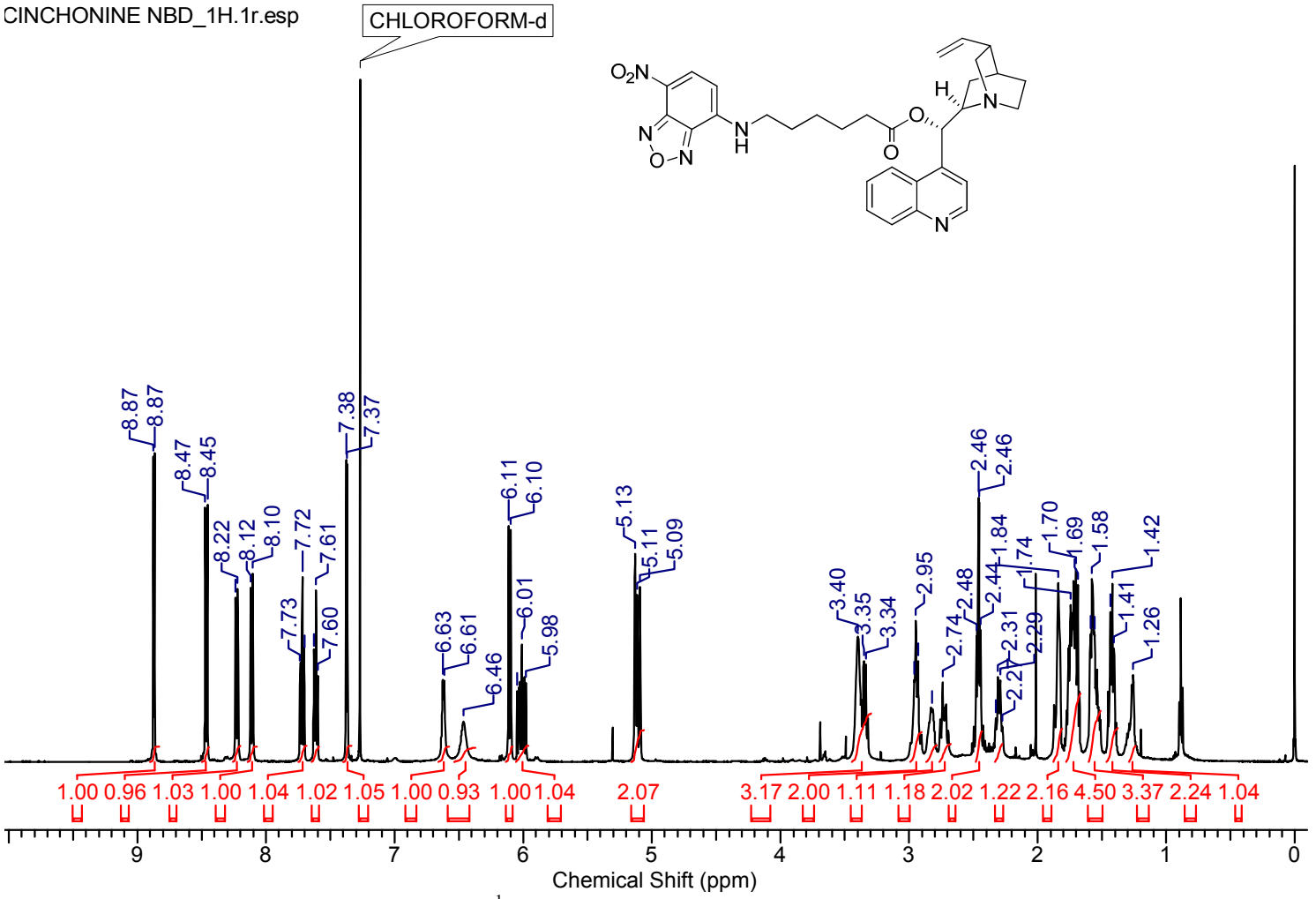

Fig. 45. ^{1}H NMR of **14a** in $CDCl_3$ at 400 MHz.

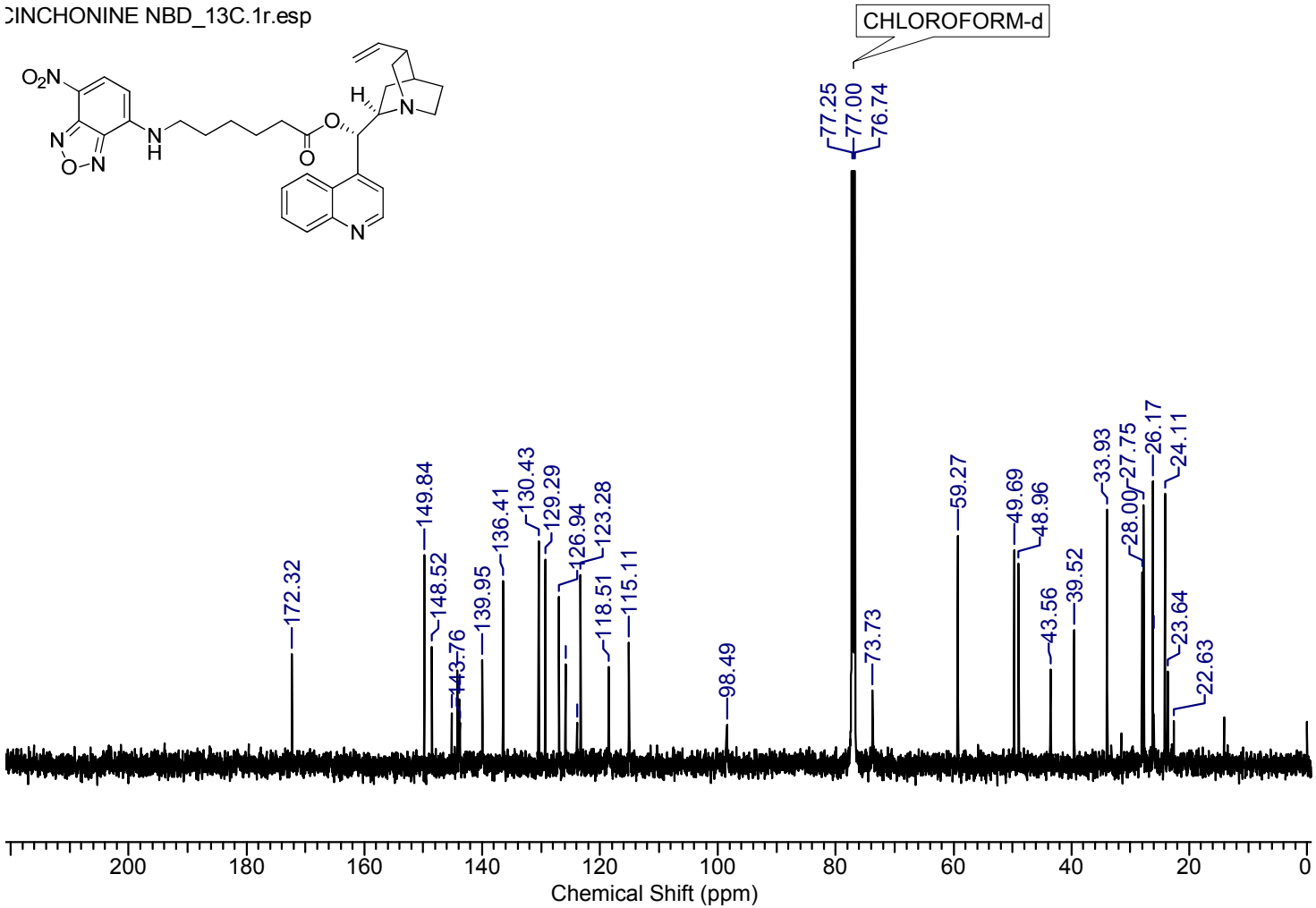

Fig. 46. ^{13}C NMR of **14a** in $CDCl_3$ at 100 MHz.

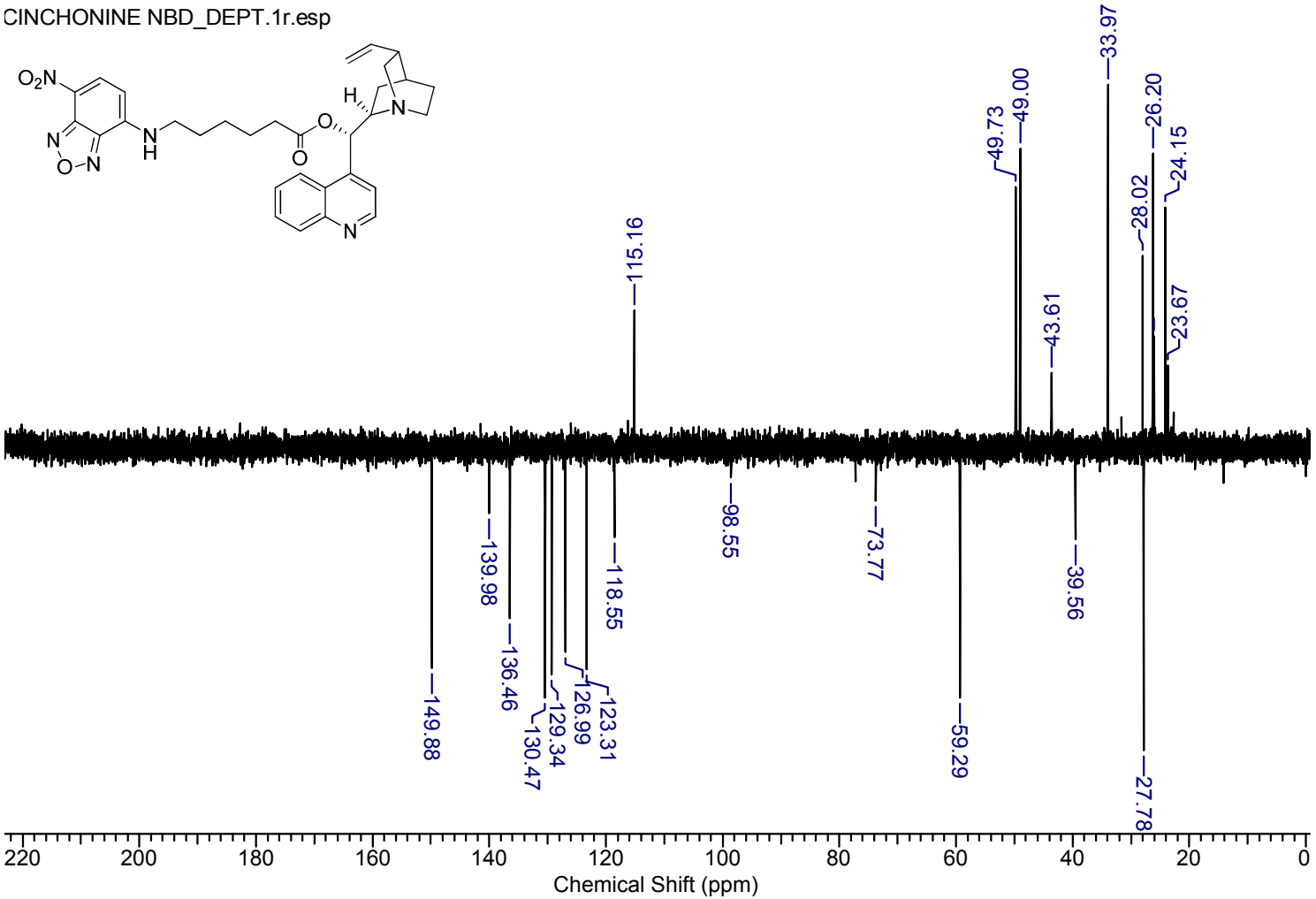

Fig. 47. DEPT-135 NMR of **14a** in $CDCl_3$ at 100 MHz.

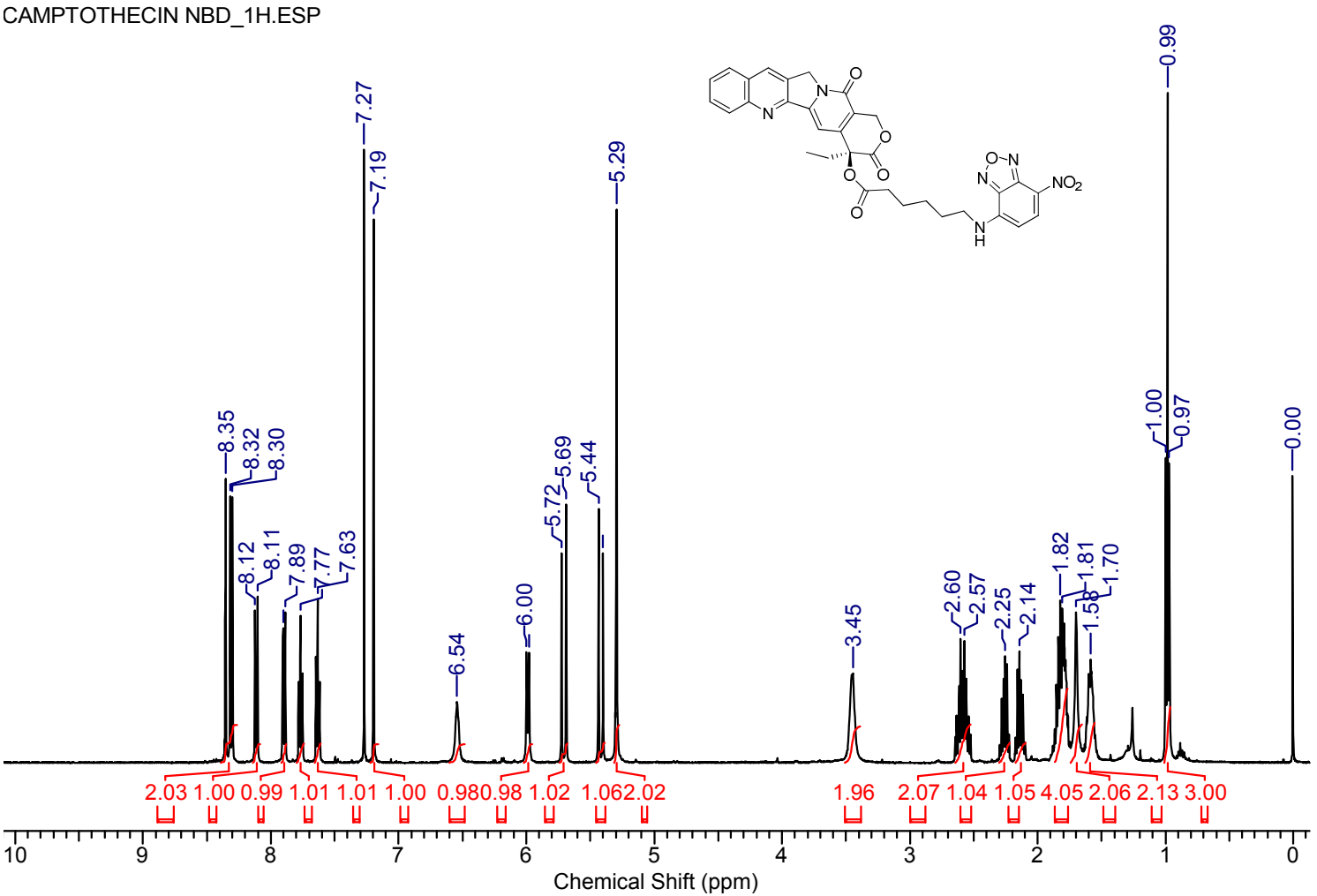

Fig. 48. ^{1}H NMR of **15a** in $CDCl_3$ at 400 MHz.

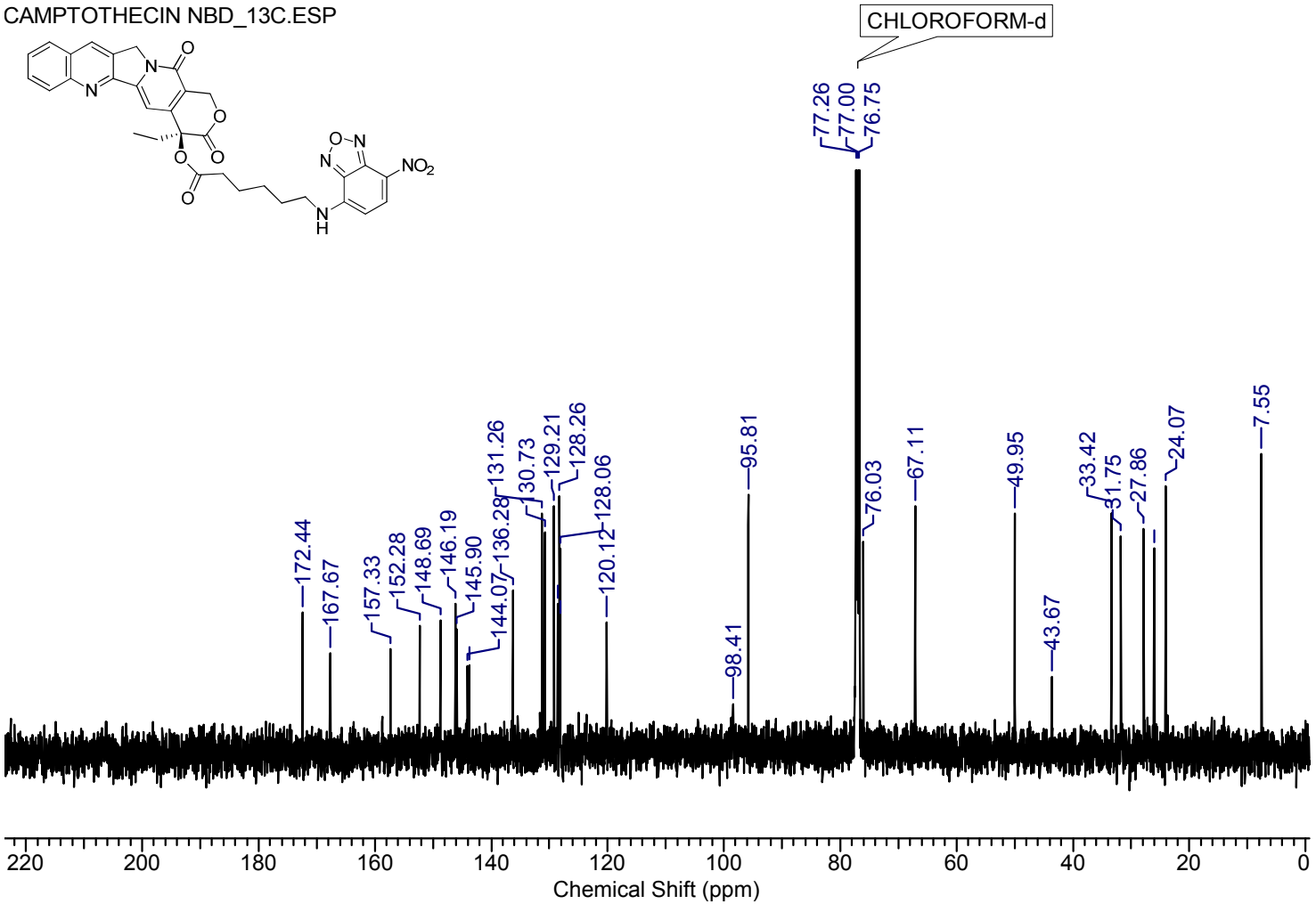

Fig. 49. ^{13}C NMR of **15a** in $CDCl_3$ at 100 MHz.

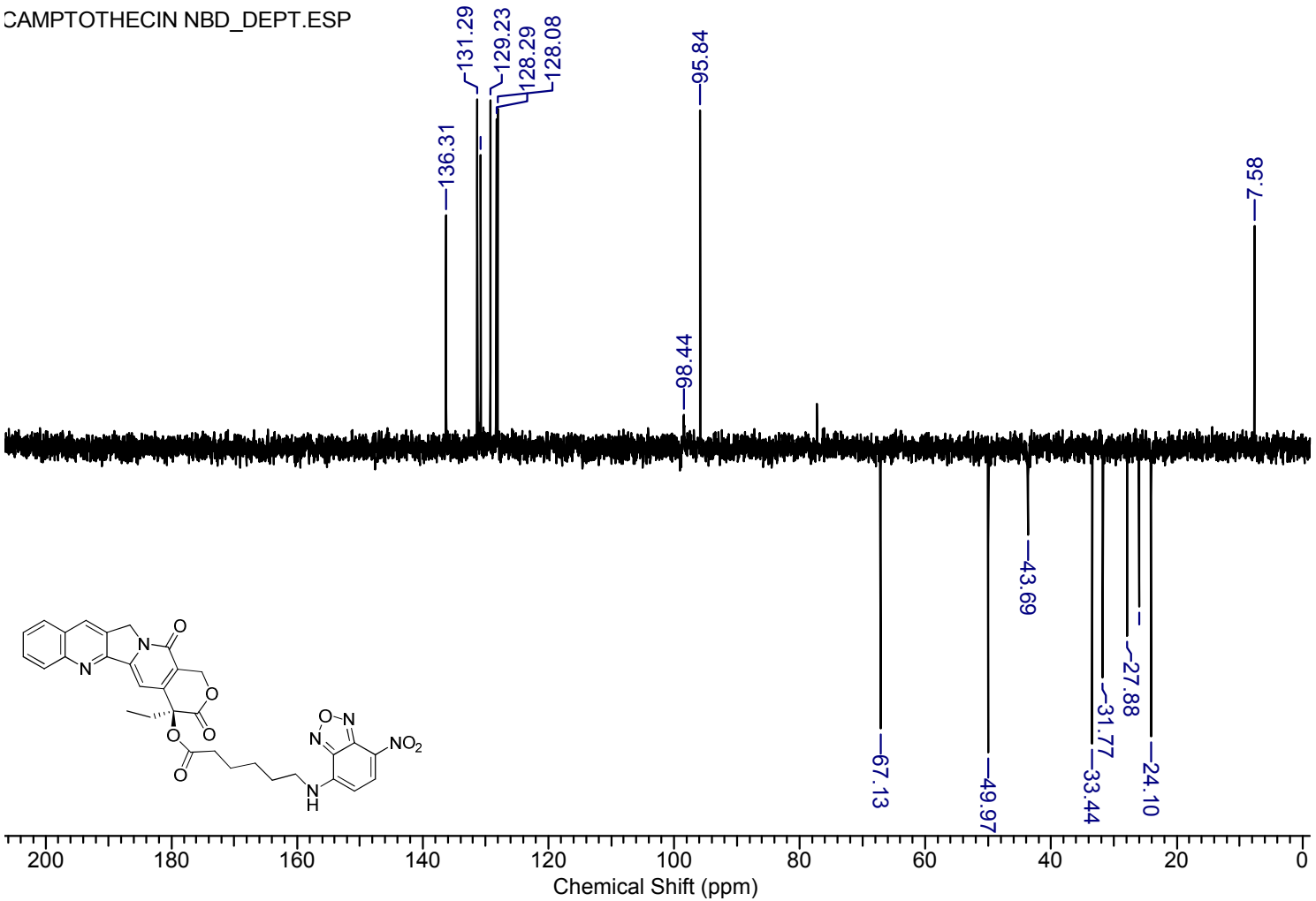

Fig. 50. DEPT-135 NMR of **15a** in $CDCl_3$ at 100 MHz.

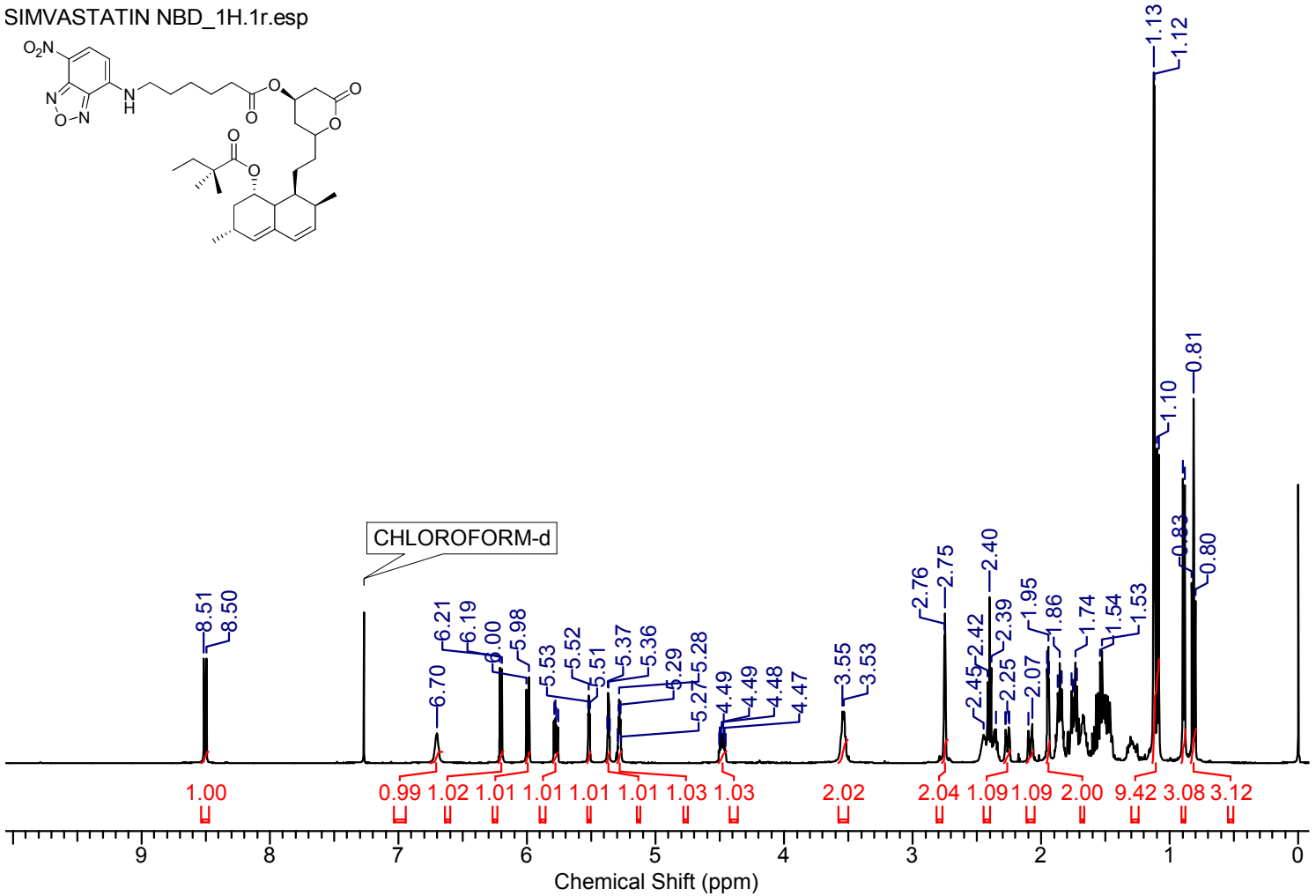

Fig. 51. ^{1}H NMR of **16a** in $CDCl_3$ at 400 MHz.

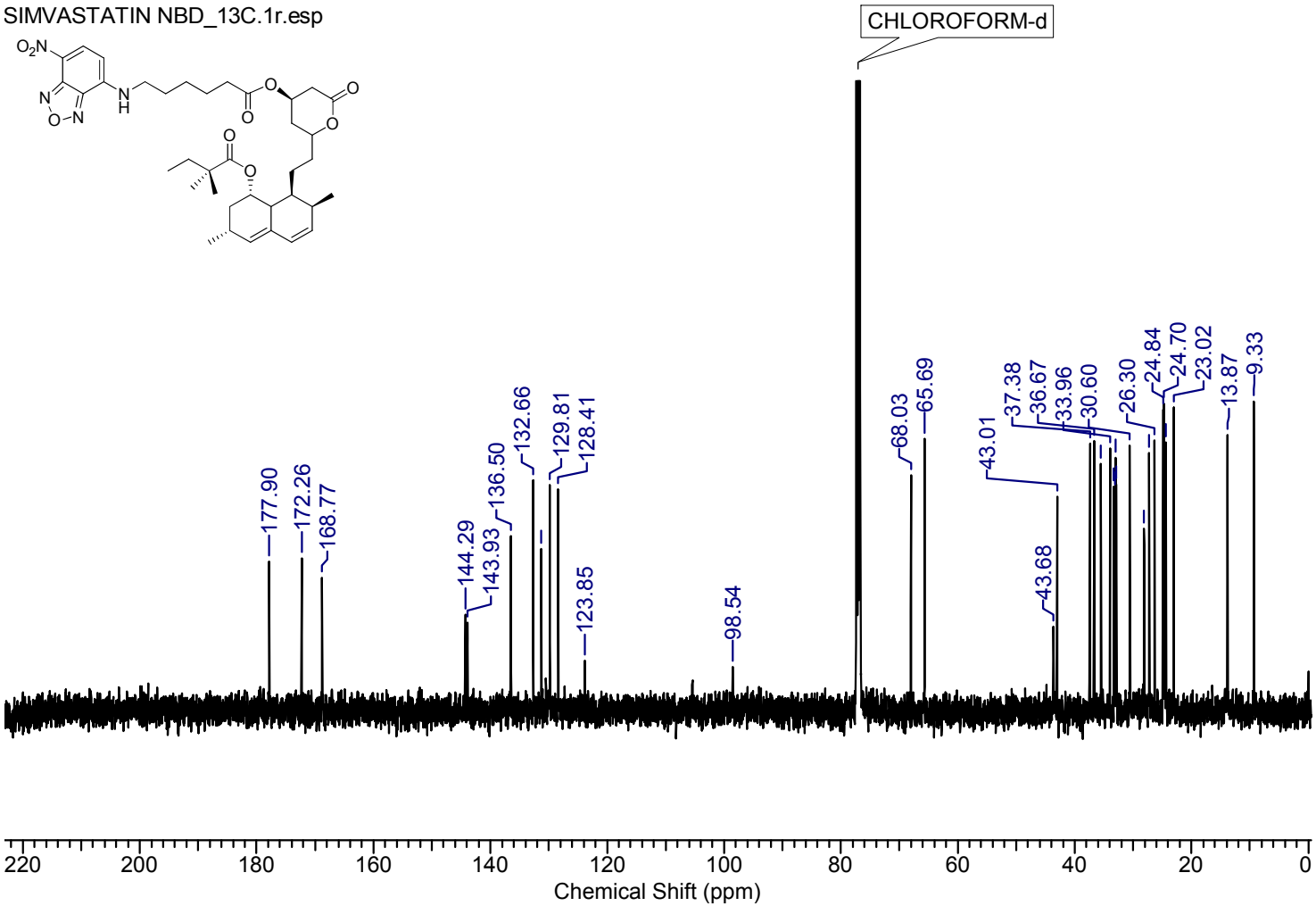

Fig. 52. ^{13}C NMR of **16a** in $CDCl_3$ at 100 MHz.

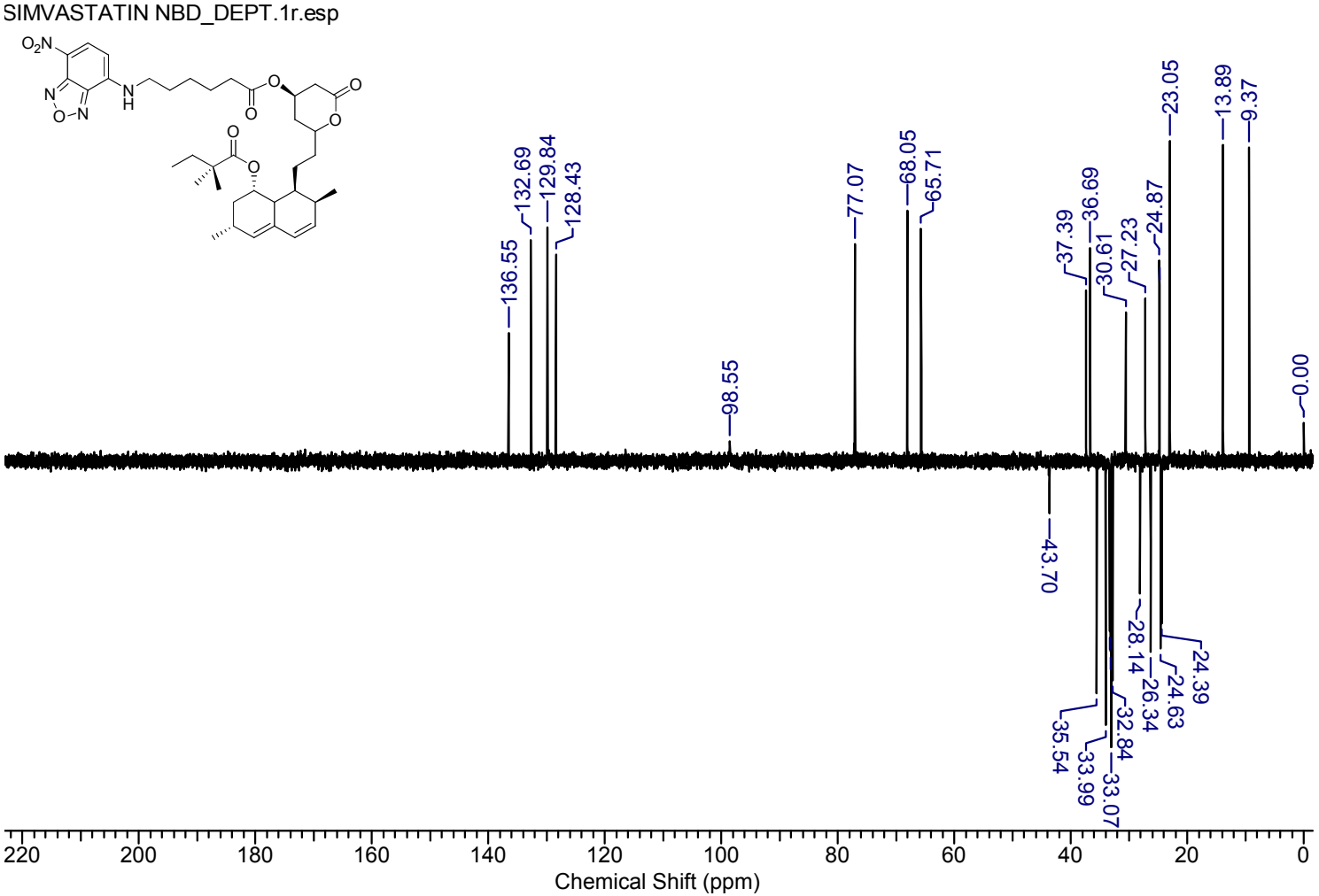

Fig. 53. DEPT-135 NMR of **16a** in $CDCl_3$ at 100 MHz.

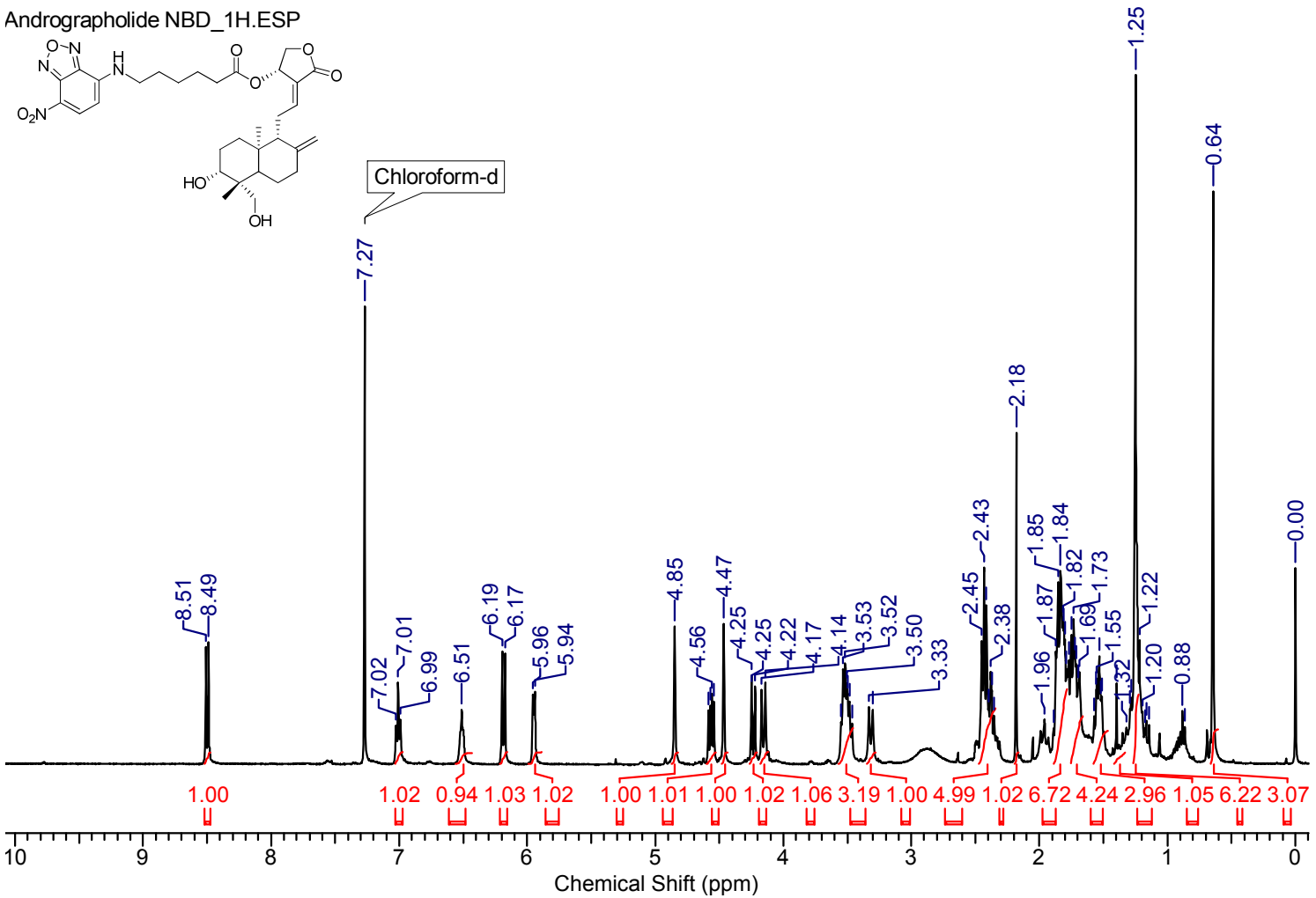

Fig. 54. ^{1}H NMR of **17a** in $CDCl_3$ at 400 MHz.

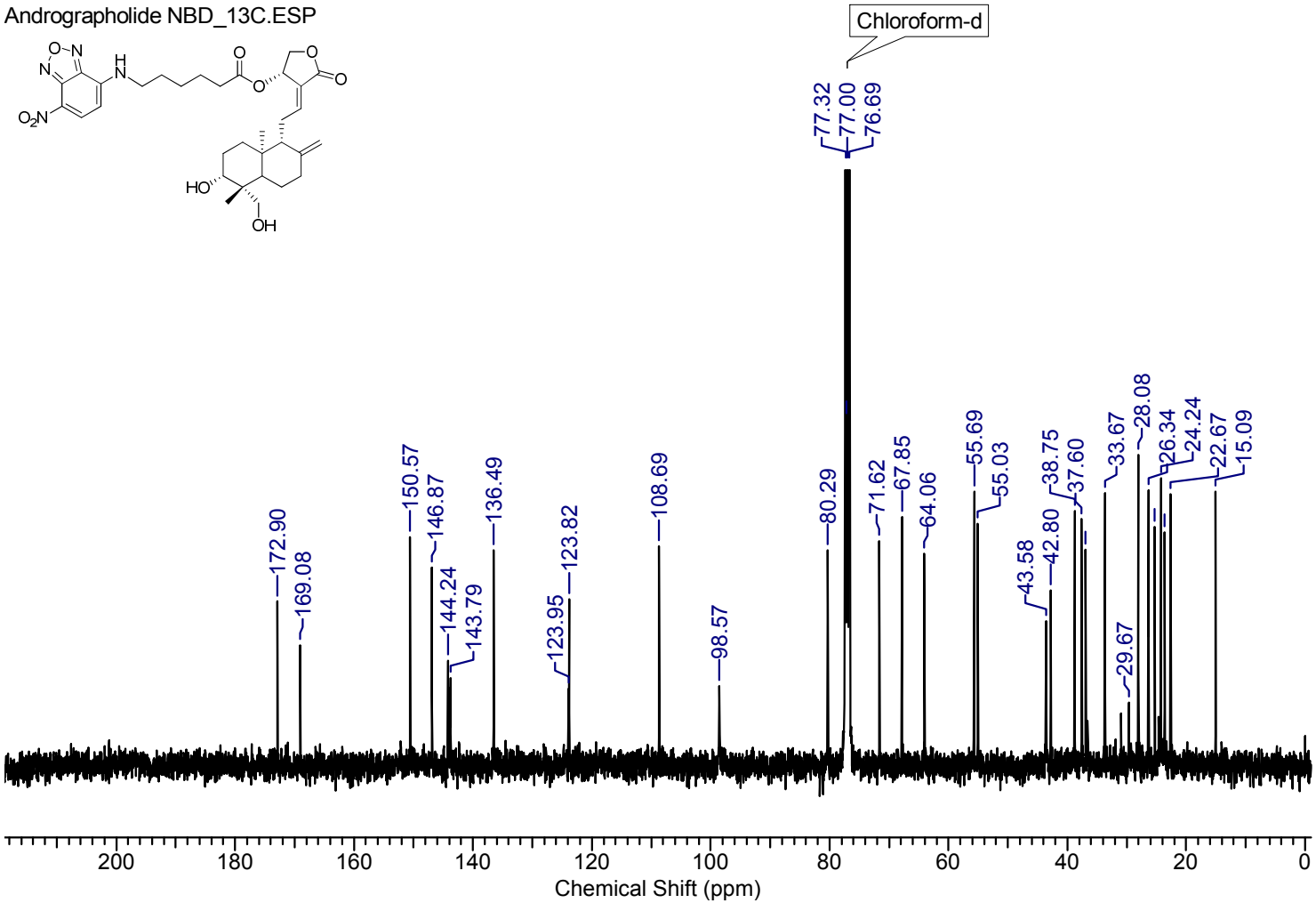

Fig. 55. ^{13}C NMR of **17a** in $CDCl_3$ at 100 MHz.

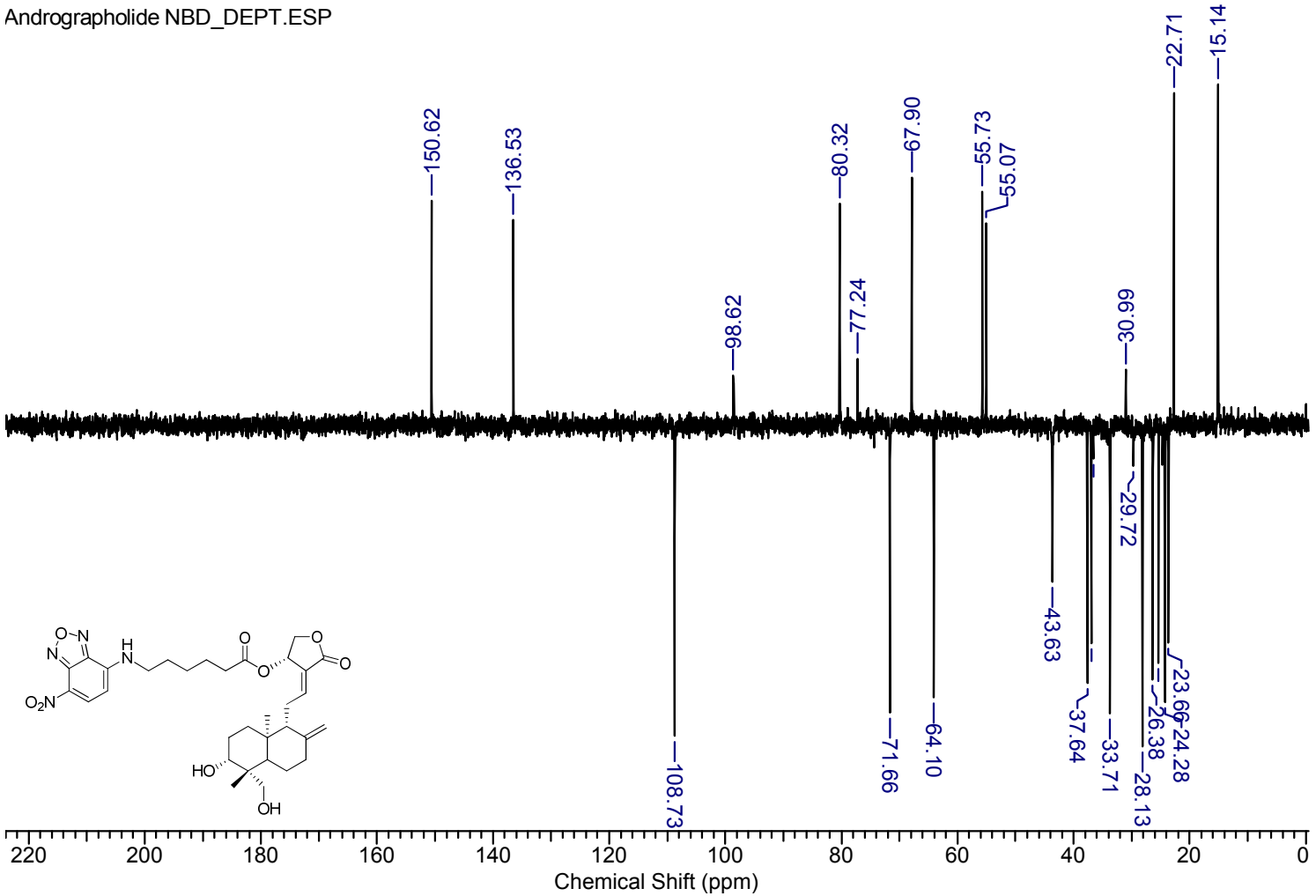

Fig. 56. DEPT-135 NMR of **17a** in $CDCl_3$ at 100 MHz.

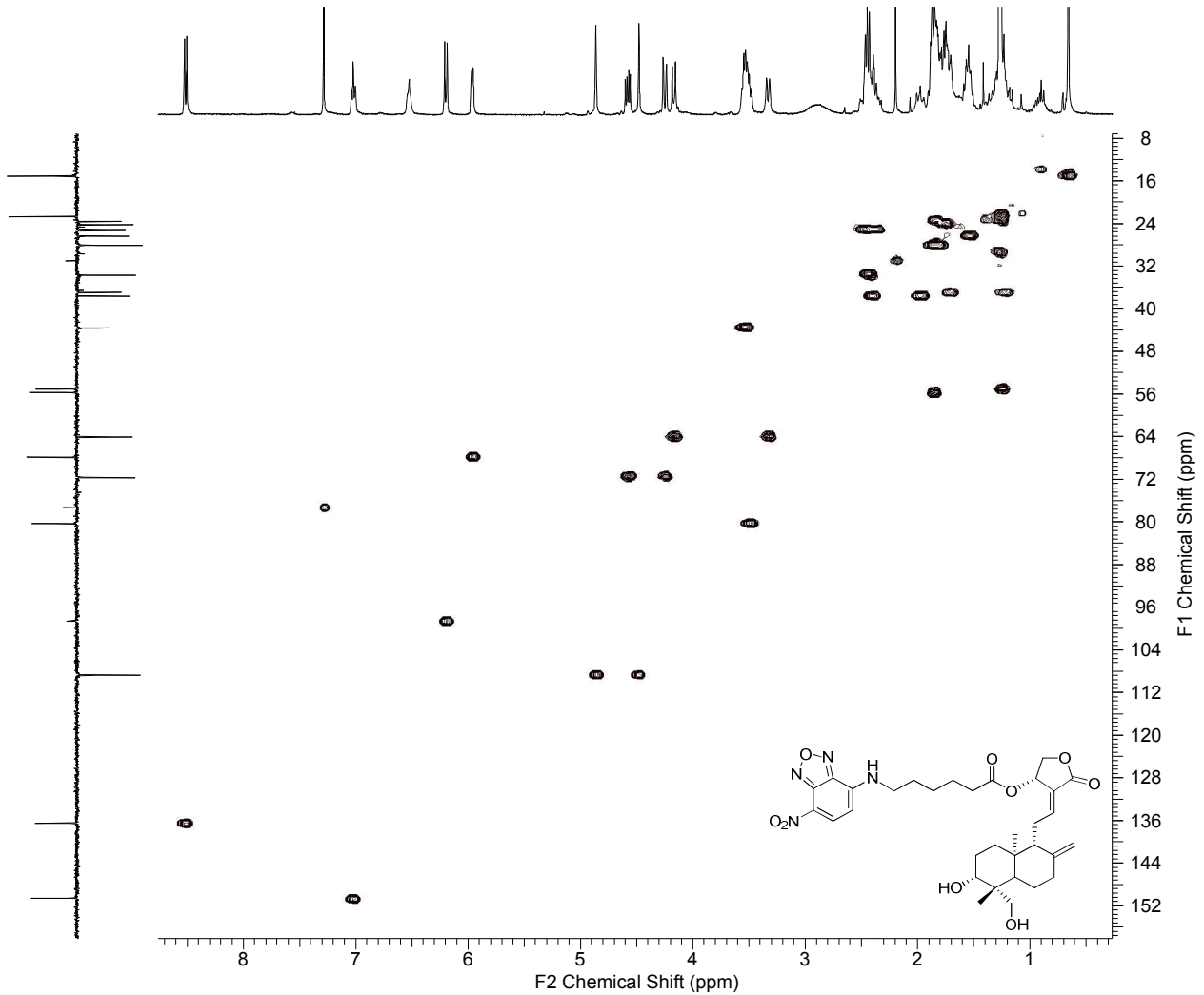

Fig. 57. HSQC NMR spectrum of **17a** in $CDCl_3$.

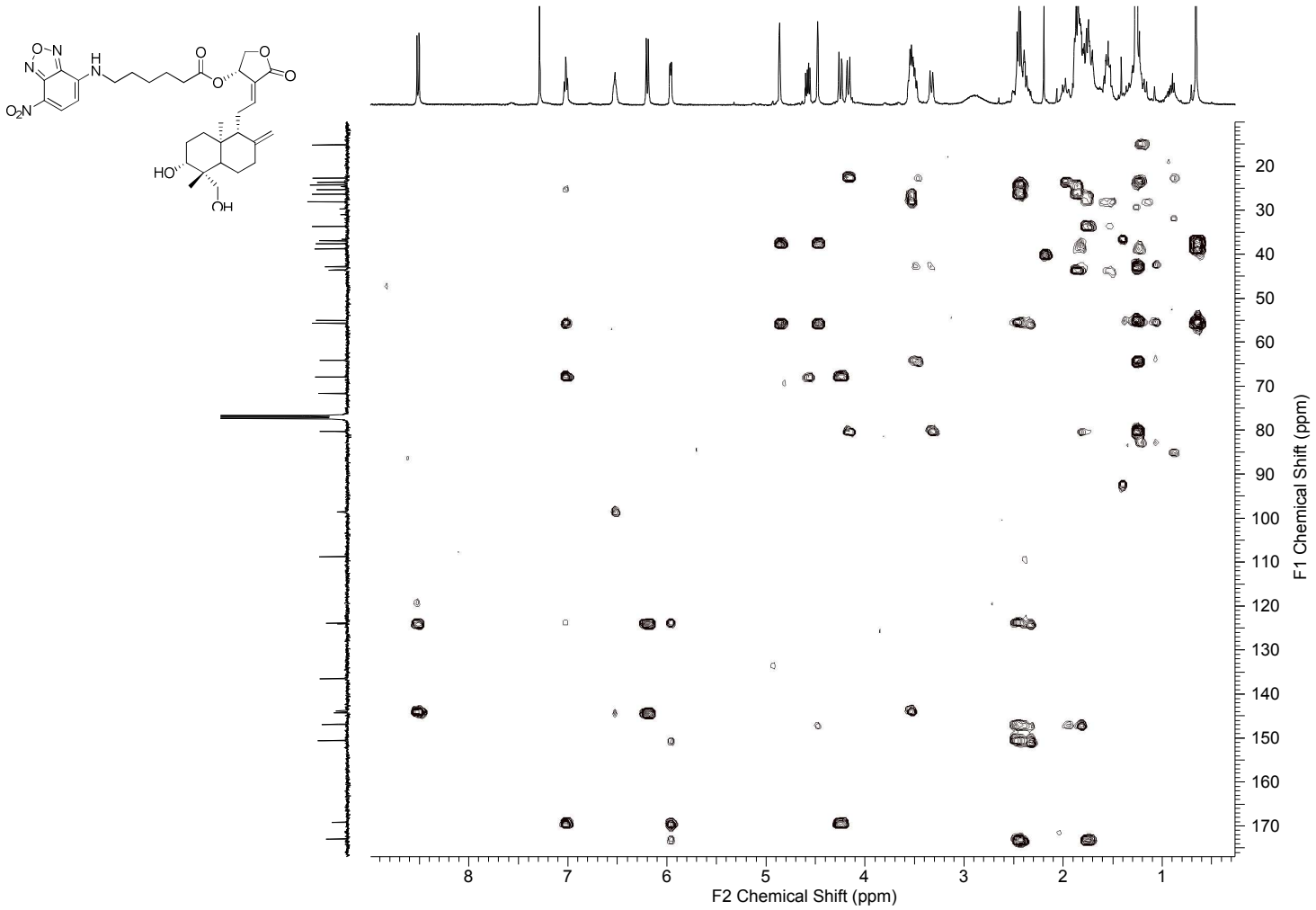

Fig. 58. HMBC NMR spectrum of **17a** in $CDCl_3$.

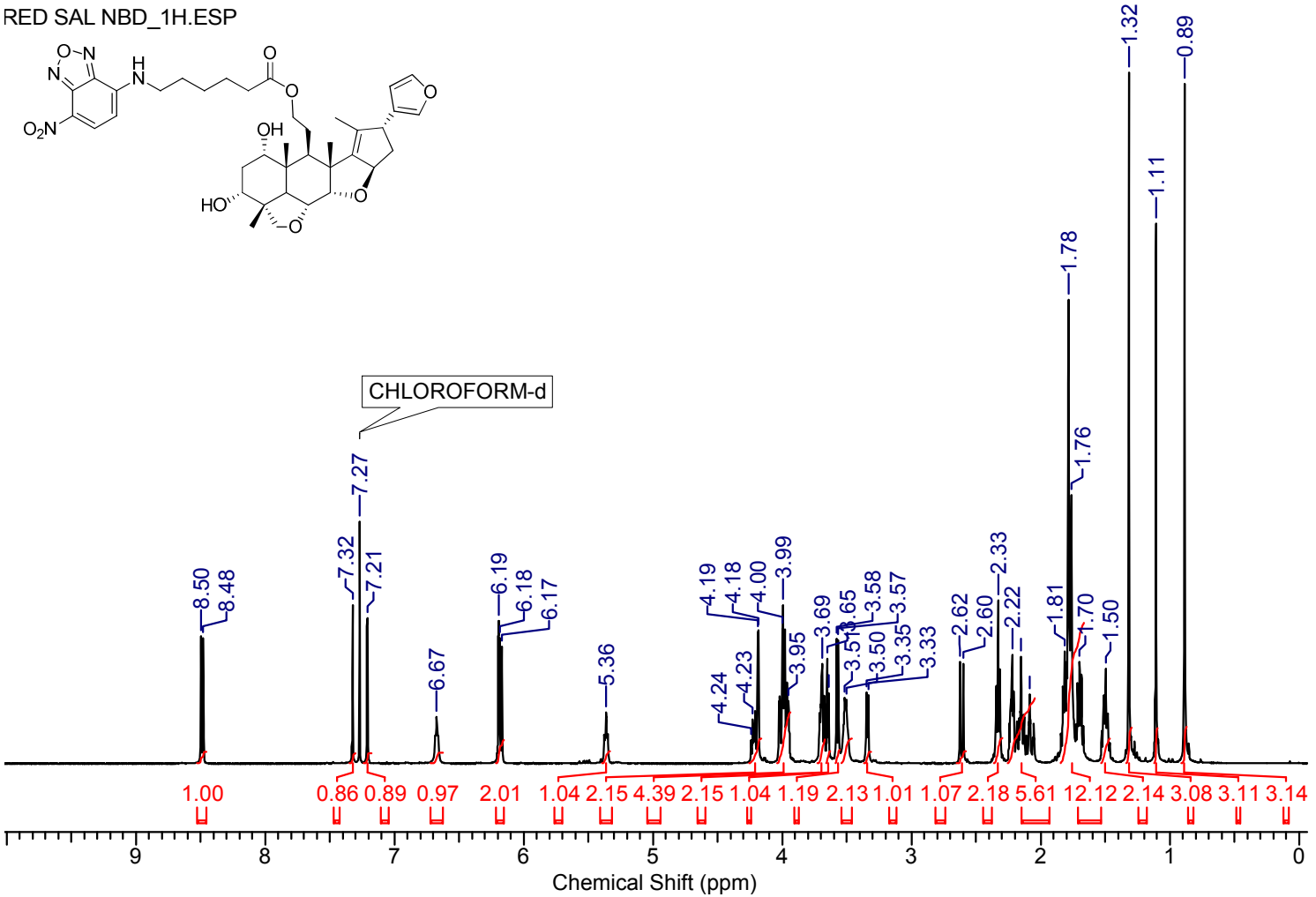

Fig. 59. ^{1}H NMR of **18a** in $CDCl_3$ at 400 MHz.

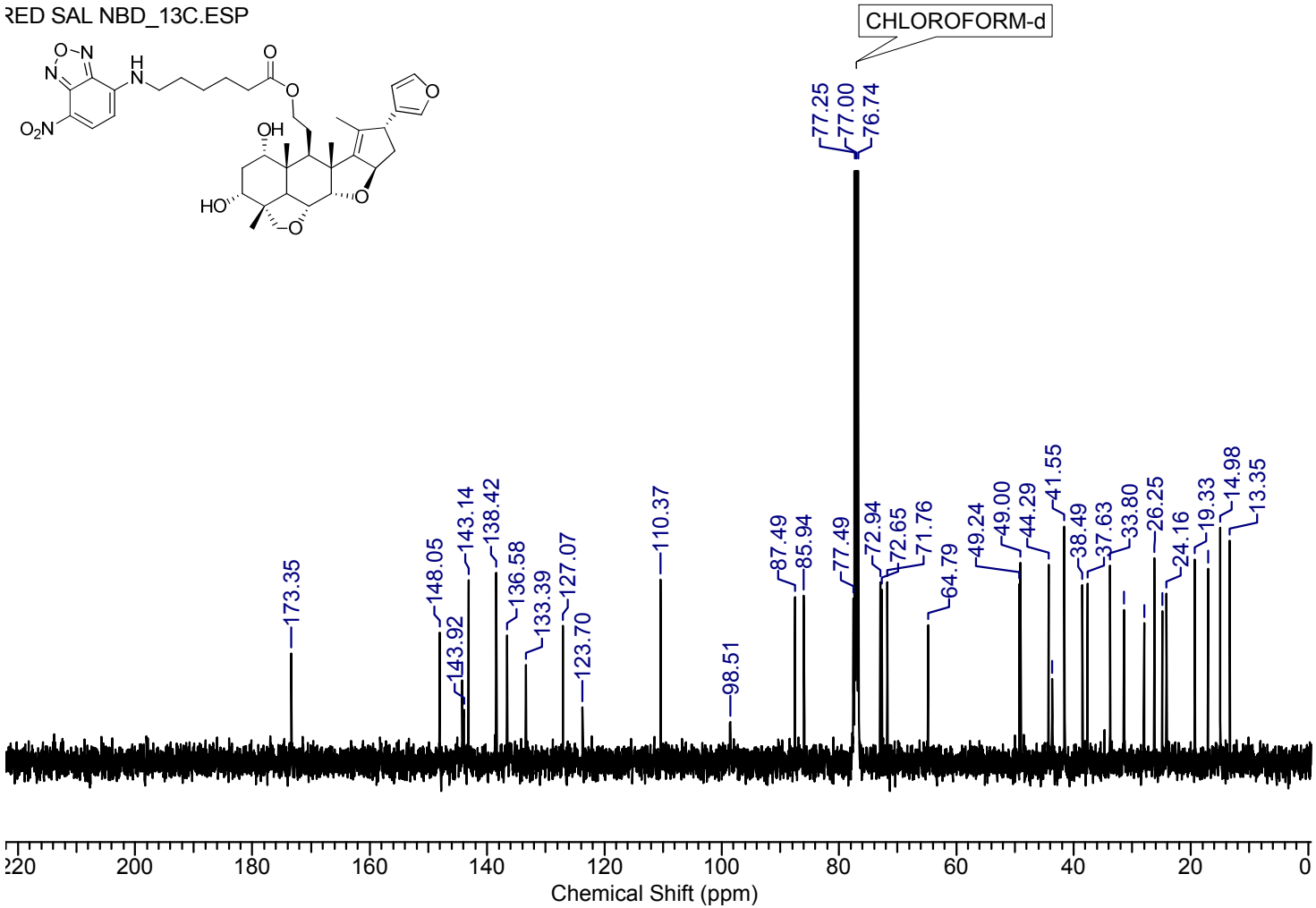

Fig. 60. ^{13}C NMR of **18a** in $CDCl_3$ at 100 MHz.

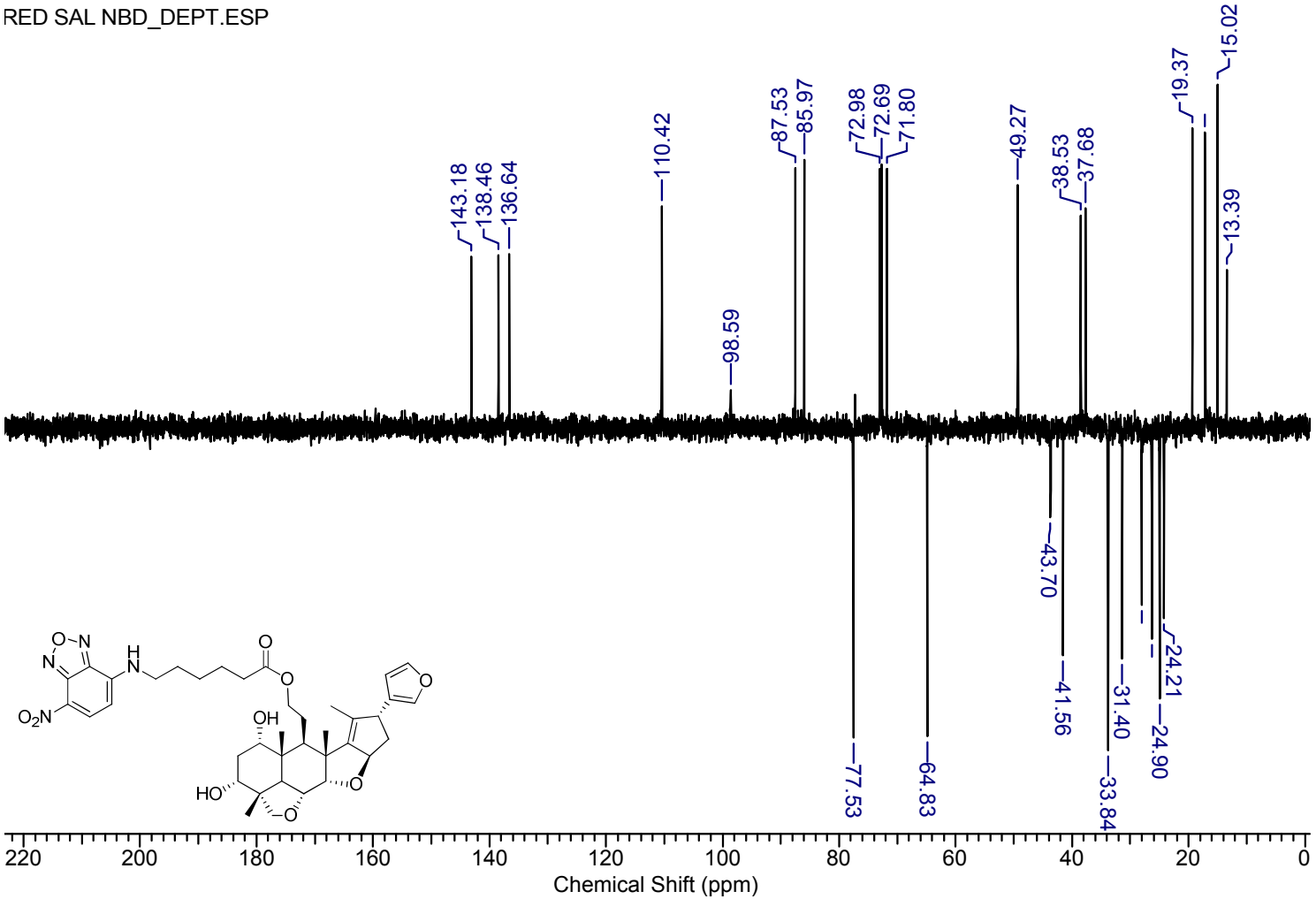

Fig. 61. DEPT-135 NMR of **18a** in $CDCl_3$ at 100 MHz.

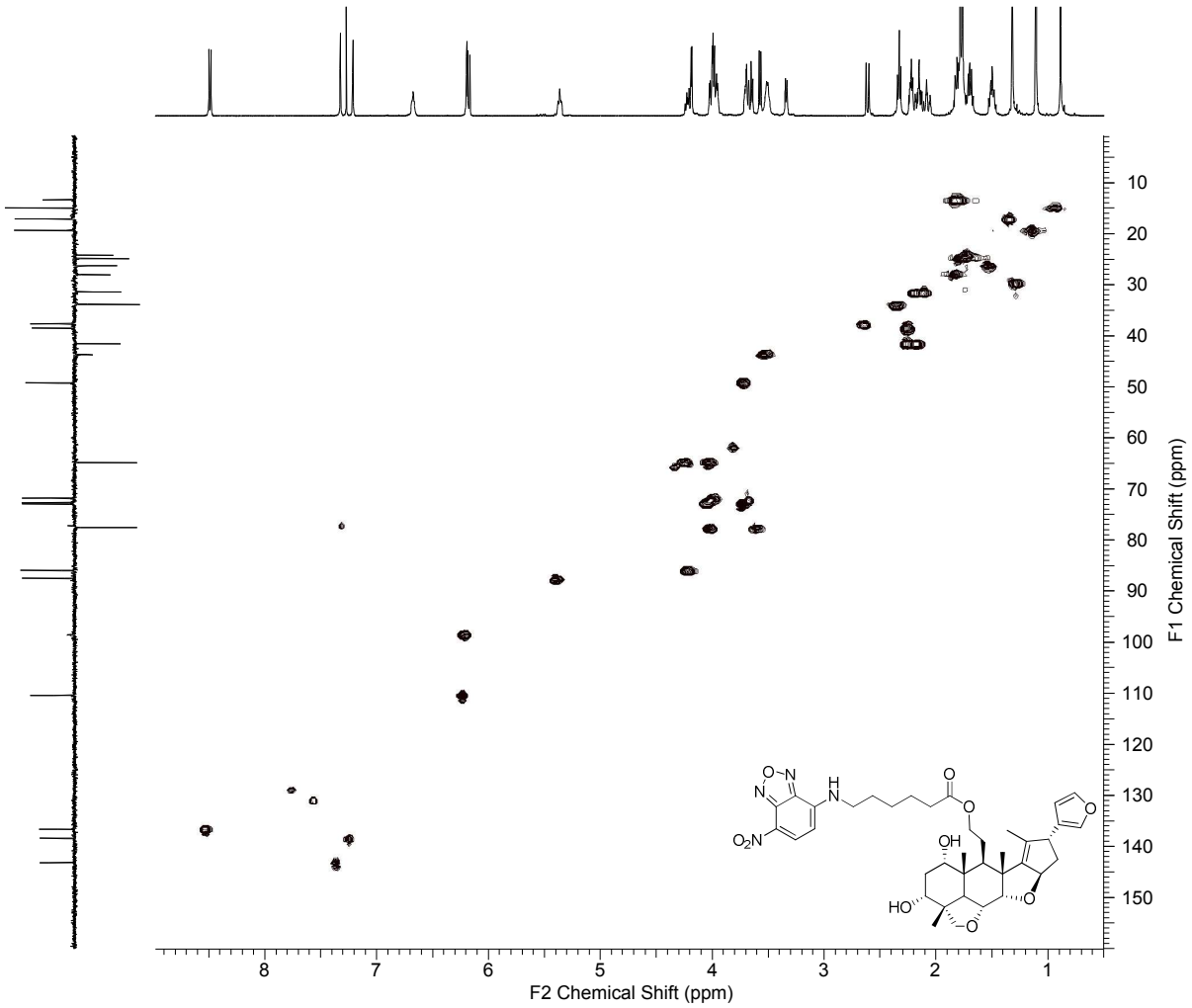

Fig. 62. HSQC NMR spectrum of **18a** in $CDCl_3$.

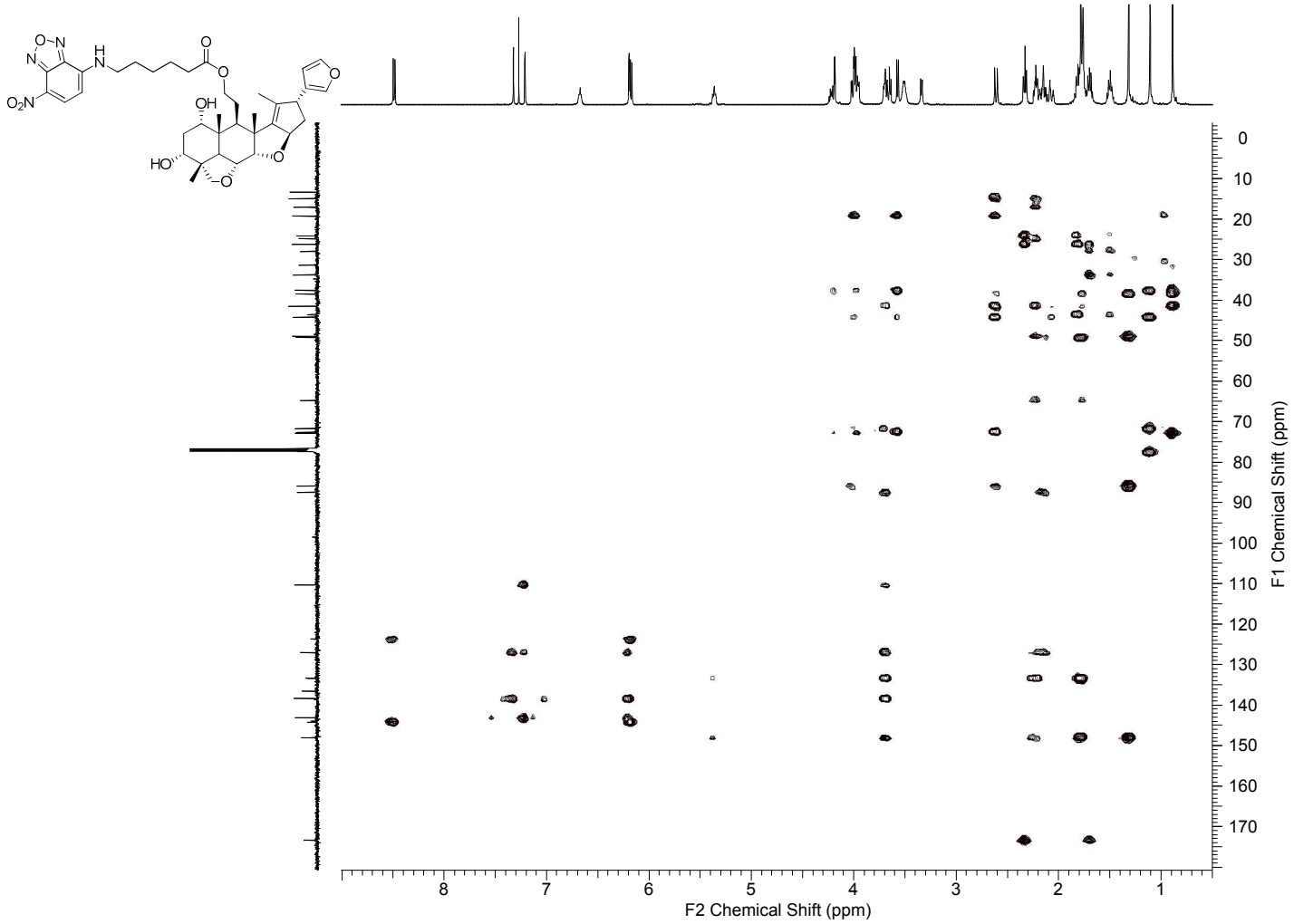

Fig. 63. HMBC NMR spectrum of **18a** in $CDCl_3$.

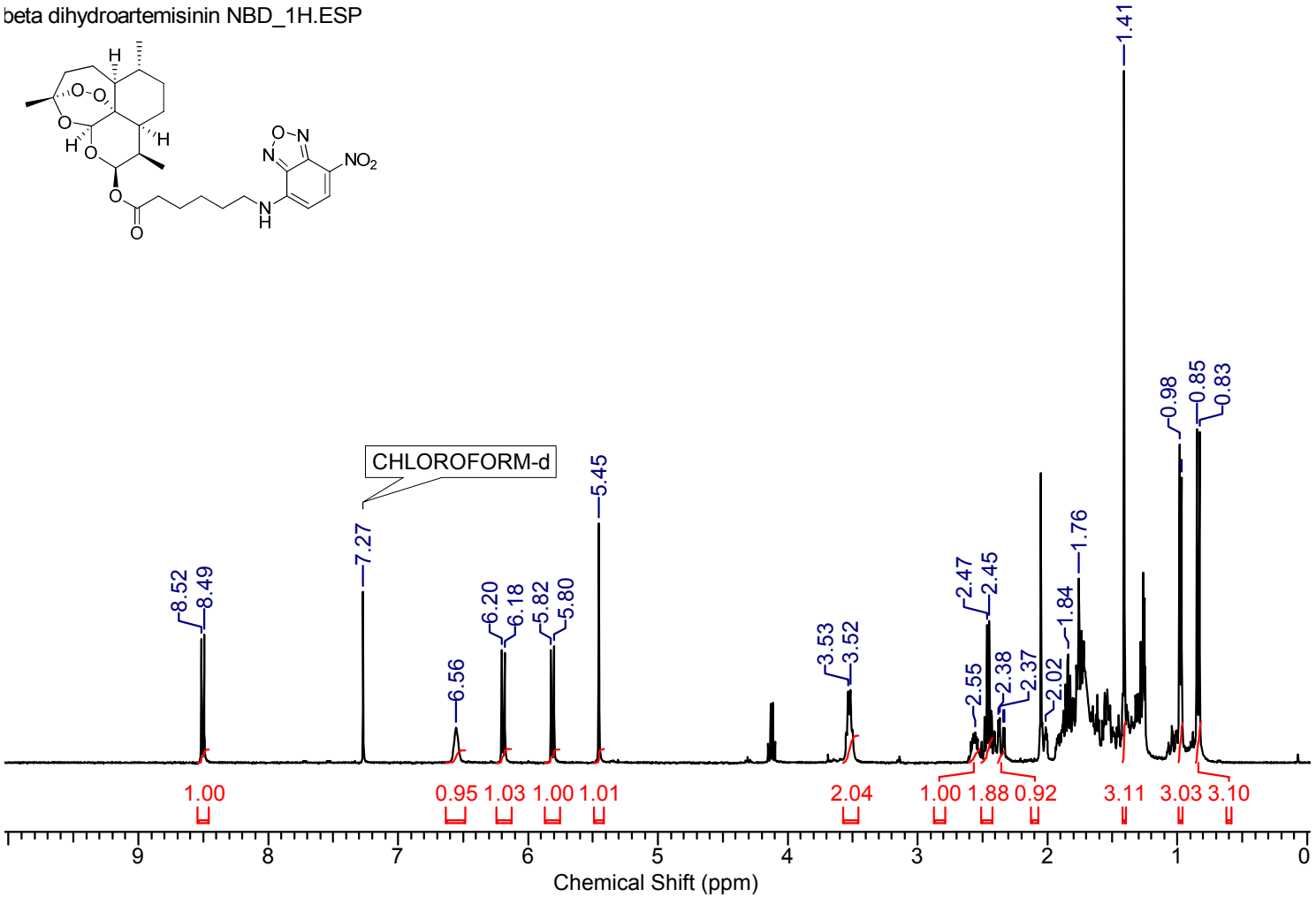

Fig. 64. ^{1}H NMR of **19a** in $CDCl_3$ at 400 MHz.

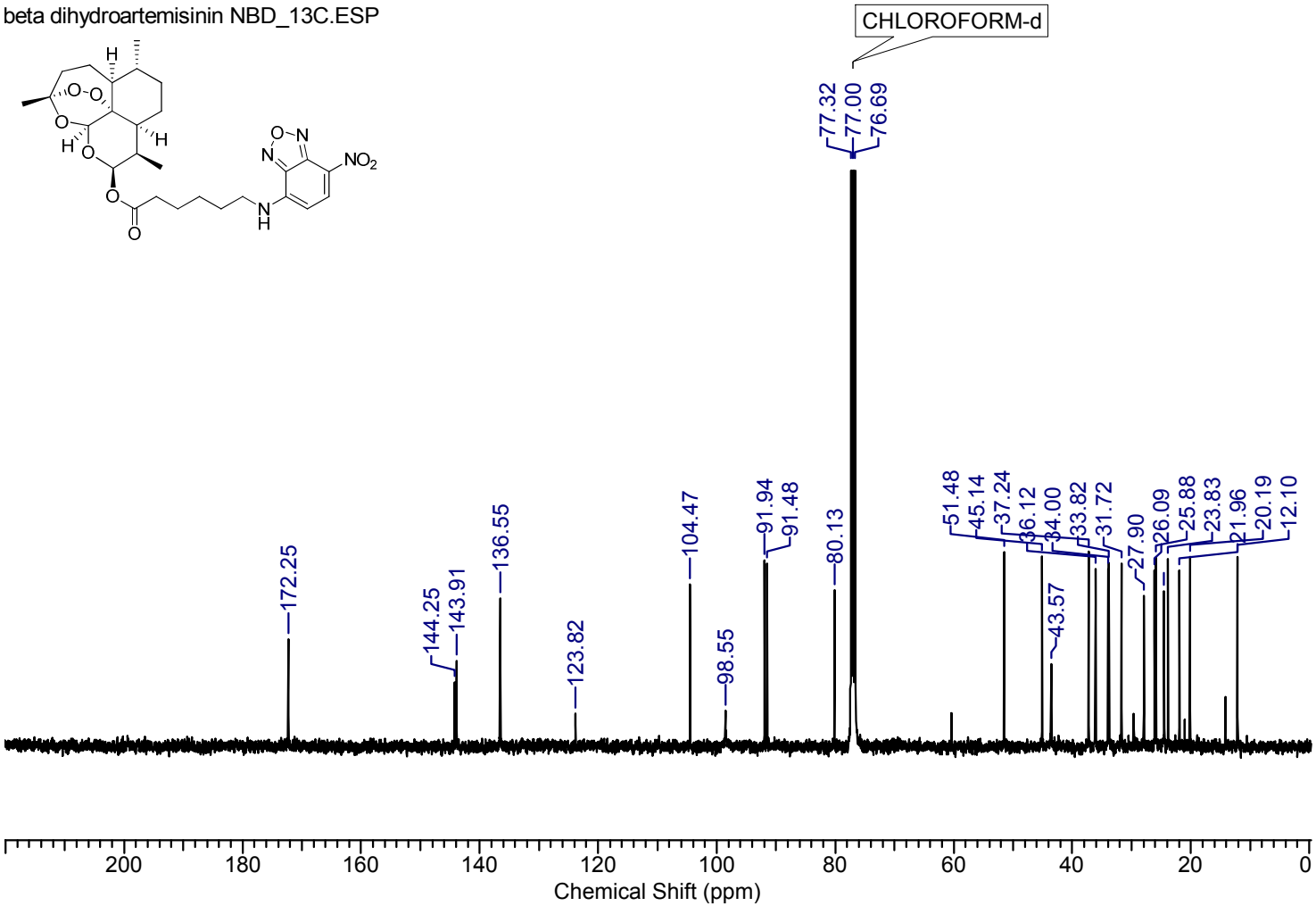

Fig. 65. ^{13}C NMR of **19a** in $CDCl_3$ at 100 MHz.

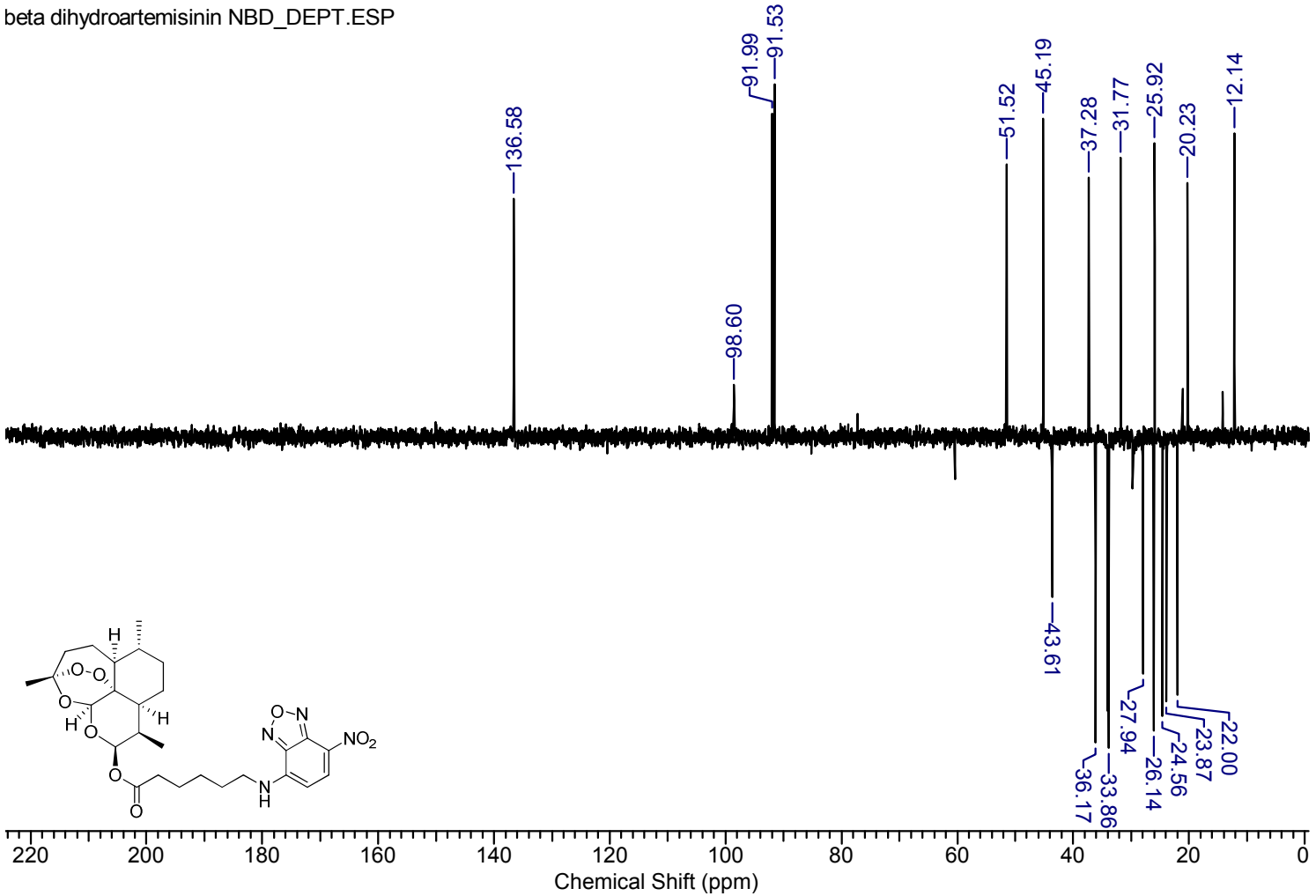

Fig. 66. DEPT-135 NMR of **19a** in $CDCl_3$ at 100 MHz.

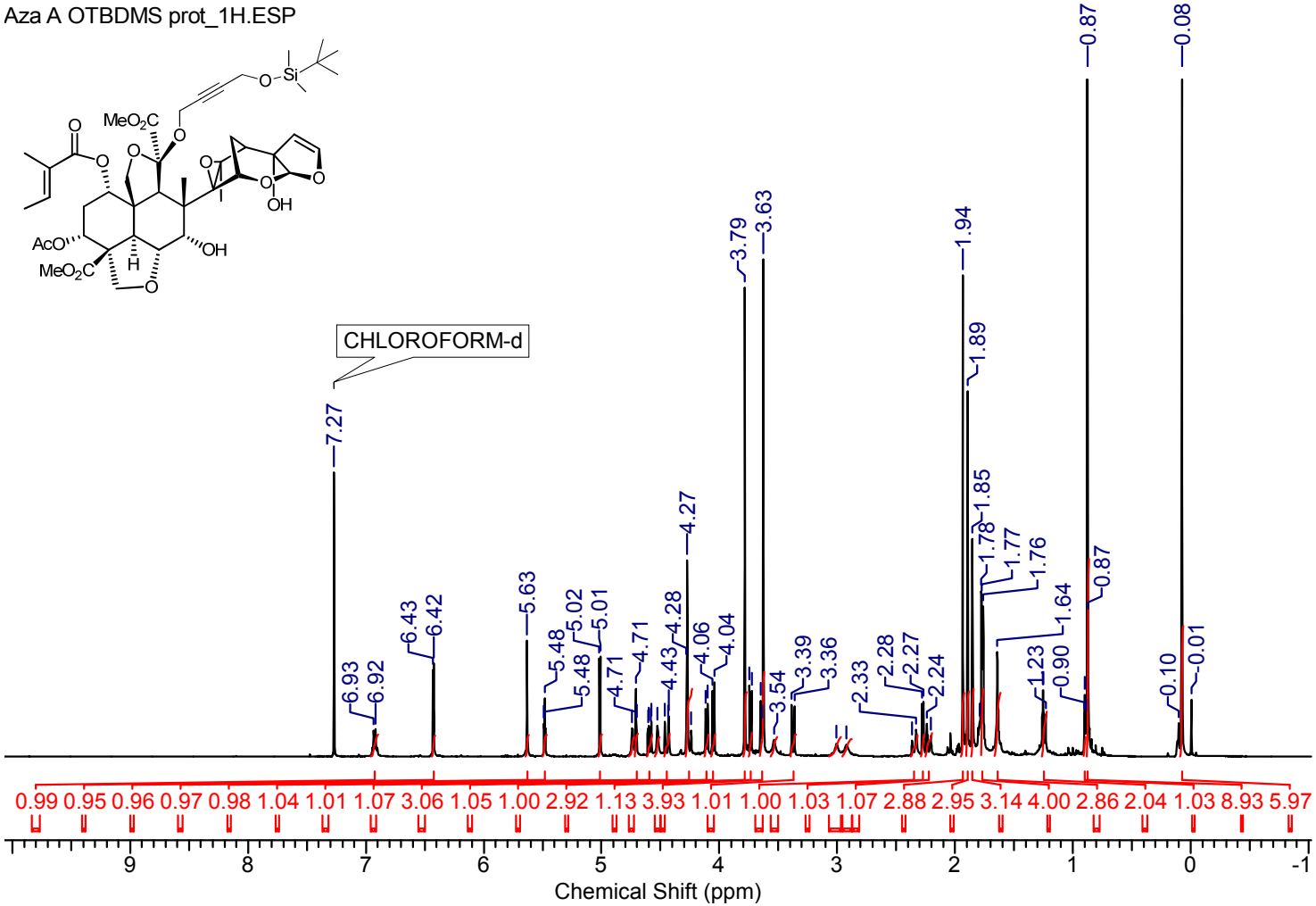

Fig. 67. ^{1}H NMR of **20a** in $CDCl_3$ at 400 MHz.

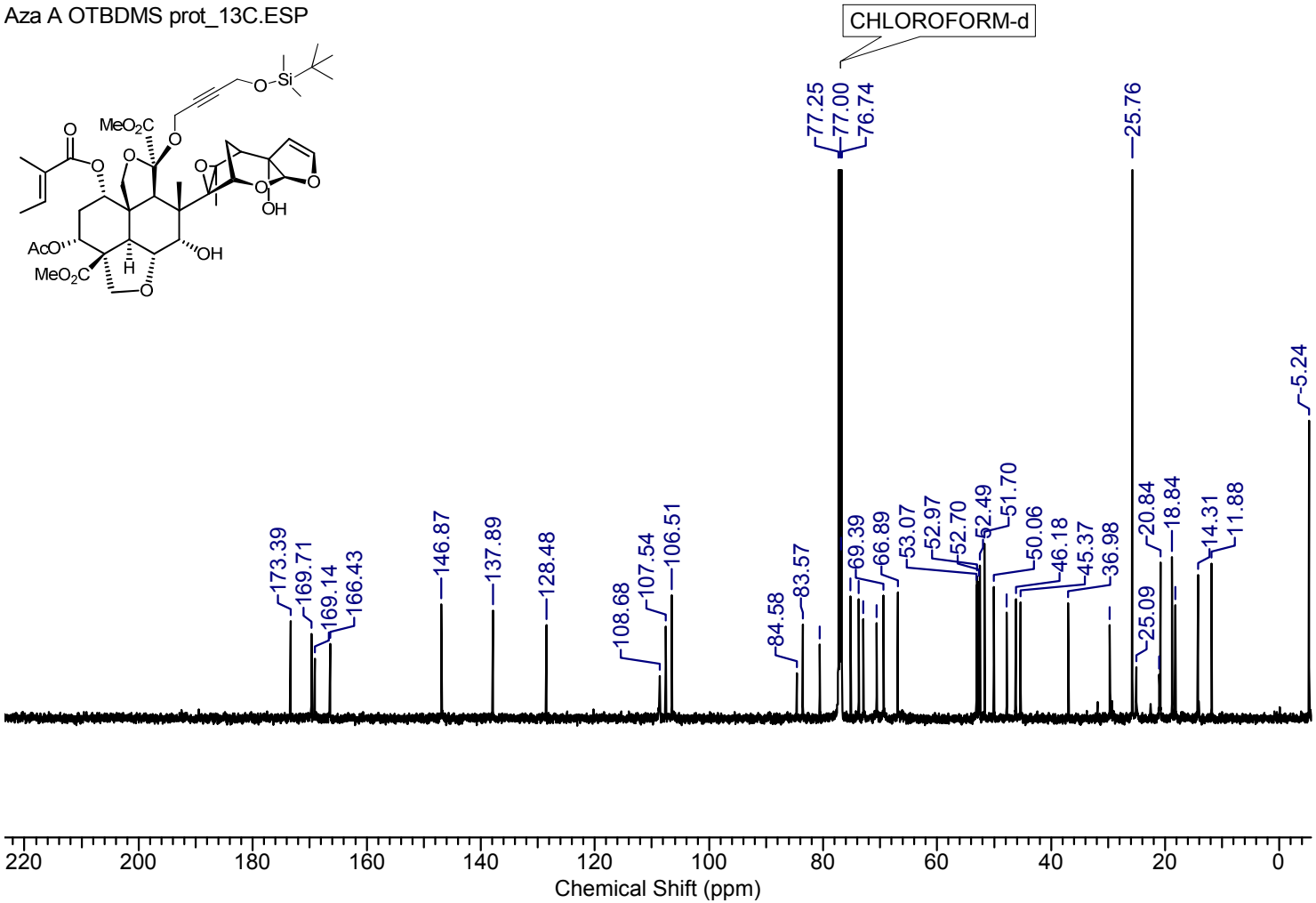

Fig. 68. ^{13}C NMR of **20a** in $CDCl_3$ at 100 MHz.

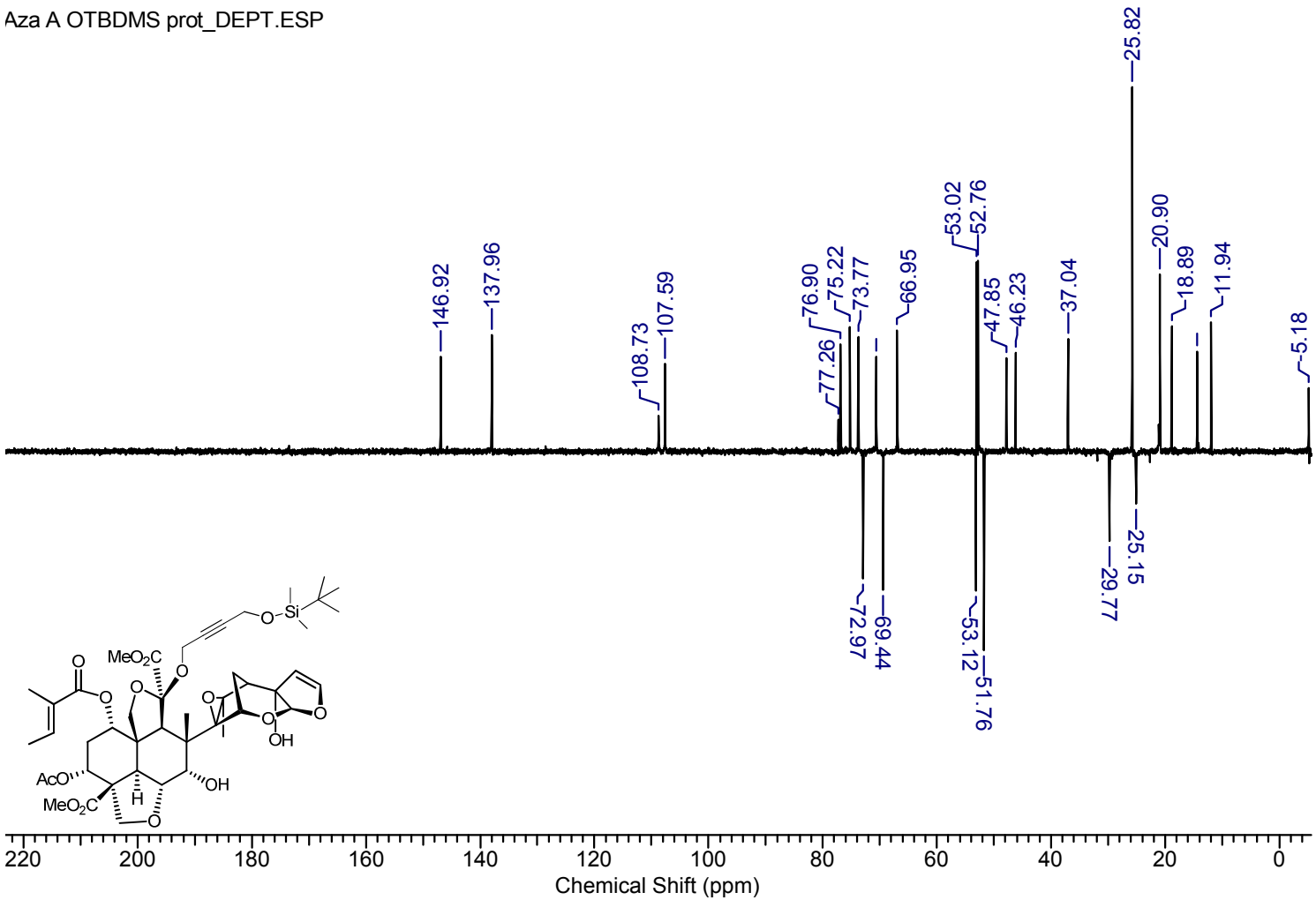

Fig. 69. DEPT-135 NMR of **20a** in $CDCl_3$ at 100 MHz.

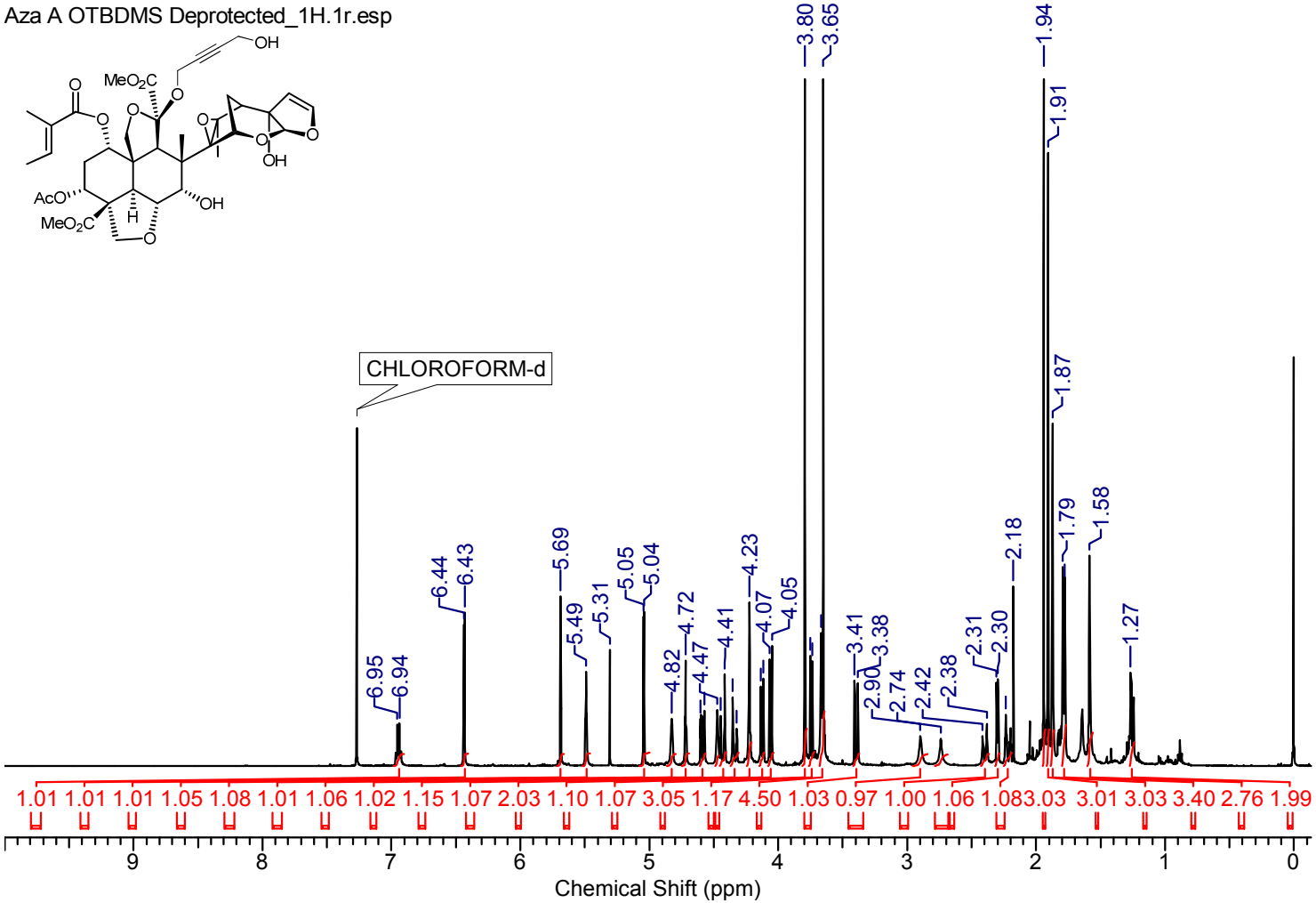

Fig. 70. ^{1}H NMR of **20b** in $CDCl_3$ at 400 MHz.

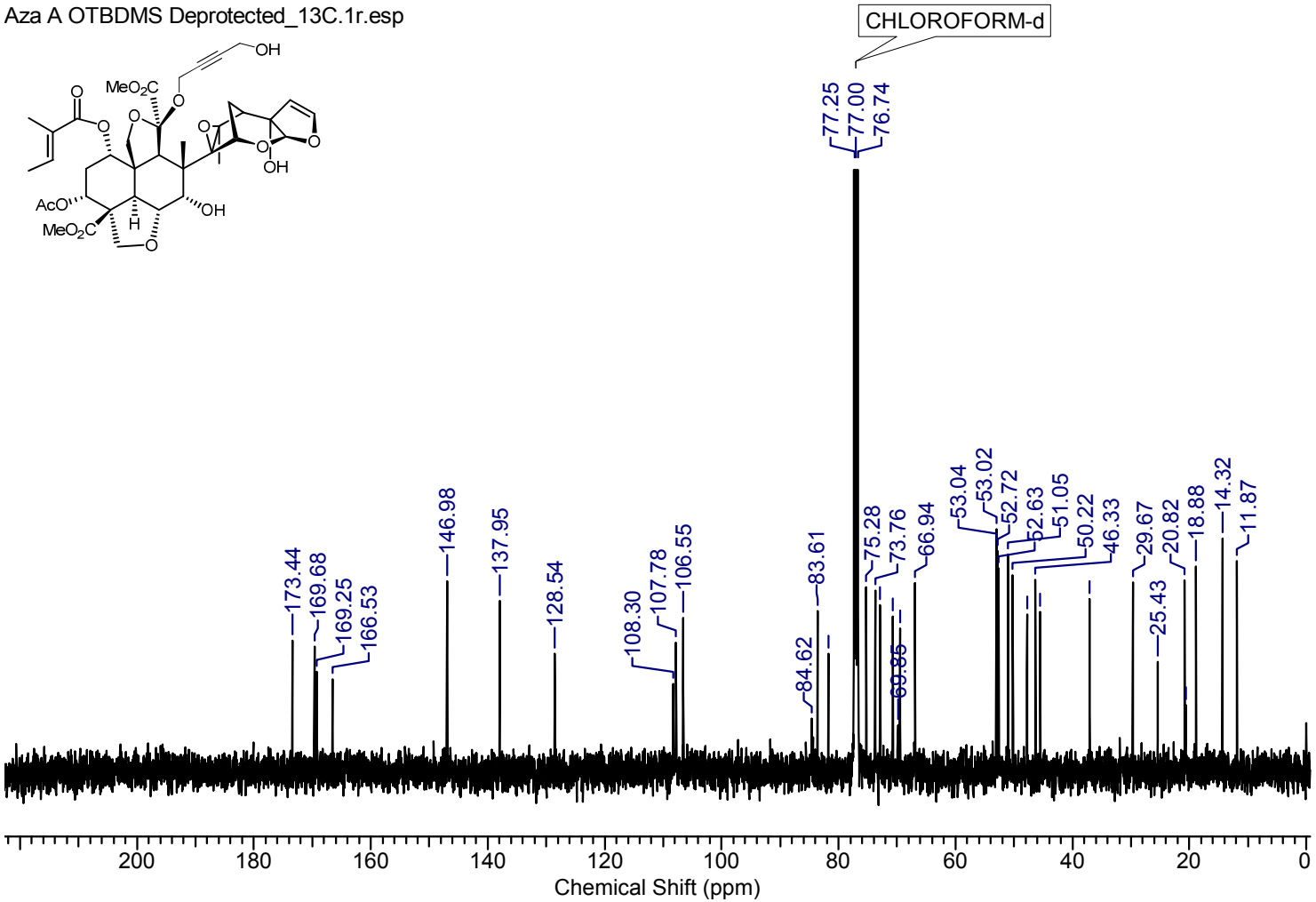

Fig. 71. ^{13}C NMR of **20b** in $CDCl_3$ at 100 MHz.

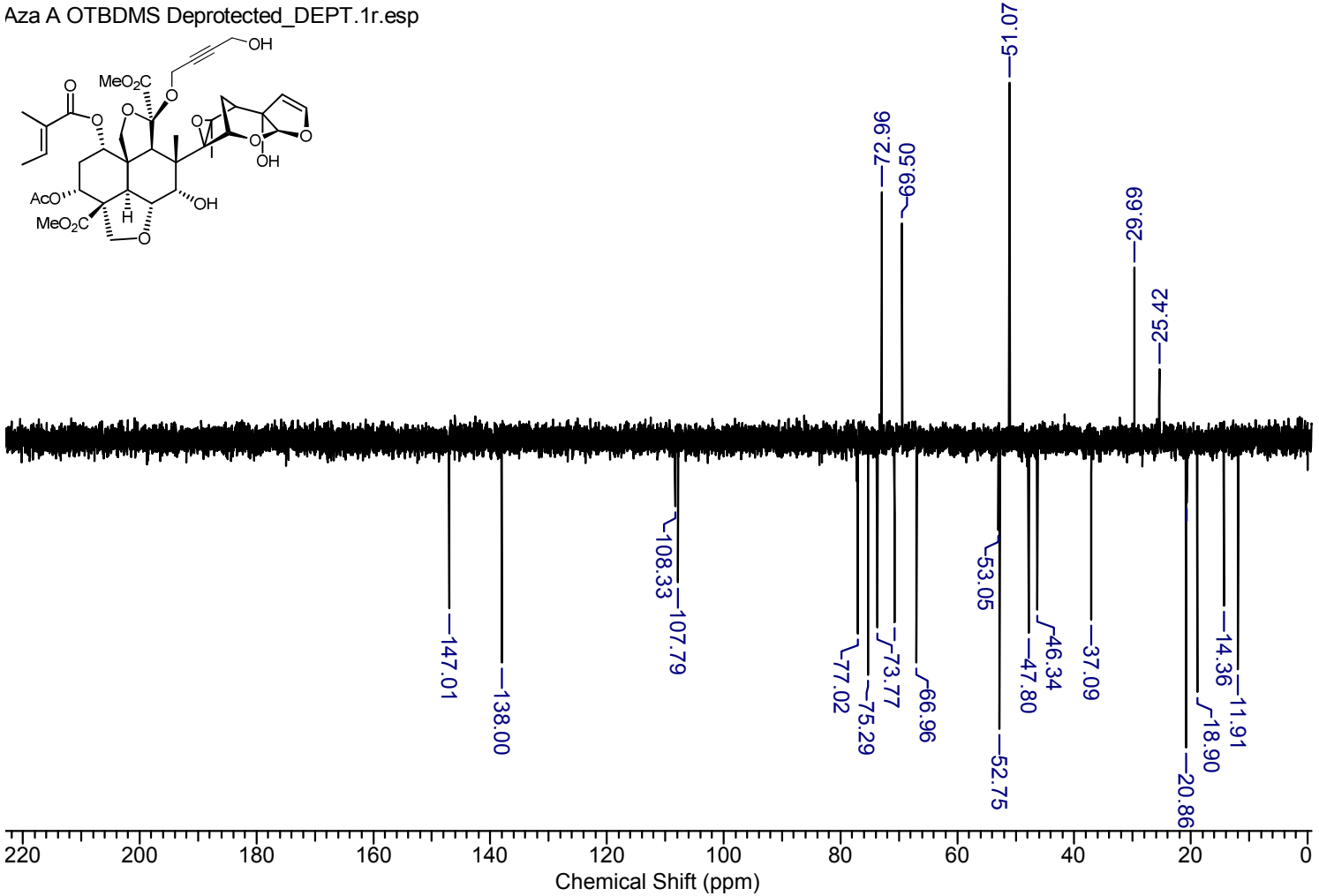

Fig. 72. DEPT-135 NMR of **20b** in $CDCl_3$ at 100 MHz.

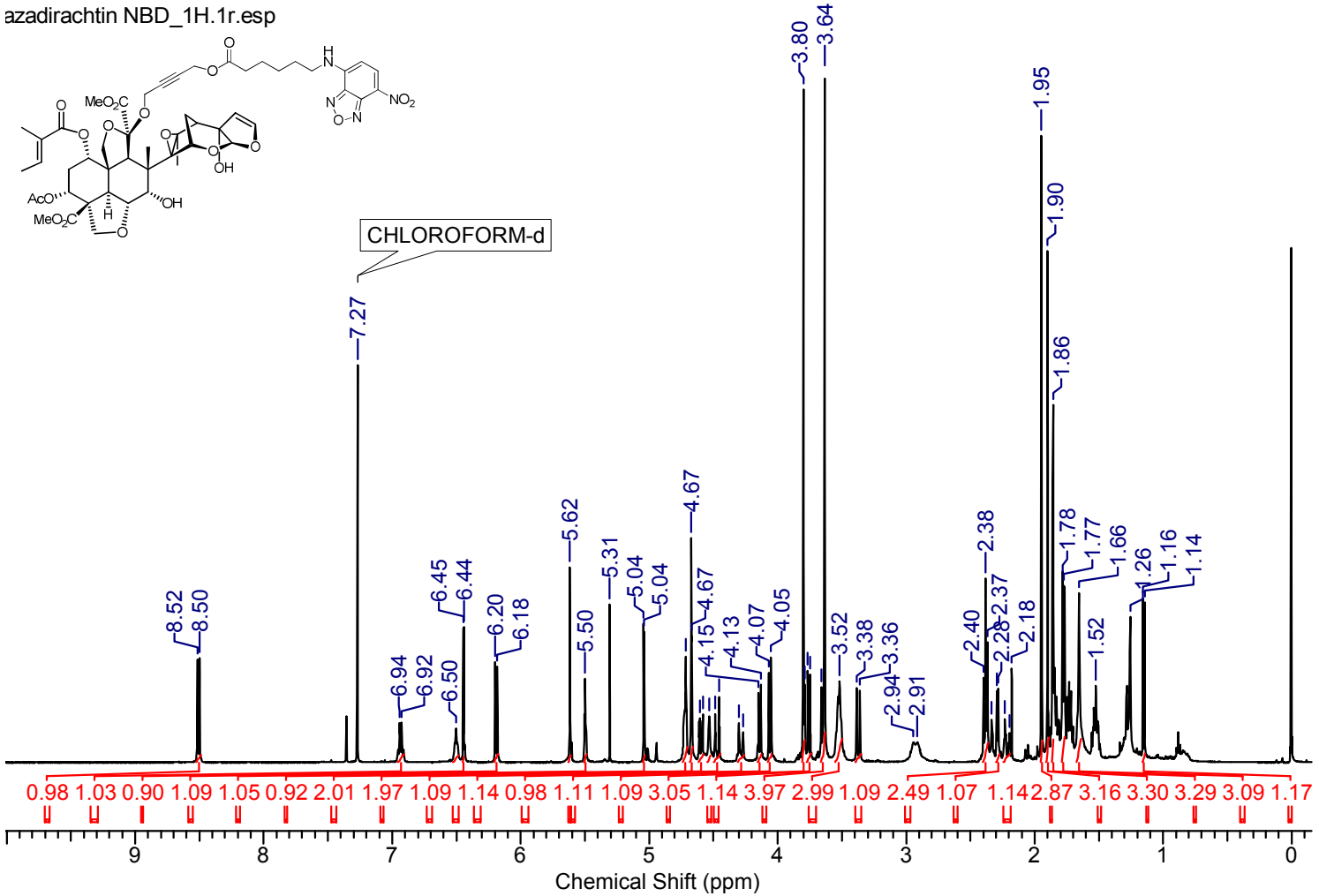

Fig. 73. ^{1}H NMR of **20c** in $CDCl_3$ at 400 MHz.

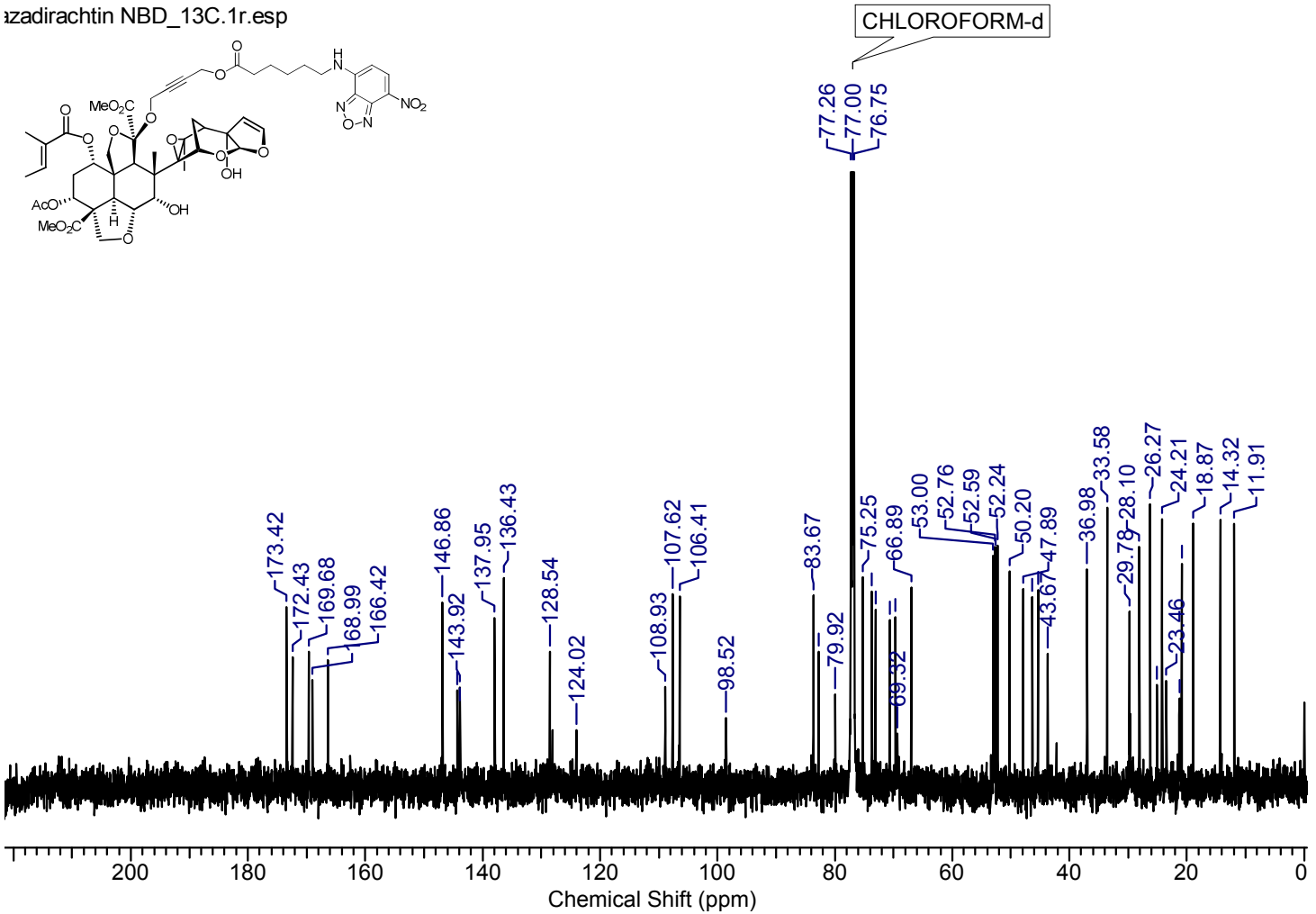

Fig. 74. ^{13}C NMR of **20c** in $CDCl_3$ at 100 MHz.

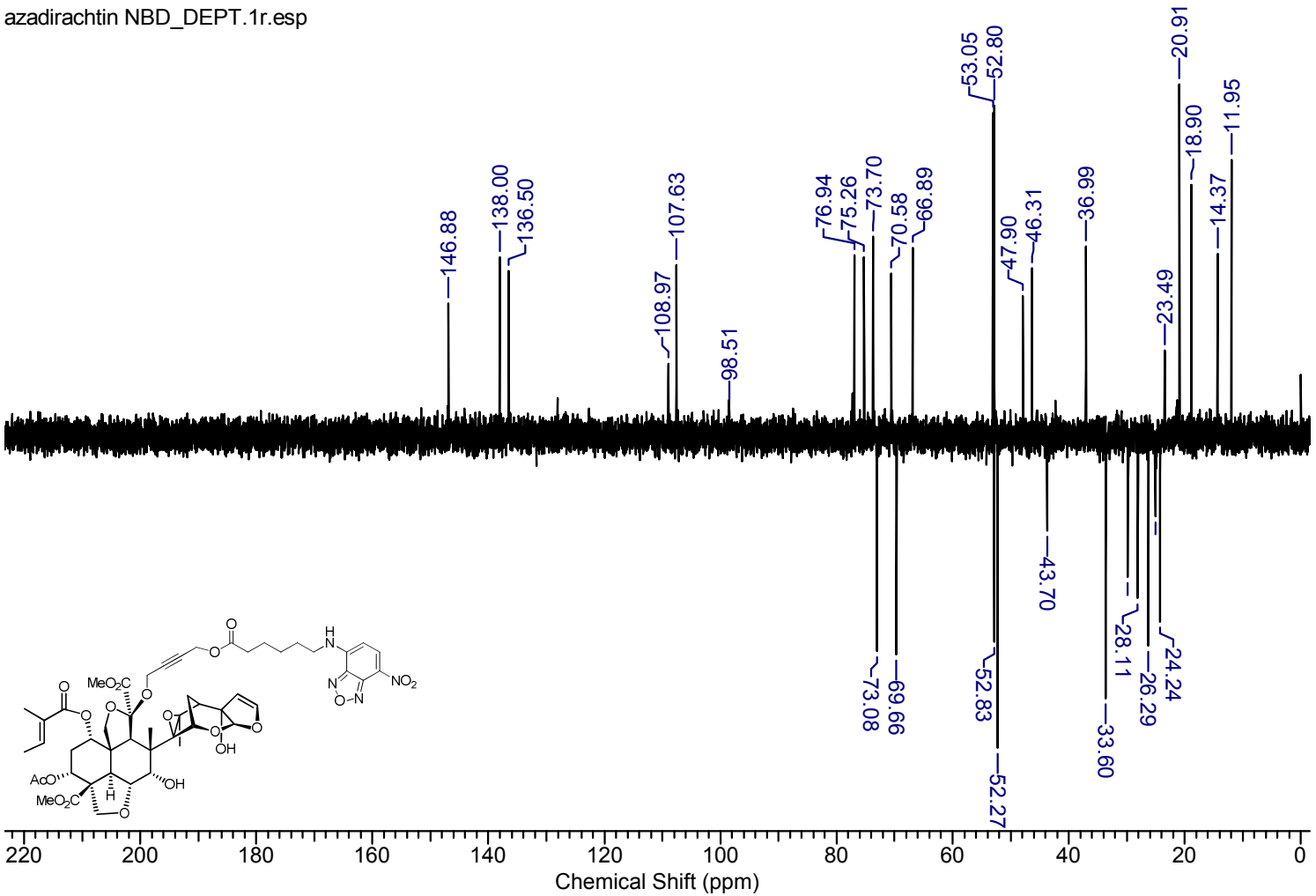

Fig. 75. DEPT-135 NMR of **20c** in $CDCl_3$ at 100 MHz.

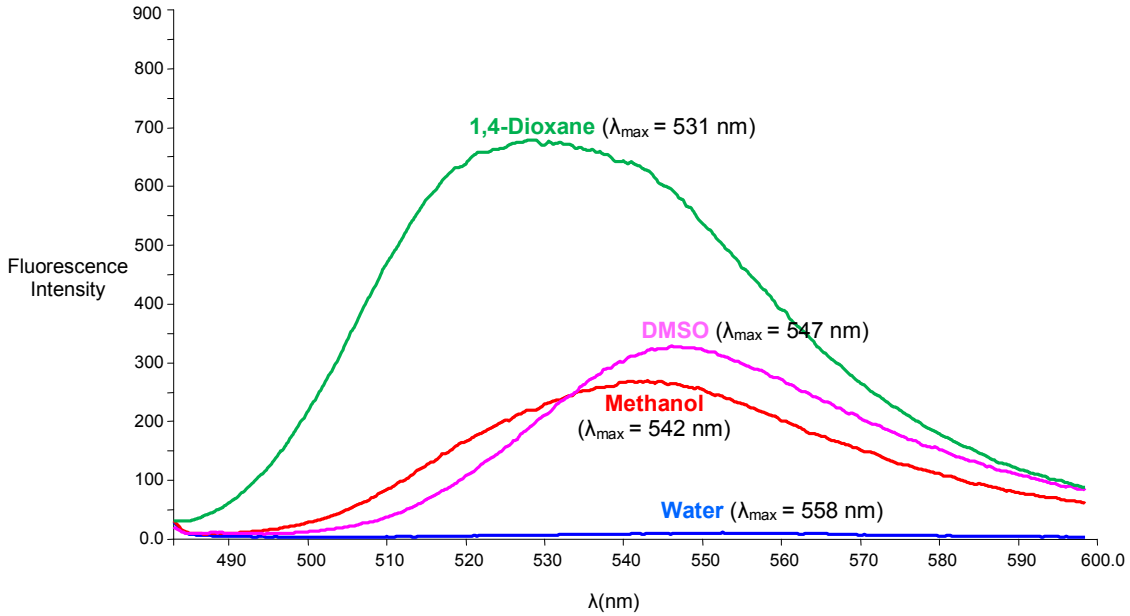

Fig. 76. Fluorescence emission spectra of **1a** (0.1 μg/mL) in solvents of different polarity (Excitation at 460 nm). Emission spectra clearly indicated that the fluorescence intensity is reduced with increase in the polarity of the environment.

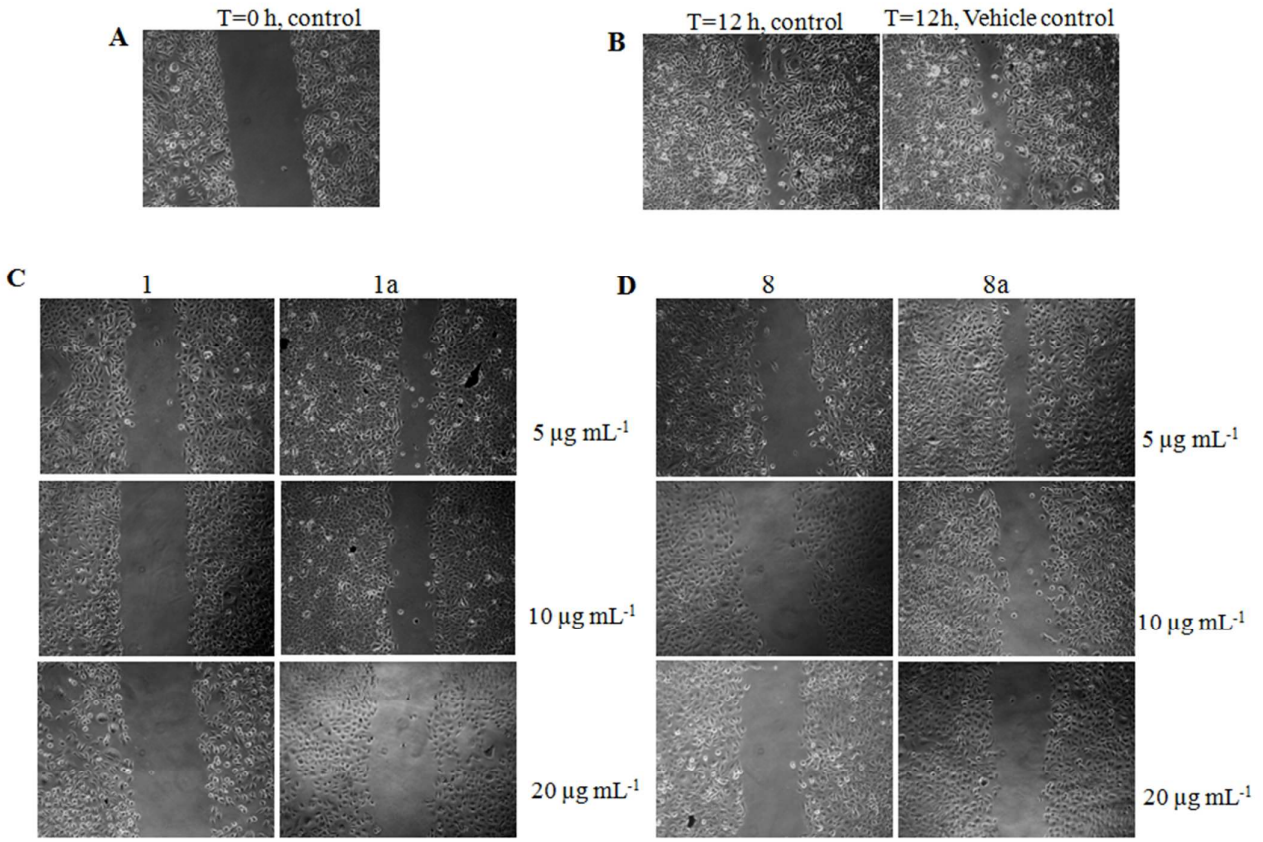

Fig. 77. Wound migration is inhibited by limonoids in MDA-MB-231 cells. **(A)** Representative wound photographed at t=0 h. **(B)** Wound photographed of control as well as vehicle control at t=12 h **(C)** Cells were treated with **1** and **1a** (0-20 µg/mL) and wound were photographed at t= 12 h. **(D)** Cells were treated with **8** and **8a** (0-20 µg/mL) and wound were photographed at t= 12 h.

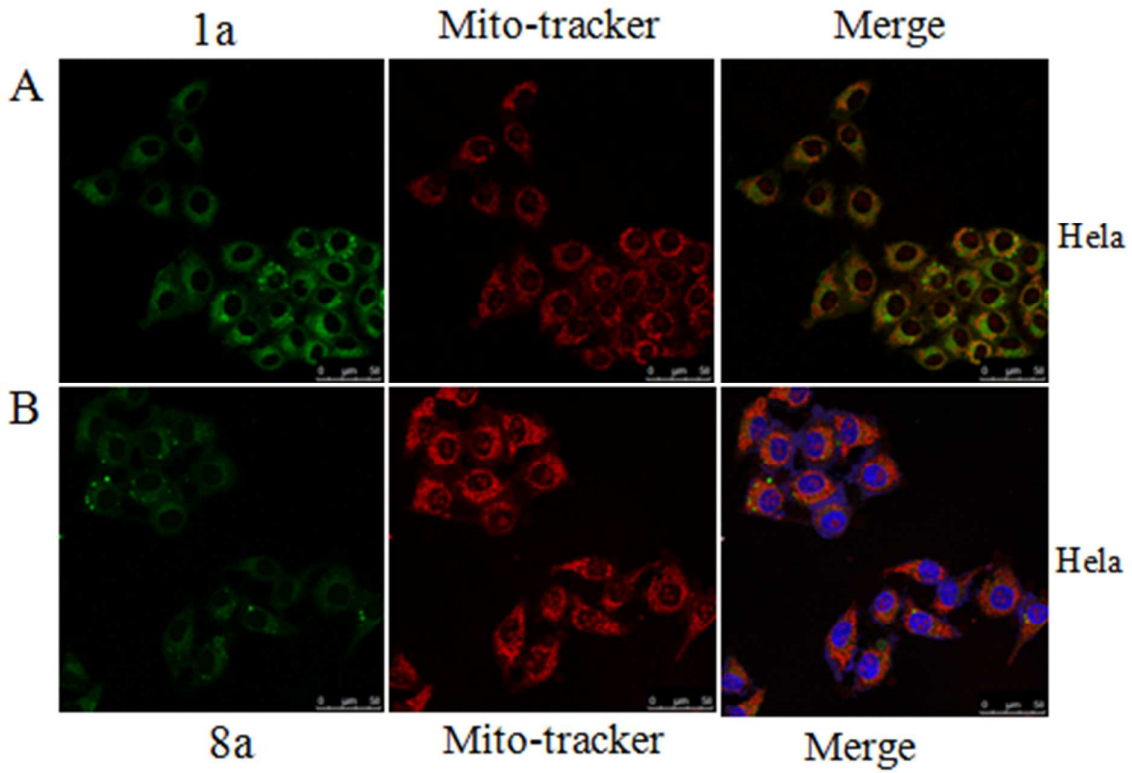

Fig. 78. (A) Hela cells were co-stained with **1a** (20 μg/mL) and Mito-tracker red (50 nM) and analyzed under confocal microscopy. **(B)** HeLa cells were co-stained with **8a** (20 μg/mL) and Mito-tracker red (50 nM) and analyzed under confocal microscopy. Nuclei were stained with DAPI. Blue: Nucleus; Red: Mitochondria; Green: NBD-labeled limonoids. Micron bar 50 μm.

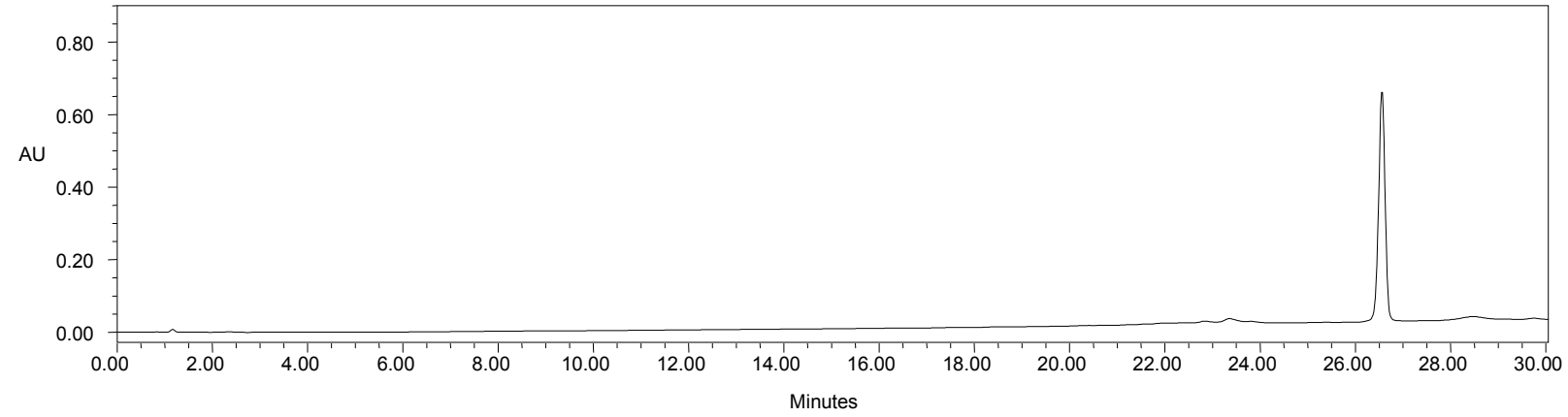

Fig. 79. HPLC profile of **1a**.

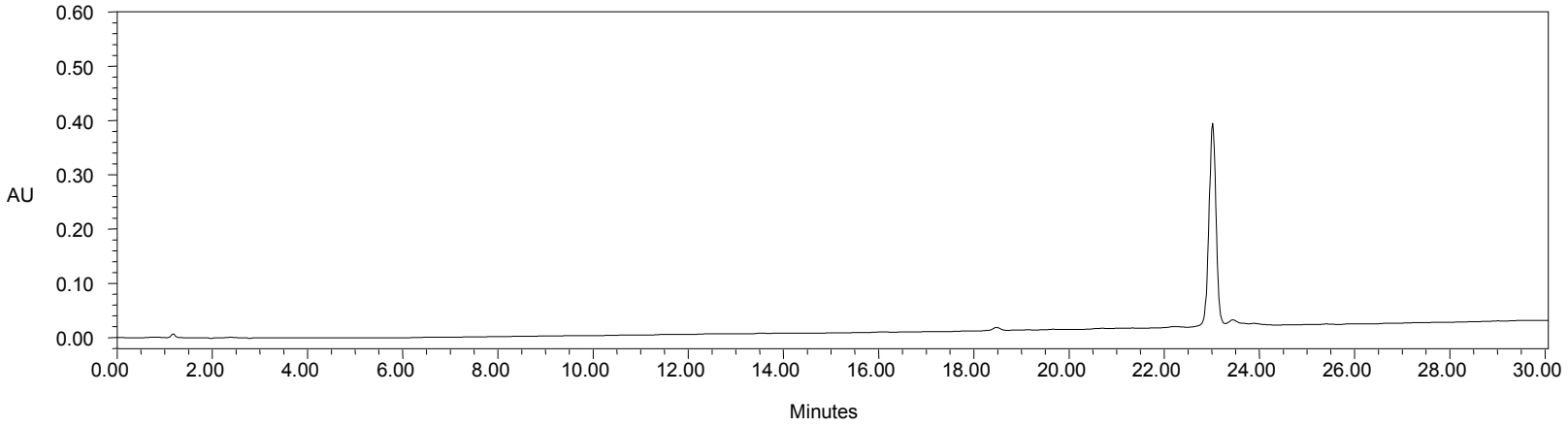

Fig. 80. HPLC profile of **8a**.

Stability of Ester Bond :

Melanoma cells (A375) in 2 mL medium were treated with **1a** (20 μg/mL) and incubated for 1 h at 37 ºC in 5 % CO_2 incubator. Before scraping, the cells were washed thrice with PBS (Phosphate-buffered saline) to remove the extracellular compounds and then lysed in lysis buffer (Lysis buffer composition: 50 mM Tris HCl, 150 mM NaCl, 1% Sodium deoxycholate, 1% Nonidet P-40, 1% Triton-X-100, 2 mM Phenyl methyl sulfonyl fluoride, 10 mM NaF, 5 mM Dithiothreitol, Protease inhibitor cocktail as per manufacture's instruction, 300 μM Na_3VO_4, 10 mM Beta-glycerophosphate and 1 mM Benzamidine). Similarly, untreated cells were also lysed as a control experiment.

Firstly, standard NBD tagged azadiradione derivative (**1a**), alcohol (Azadiradione derivative, **1**) and acid (NBD tag) were analyzed by LC-ESI-HRMS (Fig. 81). Then, cell lysate of A375 cells treated with **1a** and two controls (lysate of untreated cells and buffer) were injected in identical conditions. By comparing R_t and HRMS with the standards, the abundance of **1a**, **1** and NBD tag was determined in the lysate of A375 cells (treated with **1a)** using extracted ion chromatograms (XIC) (Fig. 82). XICs of $[M+Na]^+$ adducts (*m/z* 752.84-753.84 for **1a**, *m/z* 316.50-317.50 for NBD tag and *m/z* 476.50-477.50 for **1**) showed the presence of only **1a** in the total ion chromatogram, whereas the corresponding alcohol (**1)** and acid (may be formed due to the hydrolysis of ester bond) were absent as depicted in Fig. 82. These results clearly ascertained the stability of the ester bond joining the tag with the studied azadiradione derivative under intracellular conditions.

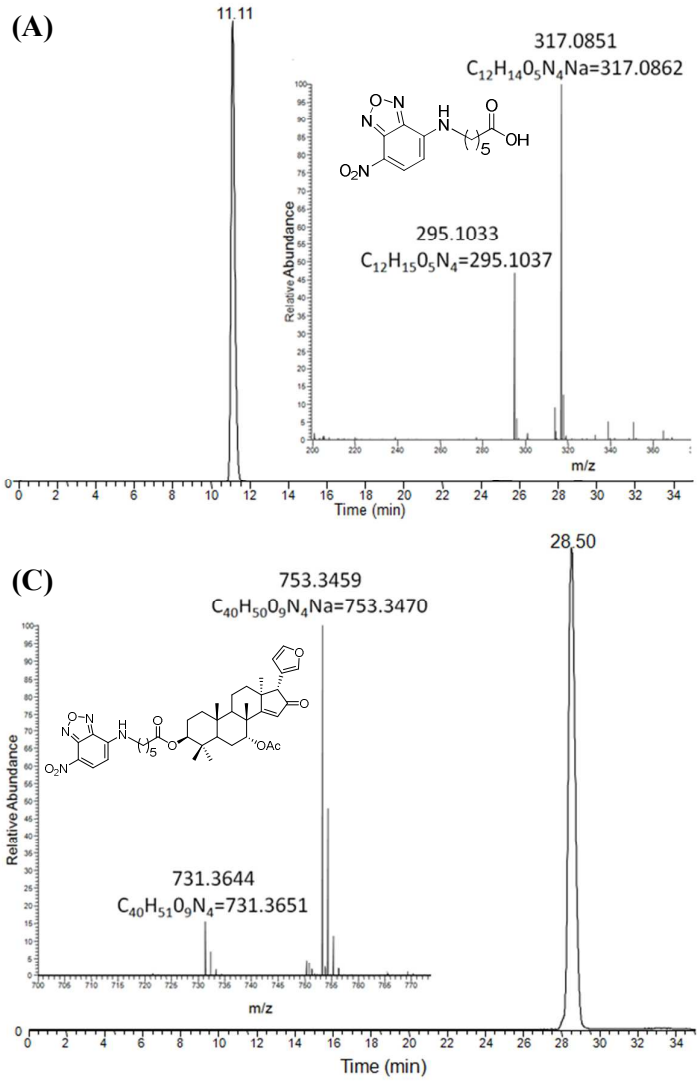

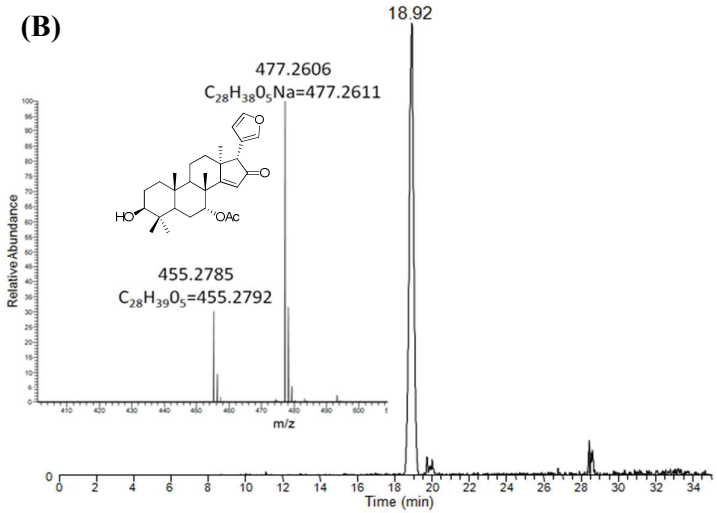

Fig. 81. LC-ESI-HRMS chromatograms and ESI-HRMS spectra (inset) of (**A**) 6-(N-(7-nitrobenz-2-oxa-1,3-diazol-4-yl)amino)hexanoic acid, (**B**) **1** and (**C**) **1a**.

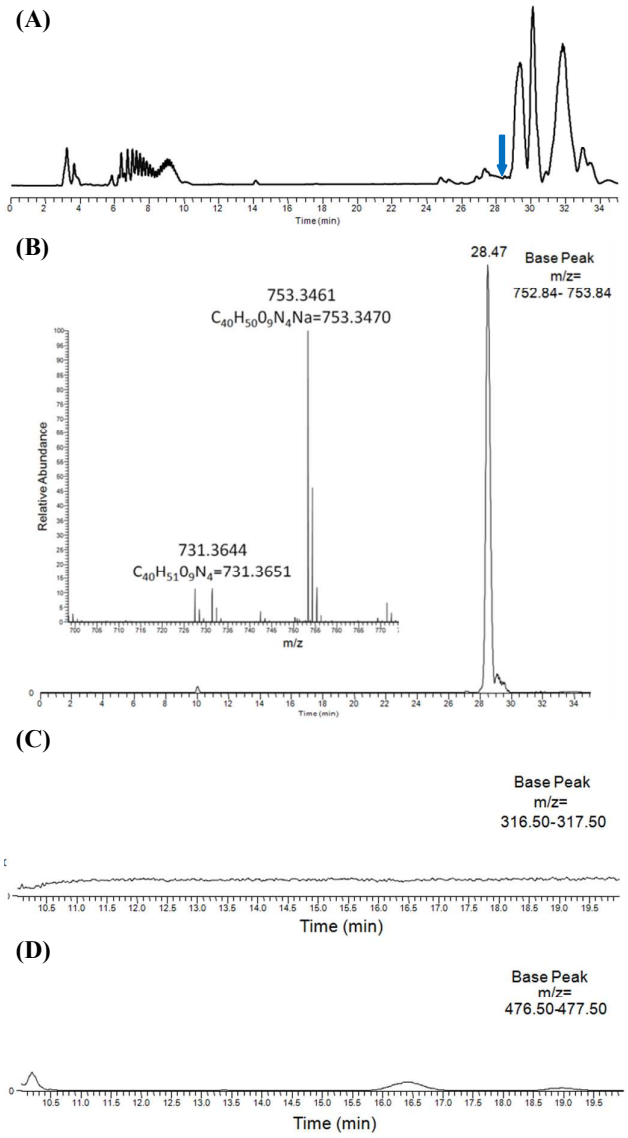

Fig. 82. (**A**) LC-ESI-HRMS total ion chromatogram of lysate of A375 cells treated with **1a** for 1 h; Extracted ion chromatograms (XIC) of *m/z* (**B**) 752.84-753.84, (**C**) 316.50-317.50 and (**D**) 476.50-477.50. XICs showed the presence of **1a** but no corresponding alcohol or acid. Thus it eliminates the probability of hydrolysis of ester bond joining the tag and studied bioactive molecule.

Characterization of NBD labeled ezetimibe (13a):

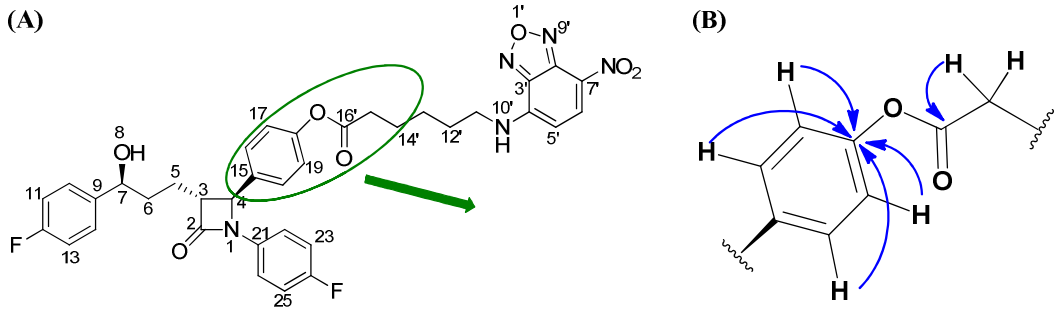

Fig. 83. (**A**) Structure and numbering of compound **13a**; (**B**) Key HMBC correlations (H→C).

The regio-selective esterification on phenolic hydroxyl group was confirmed by the extensive analyses of ^{1}H, ^{13}C, DEPT-135, HSQC and HMBC NMR spectra. Existence of an additional quaternary signal at δ_C 171.7 in ^{13}C NMR of NBD labeled ezetimibe (**13a**) suggested the esterification of hydroxyl functionality. Further, the signal at δ_C 171.7 confirmably ascribed to the ester carbonyl on the basis of HMBC correlation of C-16′ with H-15′. Except the phenolic ring (consisting of C-15, C-16, C-17, C-18, C-19 and C-20), the chemical shift values for other carbons of ezetimibe skeleton was similar to the parent (**13**). An upfield shift by 6 ppm was observed for C-18. The signals for C-15 and C-17, 19 shifted downfield by 7 ppm and 6 ppm respectively. These observations confirmed the esterification on phenolic OH-18. The correlation of C-18 (δ_C 150.6) with H-17, 19 (δ_H 7.10) and H-16, 20 (δ_H 7.34) additionally affirmed the assignment of δ_C 150.6 to C-18. The accurate allocation of the ^{1}H signals were achieved by the mutual correlations (C-16,20/H-16,20 and C-17,19/H-17,19) obtained from HSQC spectrum.

Characterization of NBD labeled andrographolide (17a):

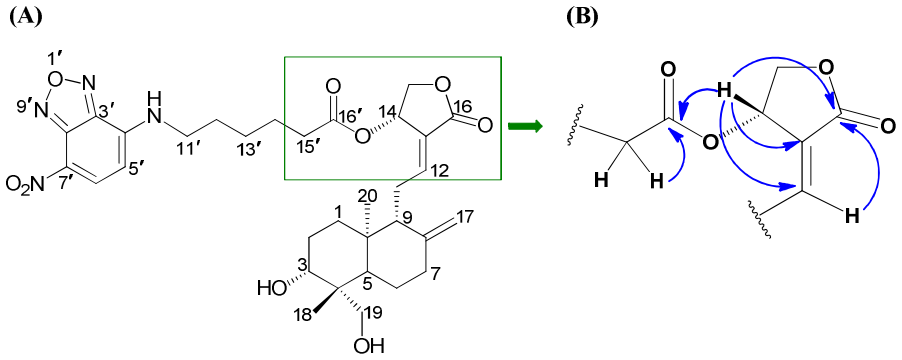

Fig. 84. (**A**) Structure and numbering of compound **17a**; (**B**) Key HMBC correlations (H→C).

The presence of ester bond in NBD tagged andrographolide (**17a**) was confirmed due to the presence of a newly appeared quaternary signal at δ_C 172.9 compared to andrographolide (**17**) and was assigned to the ester carbonyl. The chemical shift values for andrographolide skeleton in ^{13}C NMR of **17a** remained similar in comparison to **17** except for C-14, C-13 and C-15. The downfield shift of C-14 (by 3 ppm) and upfield shift of C-13 (by 5 ppm) and C-15 (by 3 ppm) indicated the esterification at 14-OH. Further the position of attachment of NBD was confirmed on the basis of HSQC and HMBC spectra. The signal at δ_H 5.94 (d, *J*=5.52 Hz) was assigned to H-14 according to the correlations of H-14 with C-12 (δ_C 150.6), C-13 (δ_C 123.8) and C-16 (δ_C 169.1) in the HMBC spectrum. The signal at δ_C 172.9 was ascribed to C-16′ due to the presence of its correlation with H-15′ (δ_H 2.43). The esterification at 14-OH was unambiguously affirmed on the basis of strong correlation between H-14 (δ_H 5.94) and C-16′ (δ_C 172.9).

Characterization of NBD labeled reduced salanin (18a):

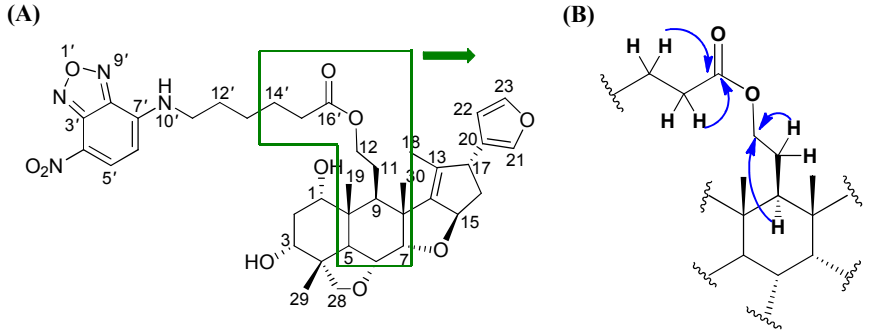

Fig. 85. (**A**) Structure and numbering of compound **18a**; (**B**) Key HMBC correlations (H→C).

Appearance of an additional quaternary signal at δ_C 173.3 in ^{13}C NMR of **18a** with respect to **18** implied the esterification of one of the hydroxyl functionalities. The correlation of C-16′ (δ_C 173.3) with H-15′ (δ_H 2.33) and H-14′ (δ_H 1.70) in HMBC spectrum further confirmed the assignment of δ_C 173.3 to the ester carbonyl. A downfield shift of 2 ppm for methylene C-12 (δ_C 64.8) was observed after esterification. The neighbouring C-11 (δ_C 64.8) underwent an upfield shift by 3 ppm. The other carbons of the esterified product (**18a**) showed similar chemical shift values with respect to the original natural product confirming the esterification on 12-OH. This was further supported by comparing DEPT-135 NMR data, since change in chemical shift values was observed only for the methylene carbons (C-12 and C-11) and not for any methine carbons. The assignment of chemical shift value for the esterified centre C-12 at δ_C 64.8 was further confirmed on the basis of HMBC correlations of C-12 (δ_C 64.8) with H-11 (δ_H 1.80) and H-9 (δ_H 2.22). All the assignments of ^1H and ^{13}C signals were supported well by the mutual correlations observed in HSQC spectrum.

Reaction kinetic studies

Kinetic studies were performed between **1** and 6-(N-(7-nitrobenz-2-oxa-1,3-diazol-4-yl)amino)hexanoic acid with higher stoichiometric reatios (1:coupling reagent=1:2 and 1:coupling reagent=1:3) of coupling reagents (DCC, EDC and DIC). 6-(N-(7-nitrobenz-2-oxa-1,3-diazol-4-yl)amino)hexanoic acid (1.0 equiv), **1** (1.0 equiv) and DMAP (1.0 equiv) were taken together and anhydrous DCM (30 mL/mmol) was added to that in an inert atmosphere. All the components were dissolved by stirring and the coupling reagnt (2.0 or 3.0 equiv of DCC, EDC or DIC) was added to the reacion mixture. The reaction was continued with stirring at room temperature. Portions of the reaction mixture was taken out periodically (0.5 hr, 1.5 hr, 3.0 hr and 5.0 hr) and analyzed by HPLC. Higher stoichiometry of coupling reagents did not show considerable variation in the extent of progress and rate of the aforementioned reaction as represented in the following figure.

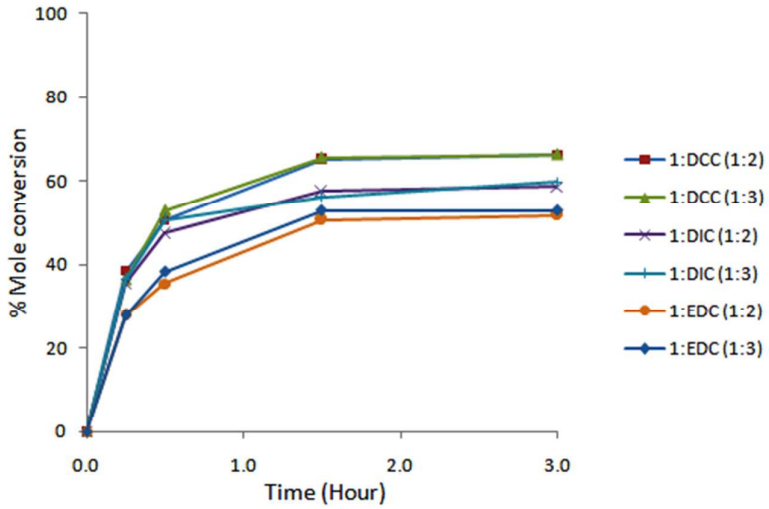

Fig. 86. Kinetic studies of coupling reaction between **1** and 6-(N-(7-nitrobenz-2-oxa-1,3-diazol-4-yl)amino)hexanoic acid using different stoichiometric ratios of **1** and coupling reagents.

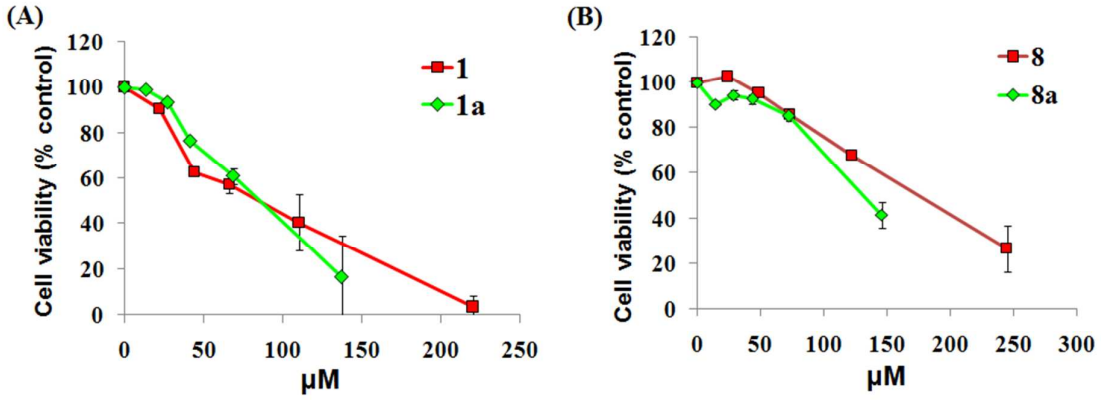

Fig. 87. (A and **B)** Graphical representation of comparative inhibition of MDA-MB-231 cell viability (MTT assay) by **1**, **1a**, **8** and **8a** (in μM concentration unit).

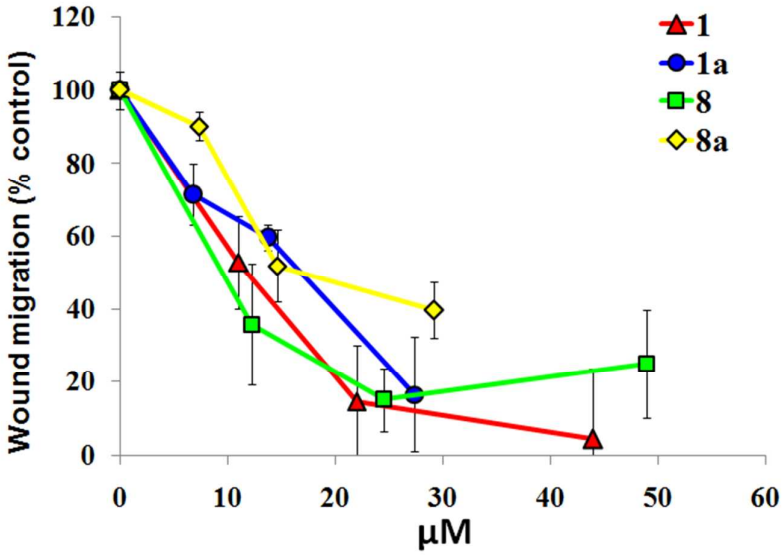

Fig. 88. Graphical representation of comparative inhibition of MDA-MB-231 cell motility (wound migration assay) by **1**, **1a**, **8** and **8a** (in μM concentration unit).